Primary fragmentation of large coal particles

CJ Badenhorst

22308245

Dissertation submitted in fulfilment of the requirements for the degree *Magister* in Chemical Engineering at the Potchefstroom Campus of the North-West University

Supervisor: Prof QP Campbell

Co-supervisor: Prof M le Roux

May 2016

DECLARATION

I, Charlotte Badenhorst, hereby declare that the dissertation entitled: "*Primary fragmentation of large coal particles*", submitted in fulfilment of the requirements for the degree ***Magister*** in ***Chemical Engineering*** at the Potchefstroom Campus of the North-West University is my own work, unless specified otherwise, and has not been submitted to any other tertiary institution in whole or in part.

Signed at Potchefstroom

_____ _____

Charlotte Badenhorst Date

ACKNOWLEDGEMENTS

The author wishes to acknowledge the following individuals and institutions for their support during the course of this project:

- Prof Quentin Campbell and Prof Marco le Roux, my study supervisors, for their guidance and the numerous learning opportunities that they gave me;
- Prof John Bunt for his insightful inputs;
- Messrs Johan de Korte, David Powell and Ms Reneta Pillay for arranging and supplying coal samples;
- Messrs Ryno van der Merwe, Frikkie de Beer, Jakobus Hoffman and Dr Ettiene Snyders from the South African Nuclear Energy Corporation (Necsa) for their individual contributions and for usage of the Mercury Intrusion Porosimetry and Micro-focus X-ray Radiography and Tomography facilities situated at Necsa;
- Sasol for using their Mercury Intrusion Porosimetry facility and especially Mrs Susanna de Jager for her assistance;
- The coal research group, technicians and laboratory personnel of the North-West University for their assistance and making sure equipment is up and running;
- Lastly to my family and friends on whom I could always depend

The work presented in this paper is based on the research supported by the South African Research Chairs Initiative of the Department of Science and Technology and National Research Foundation of South Africa (Coal Research Chair Grant No. 86880). Any opinion, finding or conclusion or recommendation expressed in this material is that of the author(s) and the NRF does not accept any liability in this regard.

ABSTRACT

When rapidly exposed to high temperatures coal tends to fragment into several pieces due to thermal and volatile release stresses. This is known as primary fragmentation and is one of the major problems opposing the optimum performance in high temperature applications such as gasifiers. Hydrodynamic and pressure drop fluctuation problems, among other things, arise in gasifiers due to this primary fragmentation. It is therefore necessary to investigate this phenomenon in detail.

In the study, *"Primary fragmentation of large coal particles"*, the fragmentation of large, almost spherical, coal particles (10, 15, 20, 25 and 30 mm) from five different coal origins in South Africa (low and high volatile, swelling and non-swelling and more or less the same ash yield samples) heated to 400, 600 and 900 °C respectively were tested. Five repeats of each combination were conducted for statistical accurate results. A horizontal tube furnace under a nitrogen atmosphere was used to test the samples (pre-heated so that heating rate was not controlled), while X-ray tomography was used to aid in the qualitative interpretation of results.

From the tomography scans small cracks could be seen throughout the particle volume. These cracks are either natural cleats or fissures formed due to handling. Upon heating new cracks formed on these initial cracks, especially on cracks between coal-mineral interfaces. The cracks that formed were well structured and orientated, either perpendicular or parallel to the bedding planes. For the high volatile samples, a major crack parallel to the bedding plane was visible which, if enough stress was applied, fragmented it into two coarse fragments. This behaviour is associated with fragmentation due to volatile release stresses. For the low volatile samples, fragmentation due to thermal stresses was more prominent with the particles fragmenting into a multitude of small pieces under certain conditions. The amount of volatiles present relative to the pore structure of a particle influenced fragmentation due to volatile release stresses. The ratio between vitrinite and fusinite content in a particle had an influence on fragmentation due to thermal stresses. Since the ash yields for the different samples were very low and clustered around 10% the influence of mineral matter could not be determined.

Fragmentation was quantified using a breakage index defined as the ratio between Sauter diameter after and before fragmentation. If the breakage index equalled one, zero fragmentation occurred, while if the breakage index was smaller or larger than one

fragmentation and swelling respectively was present. The breakage index decreased with an increase in particle size. Larger particle sizes will thus fragment more than smaller sizes.

Temperature also influenced the breakage index and it was concluded that, for the non-swelling samples, a temperature increase led to a decrease in breakage index. For the swelling samples, the breakage index, after being heated to 600 °C, was larger than for 400 °C, which was in turn larger than for the 900 °C situation. After being heated to 600 °C, swelling was able to reduce volatile release stresses and thus fragmentation, while for 900 °C volatile release and thermal stresses were too severe to be relieved by swelling. For particles heated to 400 °C swelling had not yet commenced and breakage was higher.

The relationship proposed by Dakič *et al.* (1989:916) pertains to South African coal samples. From this relationship, it is predicted that the critical diameter (largest diameter for which there is no noticeable fragmentation) of a coal sample will decrease with an increase in pore resistance number. At certain temperatures, however, the low volatile samples did not follow this relationship since they are not affected as much as the high volatile samples by the pore resistance number. Take note also that, due to the lack of variability in South African coalfields only pore resistance numbers ranging between 0 and 10 were tested. The critical diameters based on a 75% probability (at least 75% of all repeated runs fragmented) for this study for particles heated to 900 °C ranged between 10 and 20 mm, while those heated to 600 °C ranged between 15 and 25 mm. The critical diameters for particles heated to 400 °C ranged between 15 and 30 mm. The critical diameters for 900 °C were successfully compared to literature which lay between 2 and 25 mm.

Overall, the results correspond well to those from literature. For future studies, it was suggested that the influence of vitrinite and fusinite on the fragmentation behaviour should be investigated more thoroughly.

Keywords: primary fragmentation, critical particle diameter, Micro-focus X-ray tomography, breakage index, large particles

TABLE OF CONTENTS

LIST OF FIGURES

LIST OF TABLES

NOMENCLATURE

Symbol	Description	Unit
C_1	Approximate solution constant	-
C_p	Heat Capacity	J/kgK
d	Sieve size	mm
D	Tube diameter	mm
h	Convective coefficient	W/m^2K
k_f	Thermal conductivity, fluid	W/mK
k_s	Thermal conductivity, solid	W/mK
r	Radius	mm
r_n	Radius at point n	mm
r*	Spatial coordinate	-
R	Radius at surface	mm
t	Time	s
T	Temperature	K
T_i	Initial temperature	K
$\mathbf{T}_\infty$	Final temperature	K
v	Kinematic viscosity	m^2/s
V	Velocity	m/s

$\dot{V}$	Volumetric flow rate	L/min
w	Weight	g
x	Weight fraction	-
ρ	Density	g/mm^3
μ	Viscosity	Ns/m^2
μ_s	Adapted viscosity	Ns/m^2
ζ_1	Approximate solution constant	-
σ	Standard Deviation	Dependent

ABBREVIATIONS & ACRONYMS

Abbreviation/Acronym	Meaning
a.d.b	Air-dried basis
ASTM	American Society for Testing and Materials
BFB	Bubbling fluidized bed
CFB	Circulating fluidised bed
CSN	Crucible swelling number
CV	Calorific value
d.a.f	Dry ash free basis
dmmf	Dry mineral-matter free basis
DTF	Drop tube furnace
EHF	Electrical heated furnace
FB	Fluidized bed
FBDB	Fixed-Bed Dry-Bottom
Fo	Fourier Number
HGI	Hardgrove Grindability Index
HSR	Heated strip reactor
HV	High Volatile
ISO	International Organisation for Standardisation

IUPAC	International Union of Pure and Applied Chemistry
LV	Low Volatile
mmf	Moist mineral-matter free basis
MF	Muffle furnace
MIP	Mercury Intrusion Porosimetry
MIXRAD	Micro-focus X-Ray Radiography and Tomography
Necsa	South African Nuclear Energy Corporation
Nu	Nusselt Number
Pr	Prandtl Number
PRN	Pore resistance number
R^2	Linear coefficient of determination
Re	Reynolds Number
RI	Roga index
SANS	South African National Standard
SAXS	Small Angel X-Ray Scattering
TB	Thermo balance
vol.%	Volume percentage
wt.%	Weight percentage

LANGUAGE EDITOR'S CERTIFICATE

Language Editor's Certificate

TO WHOM IT MAY CONCERN

This document serves to confirm that I, the undersigned, a professional language practitioner* of

30 Kwartel Crescent, Rooihuiskraal, Centurion,

was responsible for the partial language/style editing of a dissertation submitted by

Ms C J (Charlotte) Badenhorst

a student of the Northwest University, Potchefstroom Campus, submitted for the fulfilment of the requirements for the degree

Magister in Chemical Engineering

Edited sections: Abstract
Chapters 1, 2, 3, 4, 5 and 6

A S du T Sonnekus
(Dries Sonnekus)

Professional Language Practitioner/Text Editor
Tel: 012 661 5907

*Accredited by NWU to translate/edit study guides in various disciplines.

CHAPTER 1: INTRODUCTION

"What is the extent and nature of primary thermal fragmentation on large (5 to 30 mm) coal particles?" To answer this research question an experimental proposal was developed as presented in this chapter. The proposal includes an overview on the background of the research problem as well as a motivation for studying this particular problem. The problem statement and the relevance of the research are also given. The aim and objectives are stated and the scope briefly presented. Lastly, an outline of the structure of the rest of the dissertation is also shown.

1.1 BACKGROUND & MOTIVATION

The turn of the 19th century marks the commercialisation of one of the greatest engineering processes of all times: coal gasification. Briefly coal gasification can be defined as a process in which syngas is produced from carbonaceous material (coal) when contacted with a reactant gas (Sharma *et al.,* 2012:56). Both Du Toit (2013:8) and Oboirien (2011:7) commented on the role that coal gasification plays in the generation of electricity and the production of liquid fuels. In a country such as South Africa the electricity generation and liquid fuels industries account for 85% of non-exporting coal consumption. The optimum performance of coal gasification processes is thus crucial (Department of Energy, 2015; Höök & Aleklett, 2009:10).

One of the major challenges opposing this optimum performance is the fragmentation of coal particles when rapidly exposed to the elevated heating conditions associated with gasification (especially in South African fixed-bed gasifiers). This thermal fragmentation of coal is damaging, causing hydrodynamic and pressure-drop fluctuation problems (Bunt & Waanders, 2008:2856; Höök & Aleklett, 2009:3; Van Dyk, 2001:245). Elutriation of small fragmented particles can also initiate a snowball effect in which processes downstream of the gasification process are affected by a build-up of coal pieces in the syngas (Suárez-Ruiz & Crelling, 2008:128). Fragmentation of coal particles also complicates the modelling aspects of gasification since it influences the reaction rate and kinetics (Van der Merwe, 2010a: iii). It is thus necessary to examine the extent and nature of this thermal fragmentation phenomenon thoroughly to try and understand it to a certain extent.

The focus of this dissertation is on the primary fragmentation of large coal particles which is the thermal fragmentation of coal occurring during the drying and pyrolysis stages of gasification. In Figure 1.1 the damage caused by primary fragmentation through means of a before and after comparison is given. From this figure, it can be seen that almost all of the

initial particles (1 to 5.6 mm) underwent fragmentation. Very small fragments, as well as medium size fragments, can be distinguished.

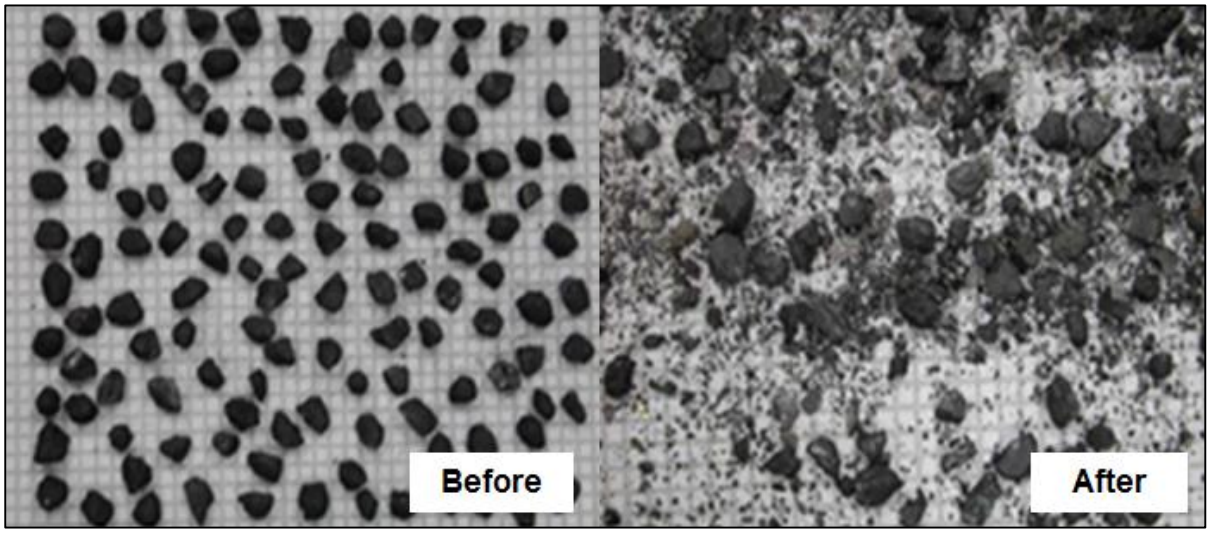

Figure 1.1: Influence of primary fragmentation on the initial feed (1 to 5.6 mm) to a real life circulating fluidised bed (CFB) gasification process (Adapted from Lee *et al.*, 2001:10).

1.2 TERMINOLOGY & DEFINITIONS

To understand the subsequent discussion (of this chapter and the rest of the dissertation) a few concepts will first be explained:

Thermal stress breakage: Primary fragmentation caused by thermal gradients in a particle when rapidly heated

Volatile pressure build-up breakage: Primary fragmentation due to a volatile pressure build-up in the pore network of a particle when rapidly heated

Critical particle diameter: Largest diameter for which there is no noticeable fragmentation

Pore resistance number: The ratio between the volatile matter and equilibrium moisture of a coal particle. Porosity is a good substitute for equilibrium moisture content. In other words the pore resistance number (PRN) is an indication of the amount of volatile matter in a particle relative to the amount of pore space available through which they can escape upon heating

Breakage index: Ratio between the Sauter diameter after and before fragmentation

Sauter diameter: Geometrical mean

Equilibrium moisture content: Moisture content at 96-97% relative humidity and 30 °C

Secondary thermal fragmentation: Secondary thermal fragmentation occurs in the char gasification stage of a gasifier when the bridges supporting the char structure burns-out (Cui & Stubington, 2001:2245).

1.3 PROBLEM STATEMENT

Research on the extent and nature of primary fragmentation on large coal particles is limited. Through examination of literature, the following aspects were identified to investigate in this dissertation:

- Causes of primary fragmentation and the extent, nature and placement of fractures forming due to primary fragmentation; and

- Factors influencing large particle fragmentation and the relationship between these factors and fragmentation.

The factors influencing large particle fragmentation include size, temperature and coal properties. These factors are considered with the focus on finding and explaining the relationship between the factors and fragmentation as was done by Dakič *et al.* (1989:911-916). In 1989 Dakič *et al.* (1989:911-916) launched an investigation into one of the most ill researched (but undoubtedly important) primary fragmentation topics namely the critical particle diameter or thermal stable size of coal particles. In their investigation they establish a relationship between the PRN of coal particles and their associated critical particle diameters. According to Oka (2004:234) the relationship is not fully developed yet since different temperatures will affect the critical diameter to different extents and should be included into this relationship. Johansson (2012:21) also stated that the relationship only pertains to bituminous coal. The effect of coal with a different rank (such as low volatile content coal) on this relationship should thus also be investigated. The influence of mineral matter was not investigated in this study.

1.4 AIM & OBJECTIVES

The aim of this dissertation is to:

- Describe the extent and nature of primary fragmentation on large (5 to 30 mm) South African coal particles.

To reach this aim the following objectives are set:

- Determine crack extent, nature and placement in large coal particles from different South African origins;

- Determine the influence of particle size (5 to 30 mm) on the primary fragmentation of large spherical South African coal particles;

- Determine the influence of temperature (400 to 900 °C) on the primary fragmentation of large South African coal particles;

- Determine the influence of coal origin on the primary fragmentation of large coal particles. The PRN values, volatile matter, swelling indices and vitrinite contents should be varied while the ash yields should be kept nearly constant; and

- Determine the relationship between temperature, particle size, coal origin and fragmentation through determining the critical particle diameters at different temperatures for particles with different PRN values.

1.5 RELEVANCE OF RESEARCH

Large particles find their application in fixed-bed gasifiers. The only significant research that has been done on the fragmentation of South African coal particles, in fixed-bed gasifiers, is that from Bunt & Waanders (2008:2856-2865). As stated previously: this study will elaborate on this research by investigating crack extent, nature and placement and examining the influence of and relationship between different variables and fragmentation.

- ***Extent, nature and placement of fractures***

  With this objective the intention is to predict where cracks will form in a particle and how these cracks will then propagate due to thermal and volatile release stresses respectively. This information is important seeing that once some sort of repeated crack network pattern can be seen it would then be easy to predict how particles will fragment time and time again. Paprika *et al.* (2013:5488-5494) then also used this type of data data to establish a model to predict fragmentation (particle size distribution) in a fluidized bed. When comparing their model results with actual experimental results a very small error between the two was found. At the end of the day the information gathered on crack extent, nature and placement in this dissertation must be able to serve as building blocks to establish a model similar to that of Paprika *et al.* (2013:5488-5494) to predict primary fragmentation in a fixed-bed gasifier. This model can then be used in kinetic studies and fixed-bed gasification modelling.

- ***Factors influencing primary fragmentation***

With this objective it is important to find a relationship between fragmentation, particle size, coal type and temperature. A similar approach as that of Dakič *et al.* (1989:911-916) will be followed in which coal type is represented by its PRN and fragmentation is represented by the critical diameter. A critical diameter for each PRN will be obtained to see whether or not a relationship between these quantities for South African coal exists. The influence of temperature on this relationship will also be investigated. At the end of the day it is hoped that the critical diameter can be obtained, for any type of South African coal, heated to any temperature, by using this relationship. Once the critical diameter is known it can be used to optimize e.g. a fixed-bed gasification process by adapting the feed particle size distribution to the process so that fragmentation can be limited.

1.6 SCOPE & STUDY OUTLINE

To study the extent and nature of primary fragmentation on large coal particles a horizontal tube furnace was pre-heated to 400, 600 and 900 °C respectively. Particles with sizes of 10, 15, 20, 25 and 30 mm were placed in the pre-heated furnace (inert conditions) until drying and devolatilisation was completed. Low as well as high volatile matter samples with different swelling numbers were tested. The breakage indices and critical particle diameters were determined to quantify breakage while Micro-focus X-ray tomography was used to make qualitative observations regarding crack extent, nature and placement.

The research, experimental plan, results and conclusions were presented in a systematically manner throughout the rest of this dissertation as indicated below:

- ***Chapter 2: Literature Review***

In this chapter crack extent, nature and placement, due to thermal stresses and volatile release stresses, were discussed. Thereafter the factors influencing fragmentation were viewed critically. The relationship between PRN and critical diameter as proposed by Dakič *et al.* (1989:911-916) was discussed in depth;

- ***Chapter 3: Experimental Methodology***

In this chapter experimental aspects were the coal origin, coal preparation and coal characterisation techniques, as well as the experimental equipment, experimental methodology and experimental data analyses for the fragmentation experiments;

- ***Chapter 4: Coal Characterisation Results & Discussion***

The characterisation analyses that were carried out on the coal samples are proximate, calorific value (CV), Mercury Intrusion Porosimetry (MIP), equilibrium moisture (air-dried samples exposed to 96-97% relative humidity and 30 °C), crucible swelling number (CSN), Roga index (RI), density, as well as petrographic analyses. In Chapter 4, the results obtained from these analyses were given and discussed in detail;

- ***Chapter 5: Fragmentation Results & Discussion***

This chapter forms the backbone of the dissertation. Crack extent, nature and placement results obtained from the Micro-focus X-ray tomography scans were discussed and compared to previous research. The relationship between critical particle diameter and PRN were given and compared to that from Dakič *et al.* (1989:911-916) and lastly the influence of different factors on the primary fragmentation of large coal particles were discussed; and

- ***Chapter 6: Conclusion & Recommendations***

In the last chapter the dissertation was summarised. Recommendations to improve the study in the future were given.

CHAPTER 2: LITERATURE REVIEW

Primary fragmentation of coal can be defined as the cleavage of a particle into two or more parts when rapidly subjected to high temperatures during drying and pyrolysis/devolatilisation (Bunt & Waanders, 2008:2857; Kijo-Kleczkowska, 2012:81; Smith & Hashemi, 2010:284; Sreekanth, 2014:503). In this chapter a review on primary fragmentation literature is given. The focus is on the causes of breakage and on factors influencing the fragmentation of coal. Case studies are also provided at the end of the chapter.

2.1 CAUSES OF PRIMARY FRAGMENTATION

Two causes, namely thermal stresses and volatile release stresses, explain the primary fragmentation of coal particles. These two causes, along with typical crack extent, nature and placement data, are discussed in detail. Elevated temperatures in these sections refer to temperatures high enough for volatiles to start escaping coal particles.

2.1.1 THERMAL STRESSES

Fragmentation due to thermal stresses is caused by the sudden exposure of a coal particle to elevated temperatures. The outer core of the particle is heated rapidly through radiation and convection, while the rest of the particle is heated more slowly through conduction. The temperature gradients caused by this will induce thermal stresses across the particle (Dacombe *et al.,* 1999:1853). These thermal stresses initiate crack formation and crack propagation in a particle, which, if pushed past its failure point, will ultimately lead to fragmentation. Dacombe *et al.* (1999:1853-1856) examined this thermal stress theory thoroughly through a detailed model predicting the radial and tangential stress components (triggered by temperature gradients) throughout a spherical particle volume.

2.1.2 VOLATILE RELEASE STRESSES

Sudden exposure of a coal particle to elevated temperatures will lead to a sudden generation and eruption of released volatiles. The developing pore structure will either accommodate this rapid release rate or cause a pressure build-up of volatiles in the pore network. It is this pressure build-up of volatiles that sources fragmentation. Dakič *et al.* (1989:911-916) investigated the volatile release stresses by determining the relationship between the critical particle size and the ratio of volatile matter relative to porosity. This relationship forms a major part of this dissertation.

2.1.3 CRACK EXTENT, NATURE AND PLACEMENT

According to Griffith's theory, new cracks would form on already existing cracks or flaws in a particle (Kelly & Spottiswood, 1982:113). These flaws can either be natural cleats or fissures formed due to handling. Hoffman (2012:91) stated that the latter can be seen as the small and thin cracks near the edges of a particle. Kelly & Spottiswood (1982:113) and Gajewski & Kijo-Kleczkowska (2006:12) also stated that the interface between two heterogeneous points forms a weakness in the particle and cracks tend to form between these interfaces.

Chirone & Massimilla (1988:273) and Campbell *et al.* (2014:24) stated that cracks have a tendency to propagate in a direction parallel to the coal bedding planes. In Figure 2.1 it can be seen that these parallel-orientated cracks then also result in the particle splitting open, and if enough stress is applied fragmenting it into large coarse chunks. If particle size increase cracks perpendicular to the bedding planes also start to form (Chirone & Massimilla, 1988:273).

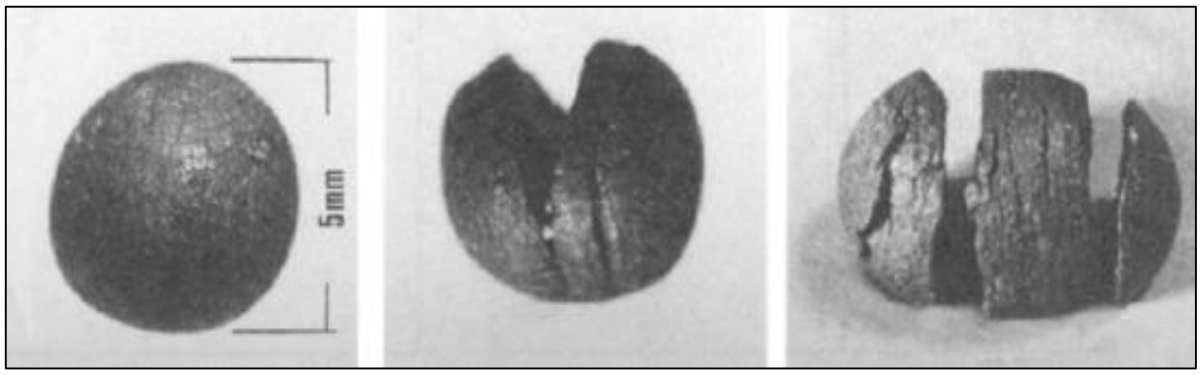

Figure 2.1: Cracks forming and propagating parallel to bedding planes in a spherical particle (Adapted from Chirone & Massimilla, 1988:273).

Chirone & Massimilla (1988:267-277) tested coal with a relatively high volatile matter implying that this type of crack propagation is due to volatile release stresses. Senneca *et al.* (2011:2937) also stated that fragmentation due to volatile release stresses produces relatively coarse fragments from the inner core of the particle. Paprika *et al.* (2007:989-990) predicted with their fragmentation model that cracks due to volatile release will initiate near the centre of the particle (where the point of highest pressure build-up is) and then propagate towards the surface of the particle in the direction of minimum pressure. For their fragmentation model Paprika *et al.* (2013:5489-5490) assumed that cracks due to volatile release will propagate from the inner zone of a particle along its radius towards either the particle surface or any empty cracks. Cracks merge with each other and cause the particle to fragment into coarse pieces (Paprika *et al.,* 2013:5489-5490).

Consider Figure 2.2. When examining fragmentation due to thermal stresses Senneca *et al.* (2010a:3) and Paprika *et al.* (2013:5489) showed that thermal stresses are dominant in the outer core of a coal particle and are mostly tensile of nature in the tangential direction. The outer core of a particle will thus fracture into numerous small pieces, while the inner core will still be partially intact (Senneca *et al.,* 2011:2937). This is known as exfoliation. It can also be seen that the time to reach equilibrium between the surface and a random point (equal distance between centre and surface) in the particle is much slower than between this point and the centre. The thermal stresses are thus more dominant in the outer core as stated previously.

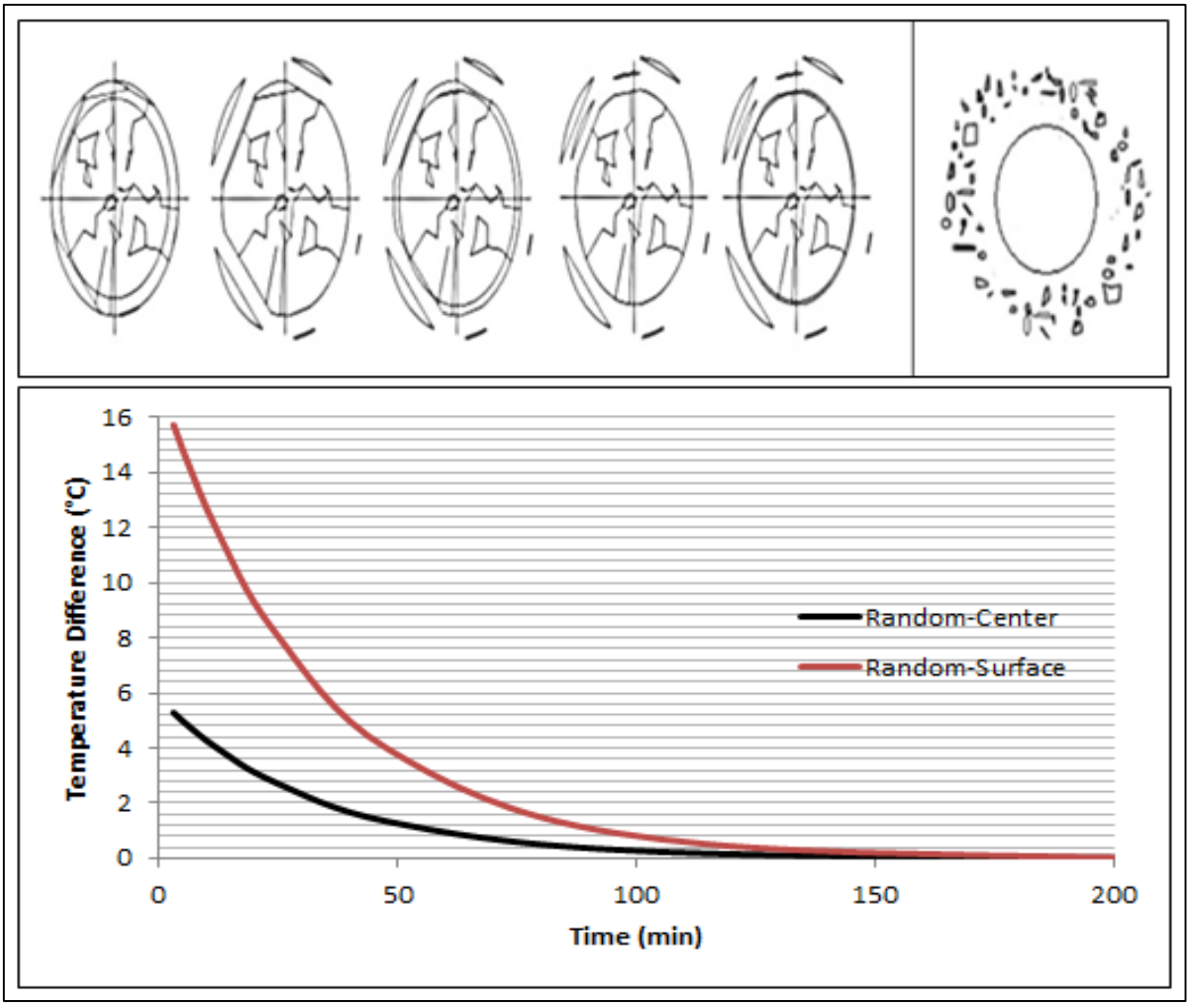

Figure 2.2: Exfoliation fragments forming from the outer core of a particle (above) and heat transfer predictions showing temperature gradients across a particle (below) (Adapted from Paprika *et al.*, 2013:5489 & Senneca *et al.*, 2013:285).

According to Senneca *et al.* (2011:2936) low volatile samples (such as anthracite and graphite) are more prone to undergo fragmentation owing to thermal stresses due to their rigid structures and high thermal conductivities. Cui *et al.* (2015:A) then also stated that for

their anthracite sample exfoliation was dominant, while for their bituminous and lignite samples coarser fragments formed.

2.2 Factors Influencing Primary Fragmentation

Factors influencing fragmentation include particle size, heating rate, bed temperature, reactor pressure and coal type (Dacombe *et al.,* 1999; Senneca *et al.,* 2011:2391-2938). The volatile matter and surface-volume ratio of a coal particle changes with a change in particle size and this is therefore a factor that is important and is discussed in more detail below (Tian, 2011:9-10). The higher the heating rate the more likely it is that fragmentation (due to thermal stresses) will occur (Badenhorst, 2013:23-24). In a fixed-bed gasifier, however, the heating rate cannot be controlled. The particles are shocked to the desired temperature by being dropped into the reactor. This factor will thus not be investigated in this study. Bed temperature is another factor that is discussed more in detail below. The temperature will affect the rate of heat transfer and therefore also the rate of devolatilisation (Sasongko & Stubington, 1996: 3913). Van Dyk (2001:247) and Senneca *et al.* (2013:2937) both tested the influence of reactor pressure on fragmentation. Although both studies found that pressure had an influence on fragmentation it was decided not to test this due to unavailability of high pressure equipment. Lastly an important factor influencing fragmentation is the coal rank. The coal rank is investigated in this study with the focus on properties affecting volatile release stresses.

2.2.1 Particle Size

In Figure 2.3 the change in centre temperature with time is given for different sized coal particles (see Appendix B for more on the construction of the figure). The time it takes for a small particle's centre to reach equilibrium temperature with its surroundings (900 °C in the example's case) is much smaller than that of a large particle. Fragmentation due to a thermal shock would thus be more severe in large coal particles assuming it is spherical.

In Figure 2.4 the centre pressure, due to volatile release, versus time is given for different size particles. When considering the influence of the volatile release stresses on the fragmentation of different sized particles Paprika *et al.* (2007:988) modelled that the increase and decrease in volatile pressure for smaller particles are rapid, while for larger particles this process takes longer. Fragmentation due to volatile release stresses will thus be more severe in larger particles than smaller particles.

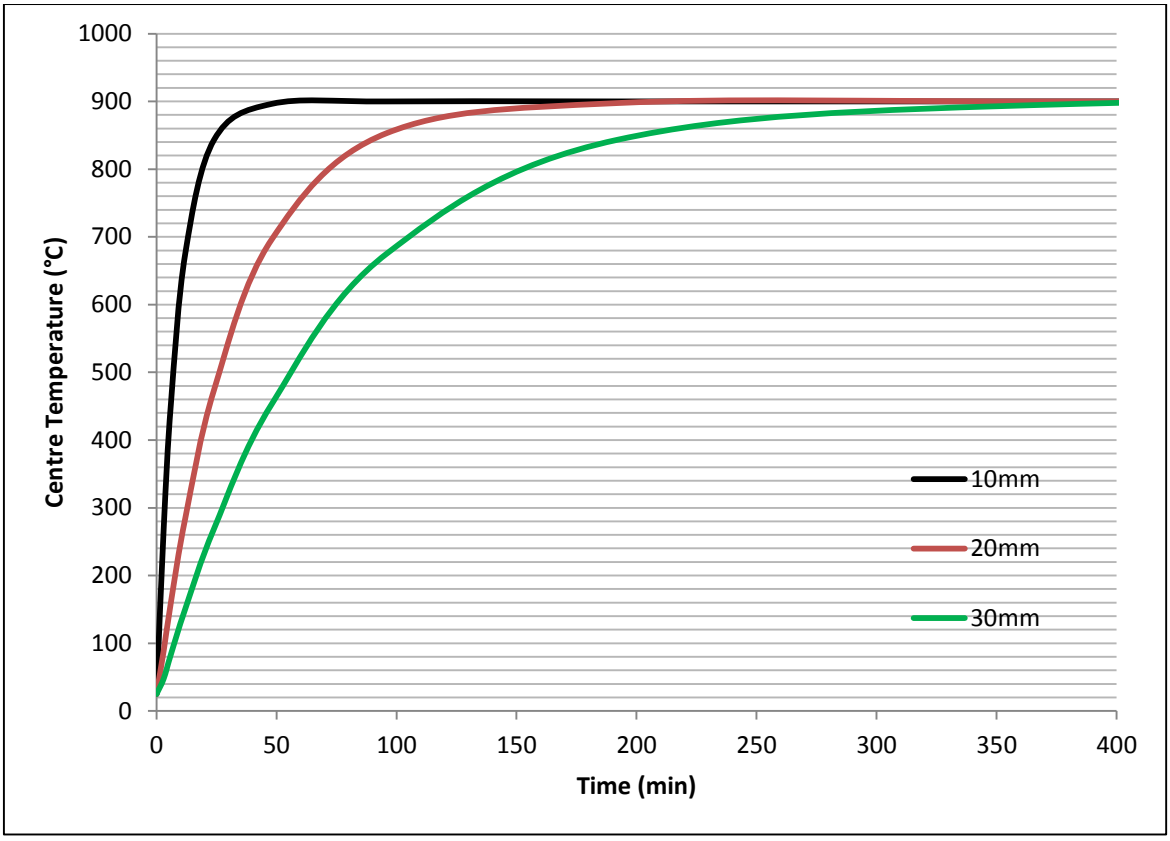

Figure 2.3: Heating times for different size, high volatile particles immersed into hot (900 °C) reactor.

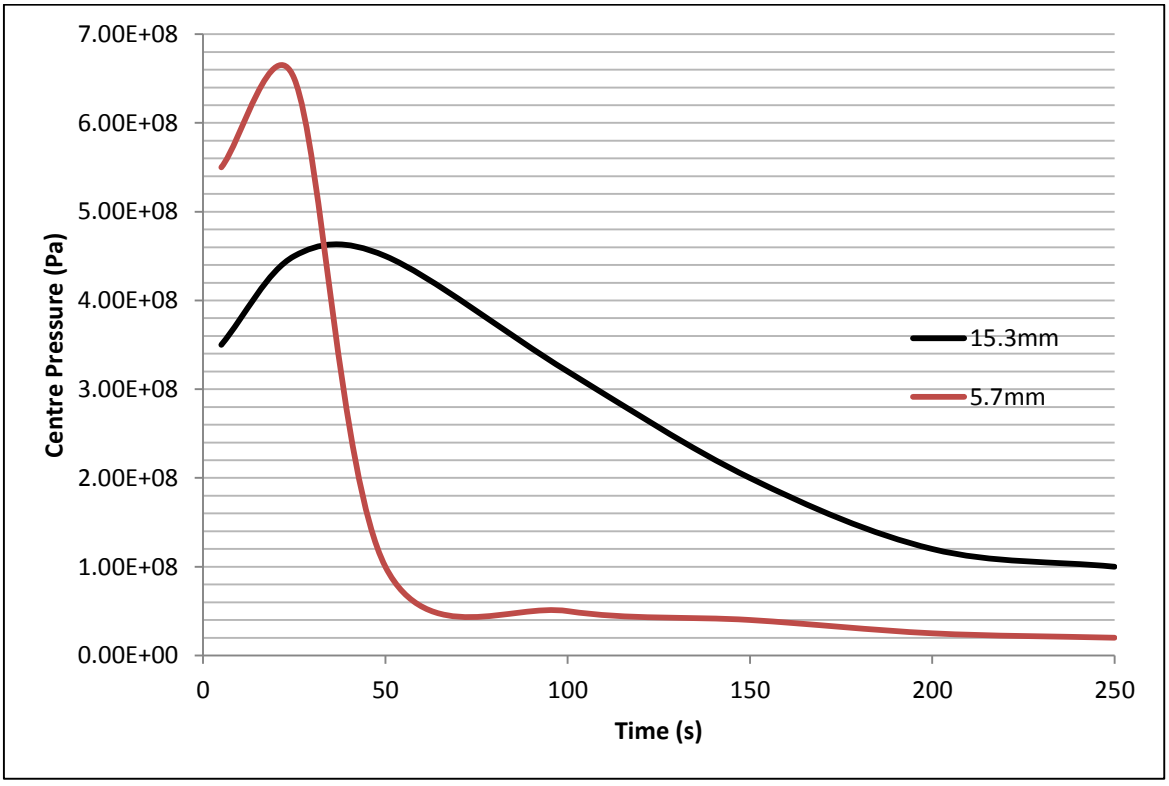

Figure 2.4: Volatile pressure build-up (centre of particle) over time for different size Kolubra particles heated to 600 °C (Adapted from Paprika *et al.*, 2007:989).

Coetzee (2011:47) stated that larger cracks are formed in large coal particles than in small coal particles. This can be because larger particles have more defects and heterogeneous boundaries, which weaken their strength and enhance fragmentation (Sreekanth *et al.,* 2008:96).

2.2.2 COAL CHARACTERISTICS

Coal characteristics influencing the primary fragmentation of large coal particles include (but are not limited to) volatile matter and porosity, moisture and ash yields, swelling behaviour and maceral composition. These characteristics are discussed separately. Other factors that can also have an influence are coal hardness, tensile strength, elastic properties and thermal properties. It was decided not to test these properties due to unavailability of testing equipment and also because these properties describe fragmentation due to thermal stresses while fragmentation due to a volatile pressure build-up is more the focus of this dissertation.

2.2.2.1 Volatile Matter & Porosity

The ratio between a particle's volatile matter and its porosity (PRN) plays a role in the fragmentation of that particle. A low PRN corresponds to a large porosity (relative to volatile matter) leaving enough space for the volatiles to escape, while a high PRN corresponds to a low porosity causing volatiles to build-up in the particle (Dakič *et al.,* 1989:915). Overall Kosowska-Galachowska and Luckos (2010:334) predicted that the combined effect of small porosity and high volatile matter causes intensive fragmentation.

Several researchers stated that the fragments produced from a coal with high volatile matter are hemispherical and inner cenosphere in shape due to devolatilisation (Zhang *et al.,* 2002:1838). This however is not fragmentation but rather thermoplastic behaviour due to a high heating rate. Dacombe *et al.* (1999:1850) stated that a peak exists in volatile matter (which is about 20% d.a.f) where the fragmentation is most severe. Before this peak value, fragmentation gradually increased and after this peak value fragmentation gradually decreased. Dacombe *et al.* (1999:1850) ascribed this peak value to the relationship between a particle's volatile matter and its compressive strength. Another reason for this peak value can be that samples above this value undergo swelling that is able to relieve internal pressure build-up and thus lower or prevent fragmentation.

Careful consideration should be implemented when investigating the influence of porosity. The International Union of Pure and Applied Chemistry (IUPAC) standard for porosity indicates that three classes of pore sizes can be identified – macropores, mesopores and micropores. In Table 2.1 information on these three classes are given as retrieved from

Laubach *et al.* (1998:175); Mandal *et al.* (2004:908) and Mazumder *et al.* (2006:205). From the table it is clear that both meso and macropores are responsible for the permeability of volatile gases. The volatile matter will travel through these pores rather than through the micropores. The volatile pressure build-up will thus depend on the volume percentages of the meso and macropores. The shape of these pores can also influence fragmentation. One should think that ink shape pores will enhance fragmentation since it prevents volatiles to escape easily while a more open pore structure will limit fragmentation.

Table 2.1: Comparison of pore size range and pore function for different types of pores in a coal particle.

Pore type	Pore size (nm)	Function
Micropores	<2	Storage space of volatile matter
Mesopores	2-50	Permeability of volatile gases
Macropores	>50	Fractures/cracks in particle
		Small % of total porosity
		Permeability of volatile gases

2.2.2.2 Moisture & Ash Yield

According to Van Dyk *et al.* (2001:6) it was estimated in a previous study (by the same authors) that the combined effect of surface and inherent moisture contributes to approximately 75% of all fragmentation in coal particles. Bunt (2006:132) also agreed that a correlation between moisture content and thermal fragmentation exists. According to Dacombe *et al.* (1999:1850), however, fragmentation for coal particles differed completely for different moisture contents and no correlation can be made. However, this opinion was formed by considering low moisture content coal. Beukman (2009:46) then stated that lignite coal with a high moisture content produced large cracks and a collapse in structure upon heating. In an experiment conducted by Chirone *et al.* (2010:4) it was found that, if bituminous coal is wetted, the fragmentation severity increases while, if anthracite is wetted, the fragmentation severity stays the same. It can thus be concluded that coal with high moisture contents will show some sort of relationship between moisture content and fragmentation while no relationship exists for low moisture coal.

When examining the influence of ash yield on the primary fragmentation behaviour of coal samples Dacombe *et al.* (1999:1859) stated that fragmentation increases with an increase in ash yield. This is because the ash yield in a coal particle relates to the mineral content in the particle and, as the ash yield increases, the mineral-coal interfaces increase producing weak spots in the particle, thus lowering the strength of the particle. Van der Merwe (2010b:66)

stated that coal particles with high densities (1600 – 2000 g/m^3), and thus high ash yields, are more prone to primary fragmentation than low-density particles due to their denser pore network structure. Consequently, pressure build-up of volatile matter is more severe in particles with a high density leading to extensive fragmentation. Cui *et al.* (2009:114) contradict these observations. They investigated the primary fragmentation of oil shale and stated that the oil shale's high ash yield and its laminated structure gives the particle a strong skeleton and fragmentation is thus less for high ash yield samples than low ash yield samples.

2.2.2.3 Swelling

The extent to which coal swell is also important since coal with a high swelling extent would be able to relieve internal pressure and prevent fragmentation (Stubington & Linjewile, 1989:159). Contradicting this is the fact that coal with a high swelling extent usually has a cenosphere type of char structure with thin and weak walls that actually facilitates fragmentation resulting in the possibility that coal with a high swelling extent will fragment more readily than one with a low swelling extent (Senneca *et al.,* 2011:2937). Boëlle *et al.* (2002:13) also stated that coal's ability to form a plastic stage during heat-up (due to swelling) is not able to release the inner stresses and fragmentation still occurs. They stated, however, that the spherical fragments produced are due to this plasticity behaviour (Boëlle *et al.,* 2002:13). Opposed to swelling, is shrinkage of a particle. Wood particles are very prone to shrinkage and this factor is then the most important contributor to fragmentation in wood particles (Sreekanth *et al.,* 2008:89).

An important factor currently not yet investigated fully is the influence that the type and concentration of the different volatile gases, in different particles, have on the fragmentation behaviour of coal. Volatile gases include hydrogen, methane, ethane, higher hydrocarbons, carbon monoxide, carbon dioxide and chemically bound water (Dakič *et al.,* 1989:912). Water, carbon monoxide and carbon dioxide escape the particle first at approximately 100 to 200 °C (Dakič *et al.,* 1989:912; Felder & Rousseau, 2005:644-649). The light hydrocarbons then come off and behave as gasses while the heavy hydrocarbons, which come thereafter, show liquid or plastic behaviour (Dakič *et al.,* 1989:912). The heavy hydrocarbons make the structure of a coal particle less brittle and it is more likely that the particle will swell and not fragment if many heavy hydrocarbons are created in the coal particle (Dakič *et al.,* 1989:912). Fragmentation also occurs if the volatiles trying to escape from a coal particle are restricted by low porosity and high volatile viscosity (Sasongko & Stubington, 1996:3916).

2.2.2.4 Petrography

Chen *et al.* (1994:137) and Stanmore *et al.* (1996:3272) stated that the brittle nature of vitrinite enhances fragmentation while fusinite limits it. The fissures that form in the vitrinite bands upon heating can be ascribed to thermal stresses and, in some instances; these fissures are actually relieving pressure build-up of volatiles instead of enhancing fragmentation (Stanmore *et al.,* 1996:3272). Campbell *et al.* (2014:24) observed some parallel cracks in and on the boundary of vitrinite rich layers. Kelly & Spottiswood (1982:113), Gajewski & Kijo-Kleczkowska (2006:12) and Tian (2011:84) also stated that the interface between two heterogeneous points sources a weakness in the coal particle and cracks tend to initiate from this interface, and breakage occurs here. Tian (2011:84) also stated that fragmentation increases with mean vitrinite reflectance value. Anthracite will therefore fragment more than lower rank samples such as bituminous.

2.2.3 TEMPERATURE

Consider Figures 2.5 and 2.6 (see Appendix B for more on the construction). From Figure 2.5 it is clear that the heating time for a particle exposed to high temperatures is longer than at low temperatures. Thermal stresses and fragmentation will thus be more severe at high temperatures.

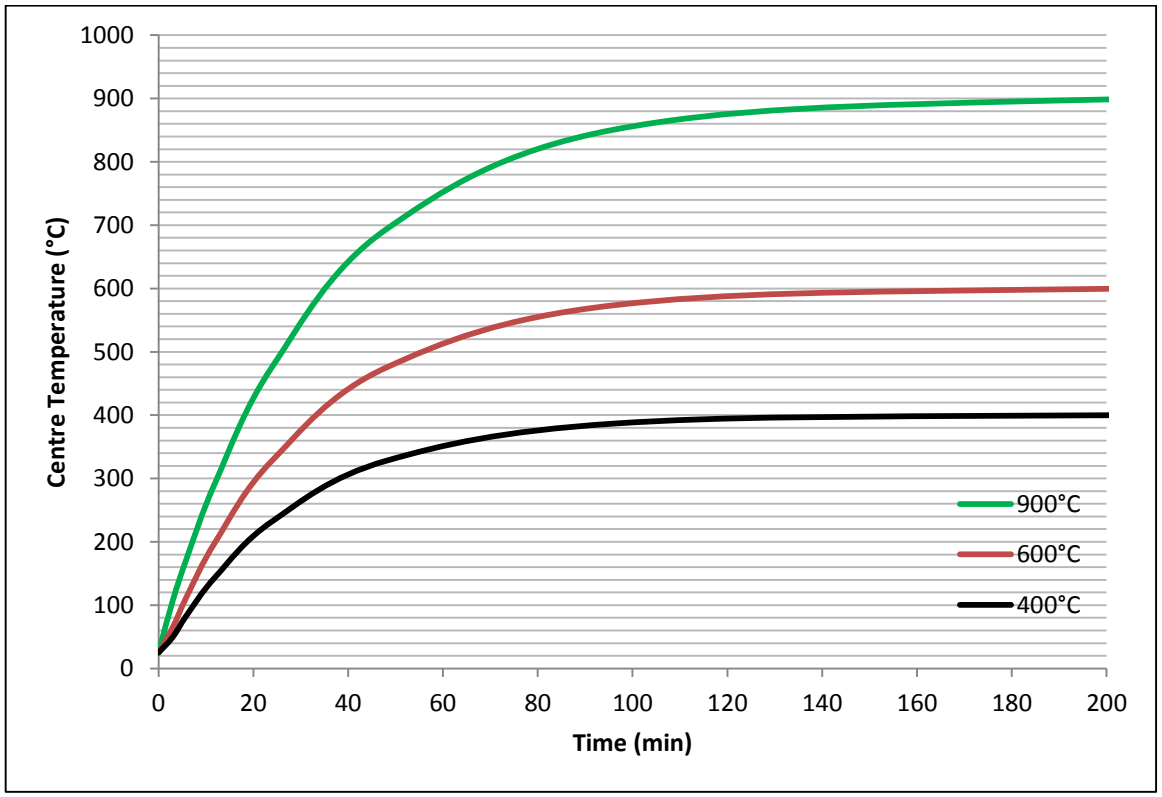

Figure 2.5: Heating times to reach different end temperatures for high volatile, 20 mm particles.

In Figure 2.6 it can be seen that a higher temperature results in a greater centre pressure and thus more fragmentation. The devolatilisation rate constant increases and the devolatilisation time decreases with increasing temperature (Tian, 2011:13). On its turn, the devolatilisation rate increases causing a higher centre pressure and ultimately fragmentation (Cui *et al.,* 2009:118; Kosowska-Galachowska & Luckos, 2010:332).

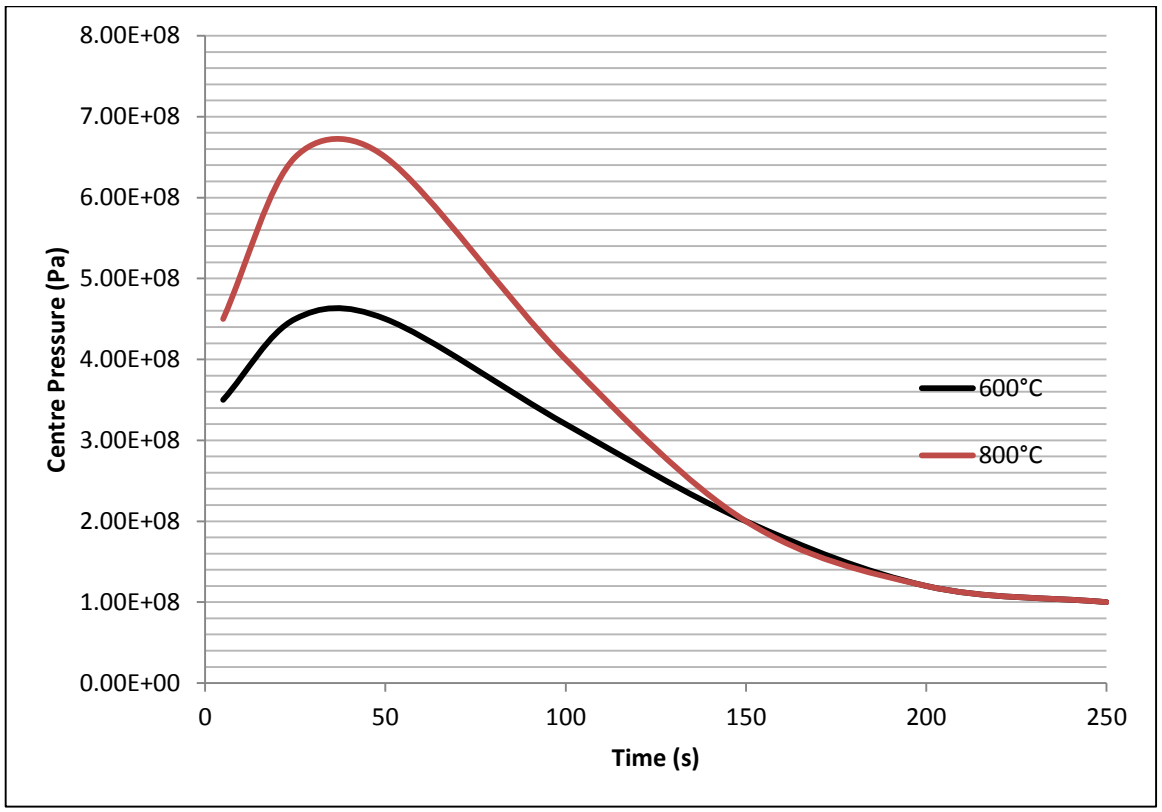

Figure 2.6: Volatile pressure build-up (particle centre) with time for a 15.3 mm particle exposed to different temperatures (Adapted from Paprika *et al.,* 2007:989).

There is however a contradiction to the statement that higher temperatures lead to fragmentation intensification. If a coal particle is heated to above its ash melting point the minerals would melt, partially relieving internal stresses, and the severity of fragmentation will reduce (Senneca *et al.,* 2010a:2; Senneca *et al.,* 2011:2937). It will also impact the thermoplastic transformations.

Microscopically Mostert (2010:60-61) stated that end-temperature had absolutely no effect on the amount and a minimal effect on the size of cracks that formed in a particle when heated. This contradicts Badenhorst's (2013:25) and Coetzee's (2011:47) viewpoint that stated that higher end-temperatures lead to an increase in the number of fractures formed. A possible explanation for this contradiction can be due to the difference in heating rate: Mostert (2010:60-61) gradually increased temperature with time, while Coetzee (2011:47)

placed particles in a pre-heated furnace. The heating rate of Badenhorst (2013:23) was also much higher than that of Mostert (2010:60-61).

2.2.4 Relationship between Size, Temperature, Coal Type & Fragmentation

In 1989 Dakič *et al.* (1989:911-916) developed a very convenient relationship to predict the primary fragmentation of coal as illustrated in Figure 2.7. From this relationship, the critical diameter (largest diameter for which there is no notable fragmentation) can be determined by only knowing the PRN of the coal sample.

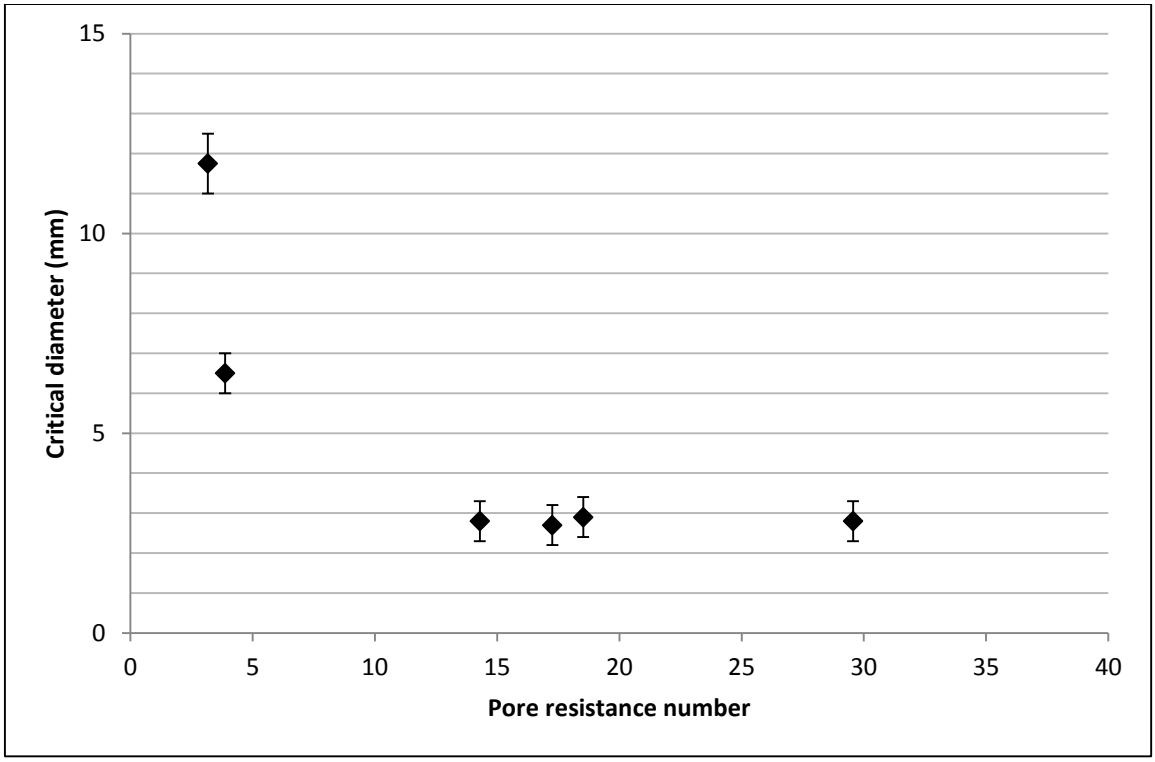

Figure 2.7: Pore resistance number versus critical diameter for high volatile samples heated to 850 °C (Adapted from Dakič *et al.*, 1989:916).

The PRN is defined as the ratio between the volatile matter and equilibrium moisture of a coal particle as indicated in Equation 2.1 (Dakič *et al.,* 1989:912).

$$PRN = \frac{Volatile\ Matter}{Equilibrium\ Moisture} \qquad \textbf{\textit{Equation 2.1}}$$

Volatile matter in wt % equilibrium moisture basis

Equilibrium moisture in wt.% equilibrium moisture basis

PRN is dimensionless

According to Dakič *et al.* (1989:912) and Thomas & Damberger (1976:25) the equilibrium moisture content is a good approximation for porosity and the PRN is thus an indication of the amount of volatile matter present relative to the amount of pore space available through which they can escape. The equilibrium moisture refers to the moisture holding capacity of a sample at 30 °C and 96 to 97% relative humidity as given in the American Society for Testing and Materials (ASTM) standard D-1412 (Speight, 2005:9).

From Figure 2.7 it can be seen that the particle size, as well as the coal characteristics, are influential on the primary fragmentation. Oka (2004:234) showed that temperature will also affect the critical diameter and should be considered in this relationship.

2.2.4.1 Particle Size

From Figure 2.7 it can be seen that for the study conducted by Dakič *et al.* (1989:916) the critical diameters ranged between 2 and 12 mm (850 °C and high volatile samples). Chirone & Massimilla (1988:274) stated that in their study particles larger than 10 mm fragmented, while those smaller than 3 mm rarely fragmented (850 °C and South African bituminous). The critical diameters for their study thus lay between 3 and 10 mm. Peeler & Poynton (1992:429) stated that for their study the critical diameters lay between 13 and 19 mm (900 °C). Coetzee (2011:46-48) and Bunt & Waanders (2008:2856) stated however that for their respective studies the thermal stable size was 25 mm (900 °C and South African bituminous coal). The difference in critical diameters for the different studies can be due to different coal samples used, as well as to different thermal conditions. The critical diameter is important for this study since one of the study's aims is to determine the relationship between it and PRN.

Previous researchers such as Zhang *et al.* (2002:1838) and Kosowska-Galachowska & Luckos (2010:332) showed that an increase in particle size leads to an increase in fragmentation. A sudden increase in fragmentation can be seen from 4 mm onwards for Zhang *et al.* (2002:1838) (size range tested: 0.63-7 mm) and from 19 mm onwards for Peeler & Poynton (1992:427) (size range tested: 1.41-28.9 mm). This suggests that there is also a size (other than the critical size) where fragmentation starts to increase drastically. Zhang *et al.* (2002:1838-1839) tested Chinese coal heated to between 500 and 900 °C while Peeler & Poynton (1992: 426) tested high as well as low volatile samples heated to 900 °C.

2.2.4.2 Coal Characteristics

The ratio between a particle's volatile matter and its porosity (PRN) plays a role in the fragmentation of that particle as can be seen from Figure 2.7. A low PRN corresponds to a large porosity (relative to volatile matter) leaving enough space for the volatiles to escape,

while a high PRN corresponds to a low porosity causing volatiles to build-up in the particle (Dakič *et al.,* 1989:915). Overall Kosowska-Galachowska and Luckos (2010:334) predicted that the combined effect of small porosity and high volatile matter causes intensive fragmentation.

Bituminous coal samples usually have small porosities and high volatile matter (Morcote *et al.,* 2010:E227). Their PRN values will thus be high and therefore their critical diameters are small. Fragmentation due to volatile release stresses is therefore dominant in these samples. Low volatile matter coals, such as anthracite, on the other hand are known for their large porosities and low volatile matter. These samples would therefore have low PRN values and therefor large critical diameters. Fragmentation due to volatile pressure build-up will thus not be as severe in anthracite samples as in bituminous samples. Thermal stresses, however, are quite severe in anthracite (low volatile) samples since these samples are renowned for their high thermal conductivities, fragility and organized structure (Senneca *et al.,* 2009:569; Senneca *et al.,* 2011:2936). This can also be the reason why He *et al.* (2007:159) stated that for their anthracite samples fragmentation occurred more readily with decreasing PRN than increasing PRN. Gajewski *et al.* (2003:125) also determined that the probability that anthracite will not fragment at all due to its low volatile matter is high.

Thermal stresses will thus be dominant in low volatile samples, such as anthracite, while fragmentation due to a pressure build-up will be dominant in high volatile samples, such as bituminous coal. From this it can be concluded or assumed that the low volatile samples will form a multitude of fines upon heating (Senneca *et al.,* 2011:2936). High volatile coal would however show more large and coarse fragments than small fragments.

2.2.4.3 Temperature

Sreekanth (2014:503-504) tested primary fragmentation in wood particles with an PRN of 6.7 and found that for particles heated to 750 °C the critical diameter is 15 mm, while at higher temperatures the critical diameter where smaller than 10 mm. In two separate studies conducted by Coetzee (2011:46-48) and Van der Merwe (2010a:68-69) respectively, South African bituminous coal was used but heating conditions differed with 50 ºC. The result was a 10 mm difference in critical diameter between these two studies. In 2009 Liu *et al.* (2009:513) attained a relationship (by using a forecasting model) relating temperature and critical diameter for quartz particles. If it is assumed that coal particles will follow the same trend it can be concluded that the larger the temperature, the smaller the critical diameter will be and the more intensive fragmentation will be (Cui *et al.,* 2015:A; He *et al.,* 2007:161 & Van Dyk, 2001:247).

2.3 CASE STUDIES

In Table 2.2 different large coal primary fragmentation case studies are given. The coal types, temperatures, particle sizes and experimental reactors used for each study are shown, as well as the main conclusions drawn from these studies. When looking at small particles research papers by Senneca *et al.* (2011:2931-2938); Senneca *et al.* (2010a:1-6); Cui *et al.* (2015:A-K) and Senneca *et al.* (2010b:366-372) can be consulted.

Table 2.2: Large particle primary fragmentation case studies from literature.

Source	Temperature (°C)	Fuel origin	Particle size (mm)	Experimental reactor	Conclusions
Ammendola *et al.* (2010)	800	Pelletised coal-wood	6×20	BFB with basket, N_2 gas	Mechanical strength limits fragmentation
Bunt & Waanders (2008)	Gasifier turn-out sample	South African bituminous	>25, 25-6.3, <6.3	FBDB	Critical diameter of 25 mm
Chirone & Massimilla (1988)	850	Non-swelling South African bituminous	1-15	FB with basket, N_2 or N_2/O_2 mixture gas	Cracks form parallel to bedding planes. Critical diameters between 3 and 10 mm
Dacombe *et al.* (1999)	Varied with furnace length	Anthracite and bituminous	1-4	DTF	Maximum fragmentation at ~20% d.a.f volatile matter
Dakič *et al.* (1989)	850	High volatile coal	2-15	FB, N_2 and/or O_2 gas	Decreasing exponential relationship between PRN and critical diameter

Source	Temperature (°C)	Fuel origin	Particle size	Experimental reactor	Conclusions
Paprika *et al.* (2015)	600 , 800, 850	Lignite	4-16	FB, N_2 gas	Large, coarse fragments
Senneca & Chirone (2009)	800-1600	Wood chips, anthracite and South African bituminous	4×4×2	HSR, He gas	Anthracite fragments the most due to thermal stresses
Peeler & Poynton (1992)	900	High and low volatile	1.41-28.9	EHF, N_2 gas	Critical diameter 13-19 mm
Senneca *et al.* (2009)	900-1400	Anthracite and South African bituminous	1-2	HSR, N_2 gas	Wetted bituminous fragmented more than anthracite
Stanmore *et al.* (1996)	850	Semi-anthracite, high volatile bituminous, medium volatile bituminous, sub-bituminous	1.2, 2.5	FB, N_2 or O_2/N_2 mixture gas	Vitrinite content influences fragmentation; Anthracite and low volatile fragments into a multitude of pieces
Stubington & Linjewile (1988)	850	High volatile coal	5-12	Tubular, N_2 gas	Swelling reduces fragmentation
Tian (2011)	800, 900, 1000	High volatile coal	5-38	DTF, N_2 gas	Agglomeration properties reduce fragmentation; mineral matter enhances fragmentation

Source	Temperature (°C)	Fuel origin	Particle size	Experimental reactor	Conclusions
Van Dyk (2001)	100-700	South African bituminous	6.7-9.5, 9.5-13.2, 13.2-19	MF, N_2 gas	Linear increase in ergun index with temperature
Lee *et al.* (2002)	750-900	Anthracite	2-12	TB, N_2 gas	Fragmentation decreases with increase in HGI

CHAPTER 3: EXPERIMENTAL METHODOLOGY

Coal samples from five different South African coal seams were obtained, prepared, characterised and used in fragmentation experimentation. In this chapter the origin of these samples, characterisation techniques and preparation methods used, as well as the experimental equipment and analyses procedures followed, are discussed.

3.1 EXPERIMENTAL METHODOLOGY

Low and high volatile samples from five different South African coal origins were chosen based on the criteria given under the coal origin section (section 3.2). These samples were exposed to three temperatures namely a low (400 °C), medium (600 °C) and a high (900 °C) temperature. The temperatures were chosen to cover a broad thermal range. To vary the particle size 10, 15, 20, 25 and 30 mm particles were tested. These sizes can be classified as “large” when it comes to fragmentation research.

In Figure 3.1, a schematic diagram of the experimental method followed is shown. The first step in the experimental method was to select, shape, characterise and density separate the coal particles used during experimentation. A thorough discussion on this is given in sections 3.2 to 3.4.

The next step was to pre-scan certain particles on an X-Ray scanner. It was decided to scan only 10 mm particles as particles larger than this tended to fragment and it would have been difficult to post-scan and reconstruct images if this was the case. Only non-swelling samples were scanned to prevent difficulty in reconstructing pre and post-scans with each other. It was decided to scan three low volatile particles at 400, 600 and 900 °C respectively and three high volatile particles at 400, 600 and 900 °C.

A horizontal tube furnace was then pre-heated to the required temperature (400, 600 and 900 °C). Pre-heating was required since the aim was to shock the particles to the desired temperatures. The heating rate was thus not controlled. Particles were placed in a special designed sample holder and inserted into the pre-heated furnace. More than one particle could be fitted into the sample holder each time since it was designed with three separate compartments. The particles were kept in the furnace until isothermal temperatures in the particles were reached and pyrolysis was completed. Heating times to reach isothermal conditions were calculated through heat transfer principals (see Appendix B). After the required heating time the furnace was cooled (gradually to room temperature with a constant flow of nitrogen) and particles were taken out and analysed for primary fragmentation behaviour.

The samples were analysed as is, separation of fragments were not done (e.g. drop of particle to separate the fragments). Analyses included taking post-scans of particles, calculating the breakage index, photographing particles and lastly determining the critical diameter for each coal origin at each temperature. At least five repeats of each size, temperature and origin combination were conducted for statistical meaningful results. In Appendix E more on the statistical analysis of number of particles are given.

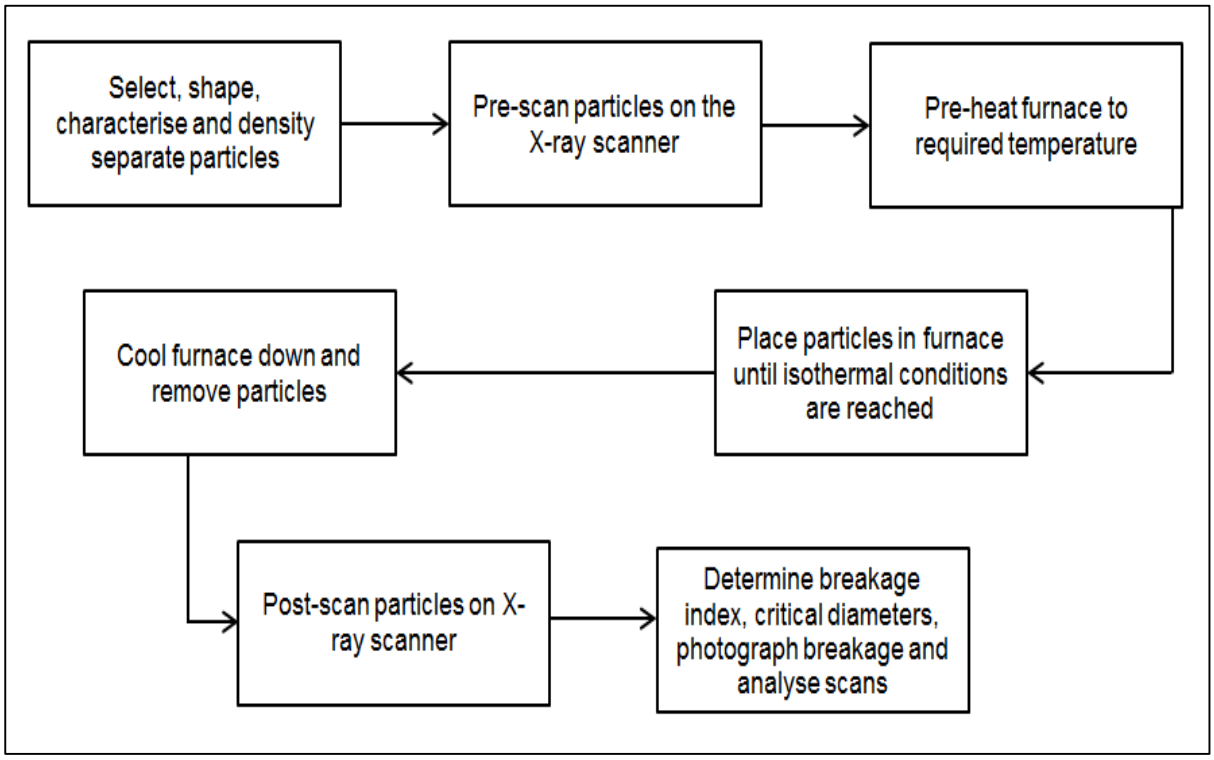

Figure 3.1: Schematic diagram of experimental methodology.

3.2 COAL ORIGIN

Five coal samples were obtained in bulk quantities from five different South African coal origins. Two of them are low volatile samples and are classified as LV1 and LV2. The rest are high volatile samples, of which one is a coking coal. The last samples would from here on out be known as HV1, HV2 and HV Coking. The high volatile samples were obtained from the Witbank and Soutpansberg coalfields respectively, while the low volatile samples were bought from different coal dealers.

When choosing the samples the criteria below were considered and Bulletin 114 by Pretorius *et al.* (2002:4-8) was consulted:

- The samples should have different PRN values;
- High and low volatile samples should be included in selection;
- Swelling coal samples should be included in selection;
- Maceral composition should be taken into account; and
- Ash yield should be kept low, and more or less the same, as far as possible

3.3 COAL PREPARATION

A 100 to 200 kg sample was acquired from each coal origin. The samples were then prepared by air-drying them on a groundsheet overnight to dry off any excess moisture. Thereafter a homogeneous representative sample from each coal origin was obtained by applying the cone-and-quarter reduction method four times, as explained by Holdich (2002:2-4) and The Southern African Coal Processing Society (2015:59-61). A riffle splitter was used to sub-divide the representative samples into smaller samples for the respective coal characterisation analyses. The remaining bulk samples were used in the fragmentation experiments. The bulk samples were sieved into size fractions so that 10, 15, 20, 25 and 30 mm particles could be handpicked easily. These handpicked particles were then shaped into spherical-like particles by using pliers and sandpaper. Minimum friction and force were applied when shaping the particles to prevent fractures forming due to handling.

In Figure 3.2, an example is given of a 25 mm particle shaped correctly. The length, width and height are all 25 mm (the diameter would thus also be more or less 25 mm) and the edges were shaped so that a somewhat spherical particle formed.

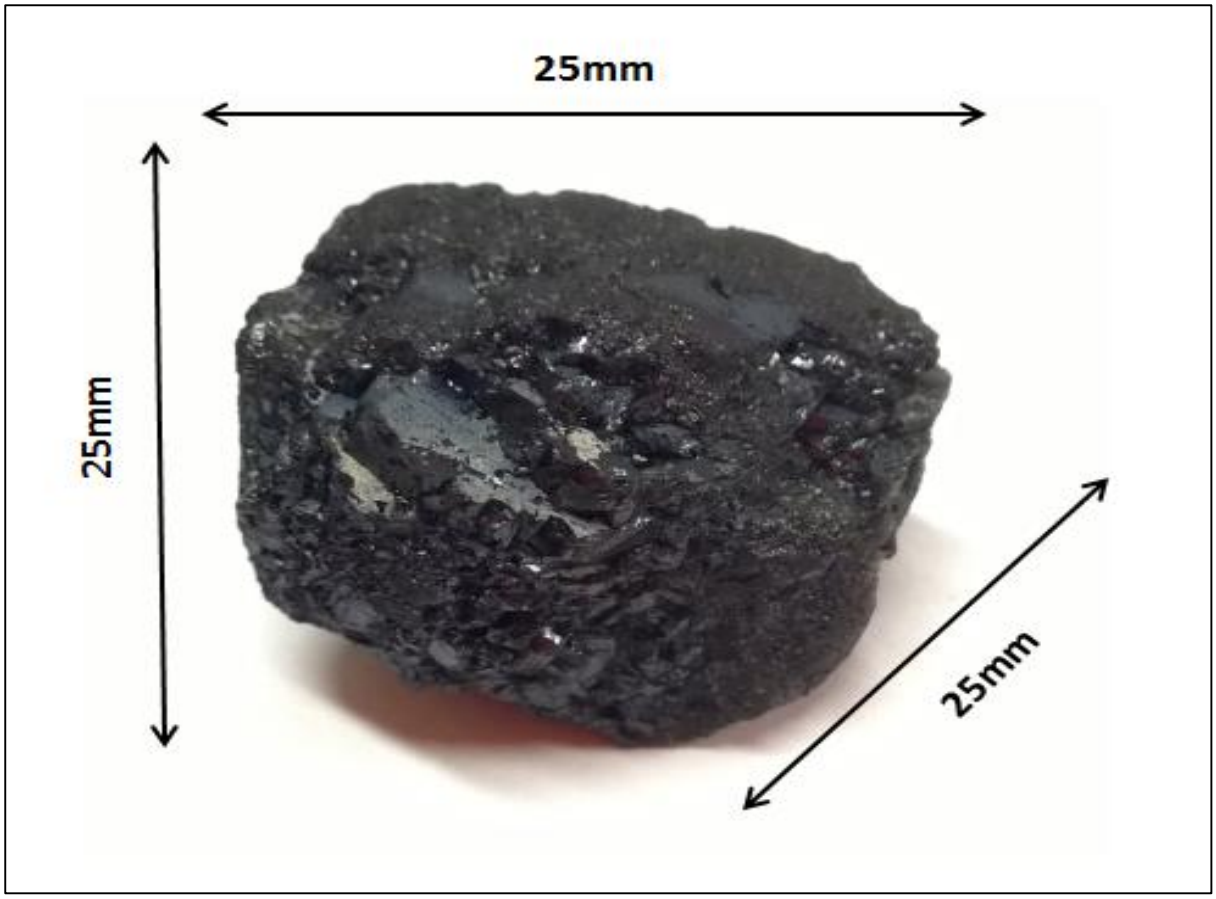

Figure 3.2: An example of a 25 mm shaped to be somewhat spherical.

Seeing that large particles were used, it was necessary to separate particles of the same coal origin to obtain particles with more or less the same mineral and microstructural properties. The mercury submersion technique was used for this purpose and is explained under the section dealing with coal characterisation.

Lastly, char samples of each coal origin were prepared at 400, 600 and 900 °C respectively in an inert, pre-heated, horizontal tube furnace (0.3 L/min nitrogen flow). The furnace was gradually cooled down to room temperature, with nitrogen still flowing through the furnace, before char samples were removed. This preparation was done to obtain the percentage volatile loss between the raw coal samples and those exposed to the different temperatures.

3.4 COAL CHARACTERISATION

As part of the coal characterisation proximate, calorific value, Mercury Intrusion Porosimetry, equilibrium moisture, Roga index, crucible swelling number, density and petrographic analyses were performed on the coal samples, while additional proximate analysis was done on the char samples.

3.4.1 PROXIMATE ANALYSIS

With the proximate analysis the weight percentages, inherent moisture, volatile matter, ash yield and fixed-carbon in the coal, as well as char (heated to 400, 600 and 900 °C respectively) samples, were determined. The samples for proximate analysis were outsourced to a third party analytical service laboratory (Bureau Veritas Testing and Inspections South Africa), which used the International Organisation for Standardisation (ISO) standards given in Table 3.1 to determine the proximate values:

Table 3.1: ISO standards used for proximate analysis.

Analysis	ISO Standard
Sample preparation	ACT-TPM-001 based on ISO 13909-4: 2001
Inherent moisture (wt.%)	ACT-TPM-010 based on ISO 11722: 1999
Ash yield (wt.%)	ACT-TPM-011 based on ISO 1171: 210
Volatile Matter (wt.%)	ACT-TPM-012 based on ISO 562:2010
Fixed carbon (wt.%)	By difference

The proximate samples were crushed to -212 μm and kept prior to analysis in a climate-controlled room operated at a temperature of 25 °C and relative humidity of 20-80%. This information was obtained from the third party analytical service to try and distinguish between moisture defined as inherent moisture and moisture defined as equilibrium moisture.

3.4.2 CALORIFIC VALUE ANALYSIS

A bomb calorimeter was used to determine the energy values of the samples. The samples were once again outsourced to a third party analytical service laboratory (Bureau Veritas Testing and Inspections South Africa) for analysis. The ISO standard they used is presented in Table 3.2.

Table 3.2: ISO standard used for calorific value analysis.

Analysis	ISO Standard
Calorific value (MJ/kg)	ACT-TPM-014 based on ISO 1928: 2009

The CV samples were crushed down to -212 μm and kept prior to analysis in a climate-controlled room operated at a temperature of 25 °C and a relative humidity of 20-80%.

3.4.3 MERCURY INTRUSION POROSIMETRY ANALYSIS

MIP analysis was conducted at the Sasol Materials Characterisation Group on a Micromeritics AutoPore IV 9500 V1.09 Mercury Porosimeter as shown in Figure 3.3. The Mercury Porosimeter was used to determine the volume percentage porosities of the different coal samples. The bulk and apparent densities could also be determined with the MIP technique.

Figure 3.3: Micromeritics AutoPore IV 9500 V1.09 Mercury Porosimeter.

MIP was used for the porosity determination above other porosity techniques due to its following advantages (León y León, 1998:343; Webb, 2001:3; Westermarck, 2000:6):

- Meso and macroporosities are determined (pore sizes through which volatiles transport); and
- Frequently used in fragmentation experiments (e.g. Dakič *et al.* (1989:912)).

There are however many disadvantages that can affect the reliability of the results. The most important disadvantage is the compression of the sample when exposed to high pressures with the result of a too large measured volume of small or medium size pores (Giesche, 2006:5; Westermarck, 2000:6). Giesche (2006:3) and Webb (2001:9) also showed that interstitial voids between packed particles might also result in a too large measurement of porosity.

For analysis a sample of 1-2 mm sized particles were used. The sample was first dried in a vacuum oven at 80 °C to remove excess moisture, prevent prolonged analysis and open up any pores blocked with moisture. The sample was then placed in a 14-0886 3 bulb volume powder penetrometer with a stem volume of 0.412 mL. The penetrometer was first connected to the low-pressure port to extract moisture and other gases from the sample's pores. The penetrometer was then placed in the high-pressure port and mercury was forced into the pores. The volume mercury forced into the pores was measured. If the pore volume exceeded 90%, or was lower than 25% of the penetrometer stem volume, the results could not be accepted as correct and the run was repeated (Van der Merwe, 2014). At least two repeats of each sample were done.

3.4.4 Equilibrium Moisture Analysis

To determine the equilibrium moisture of the coal samples the method described by Speight (2005:49) was used. The objective was to determine the moisture holding capacities of the samples at 96% relative humidity and 30 °C and relate it to the porosities of the samples to see if it is a good indication of porosity.

The first step was to insert a starting sample into the climate chamber. This starting sample consisted of 1-2 mm sized particles and about 5 g of sample was tested each time. The climate chamber (CTS C-40/100) was operated at 96% Relative Humidity and 30 °C. The samples were saturated for about 12 hours in this chamber before the new weight of the samples were taken. After this step the samples were left for 24 hours in a climate controlled room (40% Relative Humidity and 22 °C) before being weighed again (this was done to check the inherent moisture and compare it with that obtained from the proximate analysis). Lastly, the samples were dried in a moisture analyser at 105 °C. The difference before and after the moisture analyser step, and the difference between the before and after air drying step, was determined and added to give the total equilibrium moisture of the samples. For each coal sample, the equilibrium moisture analysis was repeated at least three times for statistical accurate results.

3.4.5 Crucible Swelling Number & Roga Index Analyses

The coal samples were outsourced to a third party analytical service laboratory (Bureau Veritas Testing and Inspections South Africa) for CSN and Roga index analyses. The ISO and the South African National Standard (SANS) standards used for these analyses are given in Table 3.3.

Table 3.3: ISO standard for crucible swelling number analysis and SANS standard for Roga index.

Analysis	ISO/SANS Standard
Crucible swelling number	ACT-TPM-015 based on ISO 501: 2003
Roga index	ACT-TPM-016 based on SANS 881: 2009

To determine the swelling behaviour of the samples qualitatively an in-house furnace (usually used for ash fusion temperature experiments) equipped with a video camera was used. In Figure 3.4 the Carbolite furnace, controlled with a Eurotherm 2408 controller, is shown. The video camera can be seen on the left. The coal samples were placed in the furnace which was slowly heated (in a nitrogen atmosphere) at 10 °C/min to 900 °C. Clips at every 10 °C were taken with the video camera to visualise swelling.

Figure 3.4: Carbolite furnace and camera used to obtain qualitative images of swelling.

3.4.6 Mercury Submersion Density Analysis

Because large particles were used (10, 15, 20, 25 and 30 mm), it was necessary to select particles of similar properties. This was done by assuming that similar density samples represented similar mineral contents and macrostructural properties. While this procedure seemed rudimentary, later X-ray tomographic scans supported this notion.

The mercury submersion technique was used to obtain the densities of the particles of each coal origin and, based on that, particles for use in fragmentation experiments. Mercury submersion makes use of the Archimedes principle in which the weight of displaced mercury is obtained after a particle is submerged into it.

First the coal particle's weight was taken. Thereafter a plunger was immersed in mercury and the weight was taken. Lastly, the particle was placed in the mercury and the plunger was used to push or keep the particle in the mercury (keeping it from floating) while measuring the weight. The particle's density was then determined with Equation 3.1:

$$\rho_{particle} = \rho_{Hg} \frac{w_{particle}}{w_{plunger+particle} - w_{plunger}} \qquad \textbf{Equation 3.1}$$

Density (ρ) in g/mm^3

Weight (w) in g

Once the density was known, the corresponding particle radius was calculated by using Equation 3.2:

$$r = \sqrt[3]{\frac{3w_{particle}}{4\pi\rho_{particle}}} \qquad \textbf{Equation 3.2}$$

Radius (r) in mm

To decide which particles can be used and which not, at least 30 particles (20 mm size) from each coal origin were tested. The statistical 68% empirical rule was then applied to determine the density range acceptable for each origin respectively. This rule is given in Equation 3.3:

$$\rho_{range} = \rho_{average} \pm \sigma \qquad \textbf{Equation 3.3}$$

Standard deviation (σ) in g/mm^3

The density range obtained from the 20 mm particles was used on all the particle sizes. The 10, 15, 25 and 30 mm particles were thus tested and if their densities lay in the given range, the particle was used in experimentation.

3.4.7 PETROGRAPHIC ANALYSIS

With the petrography analysis, reflectance values and maceral composition were identified for each sample. The samples for petrographic analysis were outsourced to a third party

analytical service laboratory (Bureau Veritas Testing and Inspections South Africa) which used an accredited petrography specialist. In Table 3.4 the ISO standards used for the analysis are given. The samples used were crushed to a size of -850 μm and set in an epoxy and resin mixture and ground to a polished surface necessary for the analysis. A Zeiss Axio Imager M2m and magnification of ×50 under oil immersion was used for analysis.

Table 3.4: ISO standard used for petrographic analysis.

Analysis	ISO Standard
Petrographic analysis	ACT-TPM-026 based on ISO 7404: 1994 Part 1 to 5
Maceral analysis	ISO 7404 part 3 (500 points counting)
Reflectance measurements	ISO 7404 part 5
Rank Determination	ISO 11760-Classification of Coals

3.4.8 RANK DETERMINATION

To determine the rank of the coal samples the ASTM method was used shown in Table 3.5.

Table 3.5: Rank classification method of coals by the ASTM.

Rank	Fixed carbon wt.% (dmmf)	Volatile Matter wt.% (dmmf)	Calorific value MJ/kg (mmf)
Meta-anthracite	>98	>2	...
Anthracite	92-98	2-8	...
Semi-anthracite[1]	86-92	8-14	...
Low-volatile bituminous	78-86	14-22	...
Medium-volatile bituminous	69-78	22-31	...
High-volatile A bituminous	<69	>31	>32.6[2]
High-volatile B bituminous	...	...	30.2-32.6[2]
High-volatile C bituminous	...	...	26.7-30.2
Subbituminous A	...	...	24.4-26.7
Subbituminous B	...	...	22.1-24.4
Subbituminous C	...	...	19.3-22.1
Lignite A	...	...	14.7-19.3
Lignite B	...	...	<14.7

[1]If agglomerating classify as low-volatile bituminous; [2]If fixed carbon is more than 69% do not classify based on CV

In the table fixed carbon and volatile matter are on a dry, mineral-matter free basis (dmmf) while CV is only on a mineral-matter free basis (mmf).

To determine the mineral matter (for mineral-matter-free calculations) in the samples the Parr formula was used as shown in Equation 3.4.

$$Mineral\ Matter = (1.08 \times Ash) + (0.55 \times Sulphur) \qquad \textbf{\textit{Equation 3.4}}$$

Mineral Matter in wt.% air-dried basis

Ash in wt.% air-dried basis

Sulphur in wt.% air-dried basis

3.5 EXPERIMENTAL EQUIPMENT

A horizontal tube furnace and a Micro-focus X-Ray scanner were used to test the fragmentation behaviour of the coal particles. The tube furnace was used to shock the particles thermally at different temperatures until equilibrium in the particles were reached, while the scanner was used to determine aspects regarding the crack extent, nature and placement. These two equipment pieces are now discussed separately.

3.5.1 HORIZONTAL TUBE FURNACE

In Figure 3.5 a schematic diagram of the horizontal tube furnace used for experimentation is given. Nitrogen gas (11 kg Baseline 5 supplied by African Oxygen Limited) was fed at a volumetric flow rate of 0.3 L/min to the furnace. This was to ensure an inert atmosphere in the furnace to mimic fragmentation taking place during drying and pyrolysis. The furnace was 500 mm in length with a tube diameter of 50 mm. A K-type thermocouple was used by the Rex-c100 temperature controller to control the temperature in the furnace at all times. Gas calibration data and the temperature profiles across the furnace are given and explained in Appendix A.

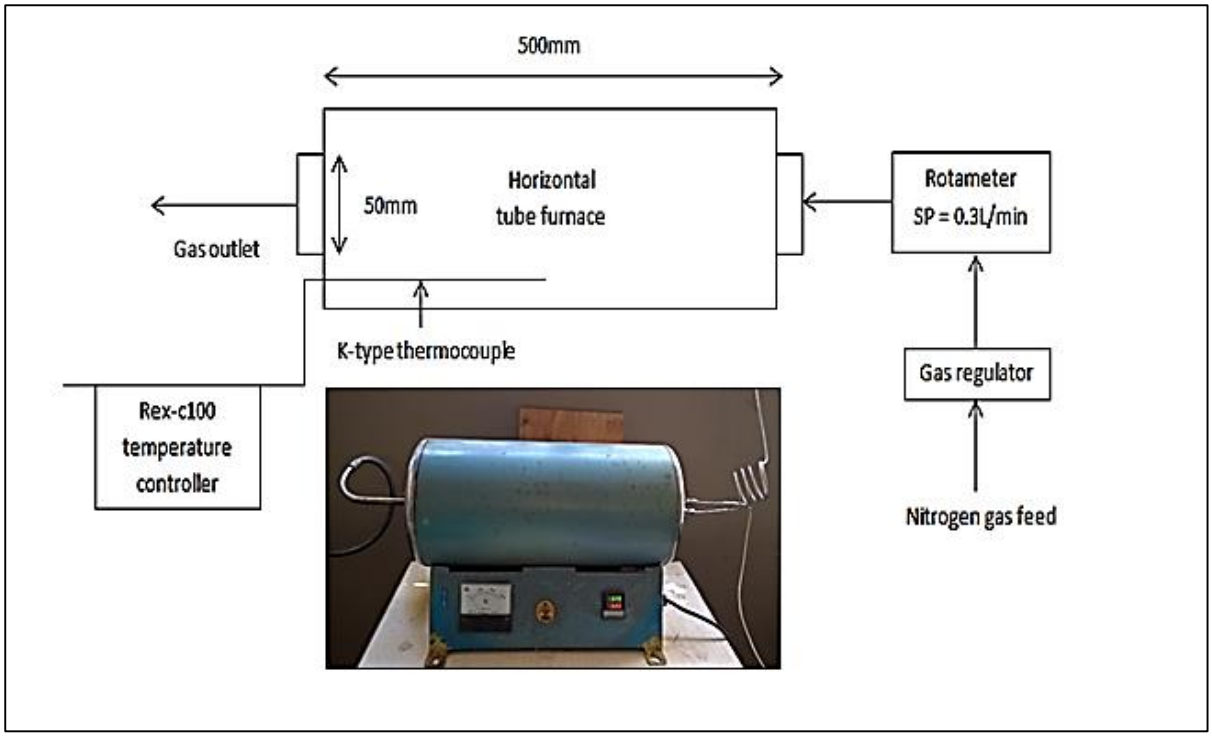

Figure 3.5: Horizontal tube furnace schematic diagram.

A sample holder manufactured from stainless steel (see Figure 3.6) was used. The sample holder was 150 mm in length and 40 mm in width with three compartments of 50 mm in length each. Ventilation holes ensured that gas flowed adequately around the particles during experimentation. The ventilation holes were small enough to keep exfoliated and very small pieces from blowing away (except for extreme cases).

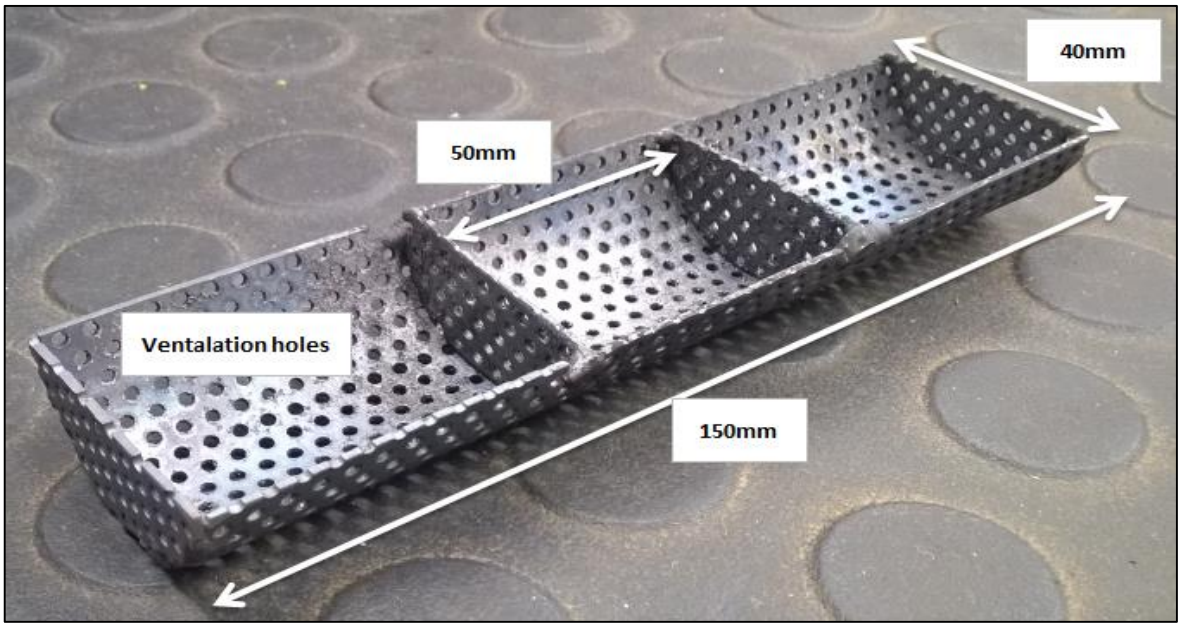

Figure 3.6: Sample holder used during experimentation.

3.5.2 X-RAY COMPUTED TOMOGRAPHY SCANNER

A Micro-focus X-Ray scanner located at the Micro-focus X-Ray Radiography and Tomography facility (MIXRAD) of the South African Nuclear Energy Corporation (Necsa) was used to construct 3D images of the coal samples before and after heating to make deductions on crack extent, nature and placement. The Nikon XTH 225 ST Micro-focus X-Ray tomography system is shown in Figure 3.7. VGStudio Max Software was used for analyses.

Figure 3.7: The Nikon XTH 225 ST Micro-focus X-Ray tomography (MIXRAD) system.

The technique of X-Ray scanning was chosen because this technique is renowned for its indestructible nature. In other words, X-Rays can penetrate the internal structure of a sample without damaging the sample (Mathews *et al.,* 2011:58; Sinha, 2007:17). The specifications for the Micro-focus X-ray tomography system are given in Appendix A.

3.6 DATA ANALYSIS

To determine the qualitative breakage behaviour of the coal samples the X-Ray scans were used to grasp crack extent, nature and placement inside a coal particle. The scans taken before and after thermal treatment were compared to each other by using VGStudio Max software. Photographs of each temperature-size-origin combination were also taken to further try to visualise crack formation and fragmentation behaviour.

To quantify the primary fragmentation of large coal particles it was first necessary to take the particle size distributions of the fragmented coal particles. The sieves where stacked according to the square root two series with the smallest sieve size taken as 2.36 mm and fragments smaller than 2.36 mm were then weighed as a single entity. The breakage index for each repeat was calculated from these distributions. The breakage index can be defined as the ratio between Sauter diameter after and before fragmentation.

The Sauter diameter (2D analysis) is calculated with Equation 3.5:

$$Sauter\ diameter = \frac{1}{\sum_i \frac{x_i}{d_i}}$$ ***Equation 3.5***

Sauter diameter in mm

Weight fraction (x) is dimensionless

Sieve size (d) in mm

In Table 3.6 an example of a breakage index calculation for a 30 mm HV1 particle heated to 600 °C is given.

Table 3.6: Breakage index calculation example.

Repeat	Sauter diameter $_{before}$ (mm)	Sauter diameter $_{after}$ (mm)	Breakage index
1	32.00	18.63	0.58
2	32.00	23.13	0.72
3	32.00	31.06	0.97
4	32.00	22.55	0.70
5	32.00	14.75	0.46

Outlier repeats were then calculated from the breakage index data as shown in Table 3.7. It can be seen from this data that, for the current example, Repeat 3 was an outlier and it was thus discarded from the data.

Table 3.7: Outlier values determination example.

Parameter	Quantity
Average	0.69
Quartile 1	0.58
Quartile 3	0.72
Inter Quartile Range	0.14
Upper outlier	0.93
Lower outlier	0.37

Once the outlier repeat was discarded, the average breakage index and the error could be calculated. For the HV1, 30 mm, 600 °C combination example the breakage index is thus 0.62 with a confidence interval of 0.19 based on a 95% confidence level. A breakage index

for each size-temperature-origin combination was obtained in this manner. Consequently, the necessary conclusions on the influence of different factors on the primary fragmentation behaviour of large coal particles could be made. If the breakage index equalled one zero fragmentation took place (the Sauter diameter before and after fragmentation is the same), and if the index was larger than one swelling occurred. For the above example the index is lower than one indicating that a 30 mm HV1 particle heated to 600 °C fragmented. Confidence intervals were calculated based on a 95% confidence level for all the breakage indices, as well as any other raw data (excluding critical diameters as explained below) and the method given in Appendix A.

To determine the critical diameters the breakage index values were once again used. After outlier repeats were discarded, the probability of breakage was determined. For the example above four out of the four legitimate repeats' breakage index was lower than one indicating that 100% of the particles fragmented. When considering another example: if four out of five repeats had a breakage index lower than one the probability of fragmentation would have been 80%. An error of 25% was tolerated meaning that, if the probability was 75%, it was concluded that fragmentation occurred for that particle size. The error value of 25% was chosen based on a sensitivity analysis. The probability for each size was observed and the cut point or critical diameter obtained. In Table 3.8 an example of the above statements is given. For this example data for LV1 heated to 600 °C was taken. From the table it can be seen that the critical diameter for LV1 particles heated to 600 °C is 22.5 ± 2.5 mm. Critical diameters larger than 30 mm and smaller than 10 mm could not be determined due to the size range tested (10-30 mm sizes). If this was the case, the critical diameters were indicated as 30 or 10 mm respectively.

Table 3.8: Critical size determination example.

Particle size (mm)	Breakage probability (%)
10	0
15	0
20	0
25	75
30	100

CHAPTER 4: COAL CHARACTERISATION RESULTS & DISCUSSION

"But, despite the complexity of coals, we nevertheless need systems for classifying and describing them" (Bunt, 2014:15). The focus of this chapter is on classifying and describing the coal used in this study. The proximate, calorific value, Mercury Intrusion Porosimetry, equilibrium moisture, crucible swelling number, Roga index, mercury submersion and petrographic analyses results are discussed.

4.1 PROXIMATE & CALORIFIC VALUE ANALYSES

Proximate and CV analyses on the raw coal samples and proximate analysis on the char samples were done. In Table 4.1 the proximate and CV results for the five coal samples are given. Results are given on a weight percentage air-dried basis (a.d.b). Three high volatile and two low volatile samples can clearly be distinguished from the data. The ash yields are more or less the same and low (with the distinction of HV Coking) as specified in the selection criteria. Contents for the three high volatile samples correspond to those typically found in South African bituminous coal as seen from studies conducted by Everson *et al.* (2013:4) and Hattingh (2012:115). The low volatile samples correspond to results obtained from Pretorius *et al.* (2002:7-8) for South African pseudo anthracite.

Table 4.1: Proximate and calorific value results for coal samples.

Analysis	LV1	LV2	HV1	HV2	HV Coking
Inherent moisture (a.d.b wt.%)[1]	1.2	1.0	2.6	2.6	0.7
Volatile Matter (a.d.b wt.%)	8.6	12.9	21.8	25.2	20.4
Ash yield (a.d.b wt.%)	15.1	12.1	12.6	15.9	25.3
Fixed carbon (a.d.b wt.%)[2]	75.1	73.9	62.9	56.4	53.7
Total (wt.%)	**100**	**100**	**100**	**100**	**100**
Calorific value (a.d.b MJ/kg)	26.59	30.72	28.03	26.89	26.12

[1]Relative Humidity: 20-80%; Temperature: 25 °C, [2]By calculation

In Table 4.2 the volatile matter (a.d.b wt.%) for the char samples, as well as their respective volatile loss percentages at 400, 600 and 900 °C, are given. In Appendix C the rest of the proximate results for the chars are given.

Table 4.2: Volatiles and percentage volatile loss results for char samples heated to 400 , 600 and 900 °C.

Analysis	LV1	LV2	HV1	HV2	HV Coking
400 °C					
Volatile Matter (a.d.b wt.%)	7.8	9.8	16.7	16.8	16.3
Volatile loss (a.d.b wt.%)[1]	0.8	3.1	5.1	8.4	4.1
600 °C					
Volatile Matter (a.d.b wt.%)	5.4	5.6	6.8	6.8	5.6
Volatile loss (a.d.b wt.%)[1]	3.2	7.3	15.0	18.4	14.8
900 °C					
Volatile Matter (a.d.b wt.%)	2.7	1.4	1.6	2.5	3.9
Volatile loss (a.d.b wt.%)[1]	5.9	11.5	20.2	22.7	16.5

[1]Volatile loss: Difference between volatile matter of the coal sample and volatiles of the char sample

To summarise the data given in Tables 4.1 and 4.2, consider Figure 4.1. From the figure it can be seen that a relationship exists between volatile loss and initial coal volatile matter at all three temperatures. The correlation is higher at higher temperatures than at lower temperatures, as can be seen from Table 4.3.

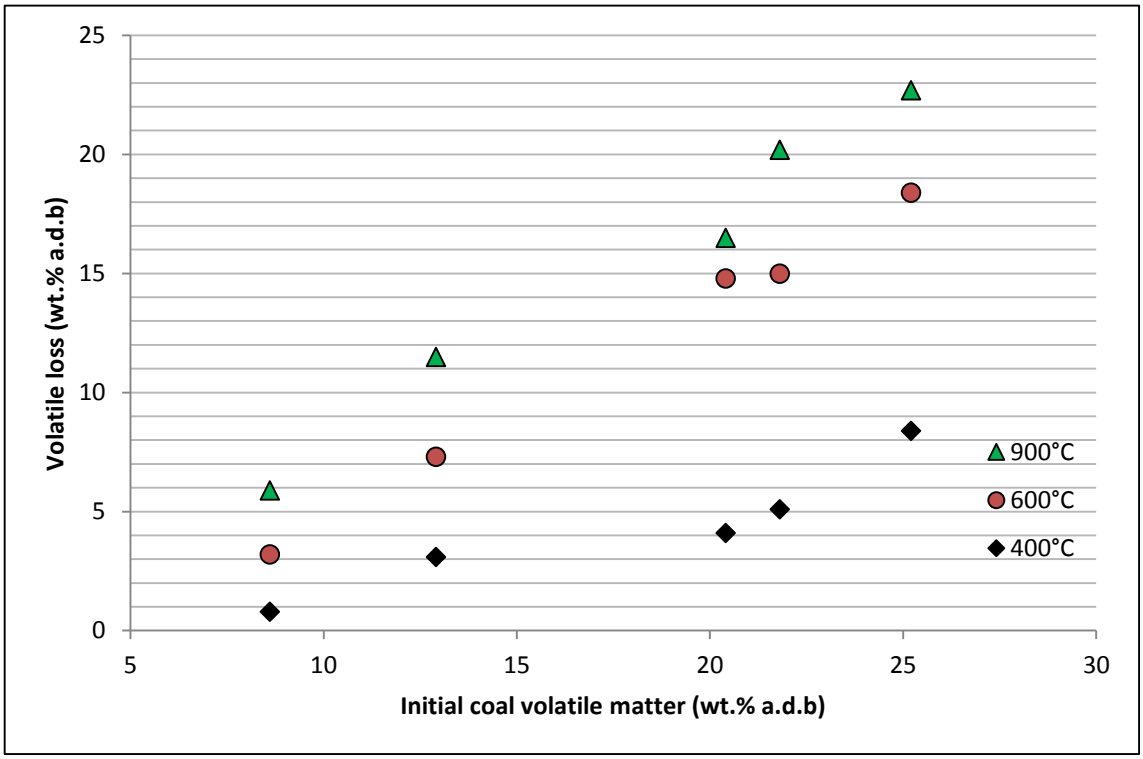

Figure 4.1: Initial coal volatile matter versus volatile loss for the different temperatures.

In Table 4.3 the slopes and linear coefficients of determination (R^2) for all three functions are given. From the table it can be seen that the R^2 values are high and the data thus fits the increasing linear trend relatively well. When observing the slope values it can be seen that, for 600 and 900 °C the slopes are equal and very close to one. This implies that almost all volatiles escaped the coal at these temperatures, while for 400 °C very little escaped. Fragmentation due to volatile release stresses will thus be more severe at high temperatures.

Table 4.3: Slopes and R^2 values for linear correlations between coal volatile matter and volatile loss at 400, 600 and 900 °C.

Temperature (°C)	Slope (a.d.b wt.%)	R^2
400	0.4	0.9
600	0.9	1.0
900	1.0	1.0

When considering Figure 4.2 it can be seen that the difference between 400 and 600 °C is more severe for the high volatile samples than for the low volatile samples. Fragmentation due to volatile release stresses will thus be more pronounced for particles heated to 600 °C than for those heated to 400 °C for the high volatile samples, while for the low volatile samples the difference will not be that severe. For the low volatile sample an almost linear increase with temperature can be seen, while for the high volatile sample a non-linear function that tapers off at high temperatures can be fit to the data.

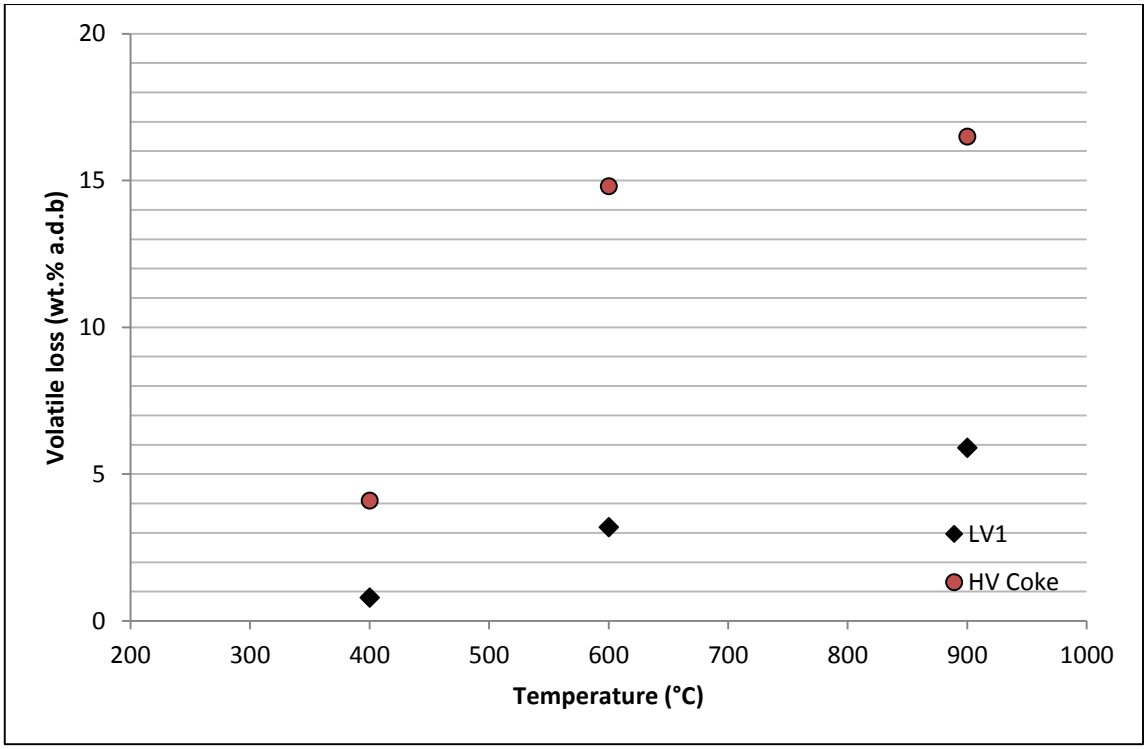

Figure 4.2: Temperature versus volatile loss for LV1 and HV Coking samples.

4.2 MERCURY INTRUSION POROSIMETRY & EQUILIBRIUM MOISTURE ANALYSES

The MIP technique was used to investigate the macro and 41esopores structure of the coal samples. The equilibrium moisture for each coal sample was also determined and related to the porosity of that sample. In Table 4.4 this porosity (vol.%) versus equilibrium moisture (wt.%) data are given. From the data in Table 4.4 it can be seen that a good correlation between porosity and equilibrium moisture exists.

Table 4.4: Porosity (vol.%) versus equilibrium moisture (wt.%) data for the different coal samples.

Coal origin	Porosity (vol.%)[1]	Equilibrium moisture (wt.%)[1,2]
LV1	5.1 ± 2.7	3.0 ± 0.2
LV2	6.1 ± 0.9	2.6 ± 0.3
HV1	5.1 ± 0.9	4.1 ± 0.2
HV2	4.9 ± 8.1	3.7 ± 0.3
HV Coking	3.2 ± 0.9	1.8 ± 1.5

[1]Confidence interval based on a 95% confidence level, [2]Relative Humidity: 96%; Temperature: 30 °C,

When considering Figure 4.3 it can be concluded that this correlation is of linear nature. The R^2 value of the correlation illustrated is 0.6 and the slope 1.1. It can thus be stated that the

equilibrium moisture for a coal sample is a good indication of its porosity. This corresponds to the conclusion drawn by Thomas & Damberger (1976:25) on Illinois coal. Ryan (2006:142) and De Korte (2000:3-4) also indicated that such a relationship exists. When plotting the porosity versus inherent moisture (moisture capacity at 20-80% relative humidity and 25 °C) it was found that the fit was not as good as between equilibrium moisture and porosity.

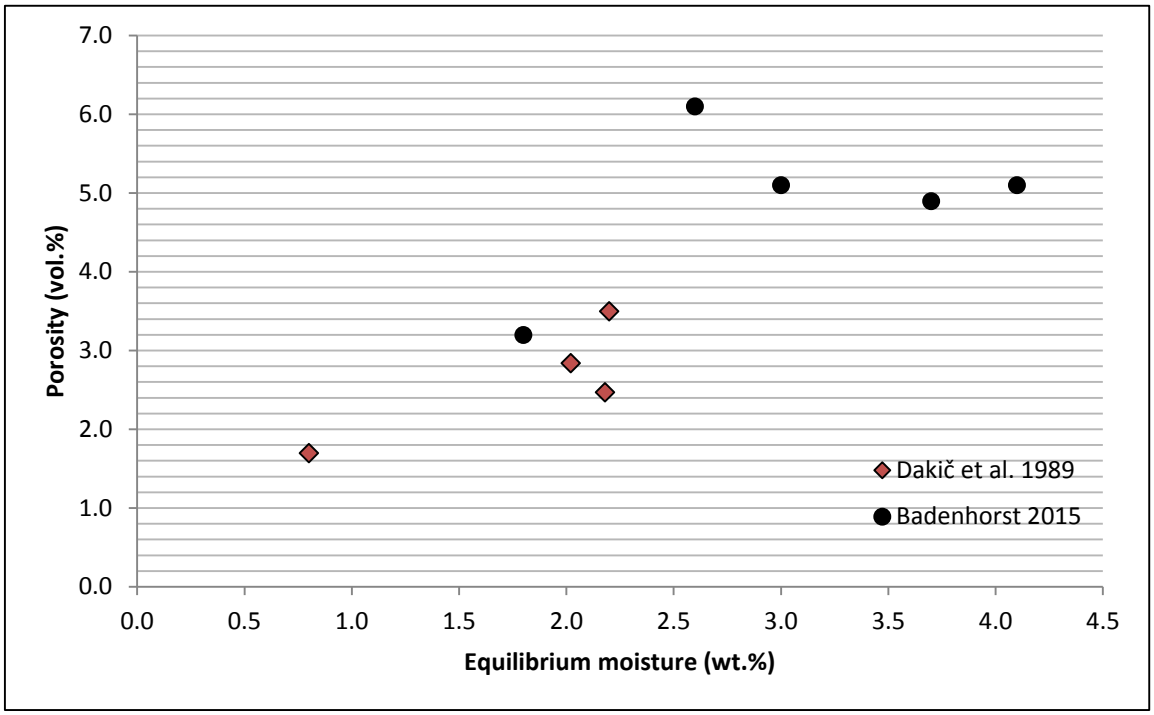

Figure 4.3: Equilibrium moisture versus porosity.

The differences that are present between the porosity and equilibrium moisture values can possible be because with the MIP technique the mercury is forced into the pores, which can cause a collapse in structure and therefore an inaccurate measurement of too large porosity is taken (Webb, 2001:15-16; Westermarck, 2000:6). Webb (2001:9) also remarked that interstitial voids between packed particles could also result in a too large measurement of porosity. When considering the fact that hydrocarbons and CO_2 are originally trapped in coal pores and removed during MIP but not during equilibrium moisture measurements, one can also see why the equilibrium moisture values are smaller than the porosities (Thomas & Damberger, 1976:25). Experimental errors and the heterogenic nature (maceral differences) of coal can also explain the deviations.

In Figure 4.4 a MIP cumulative intrusion/extrusion curve for LV1 is shown. From the figure it can be seen that the intrusion volume increases exponentially with pressure. If interstitial voids were present or a collapse of structure occurred the curve would have deviated from

this trend as discussed by Webb & Orr (1997:158) and Webb (2001:15). The same trend was seen for all five coal samples and it can thus be concluded that these two factors did not affect the results. The porosity data is thus relatively accurate when compared to the errors made during equilibrium moisture testing when hydrocarbons and CO_2 molecules are still present in the pore structure.

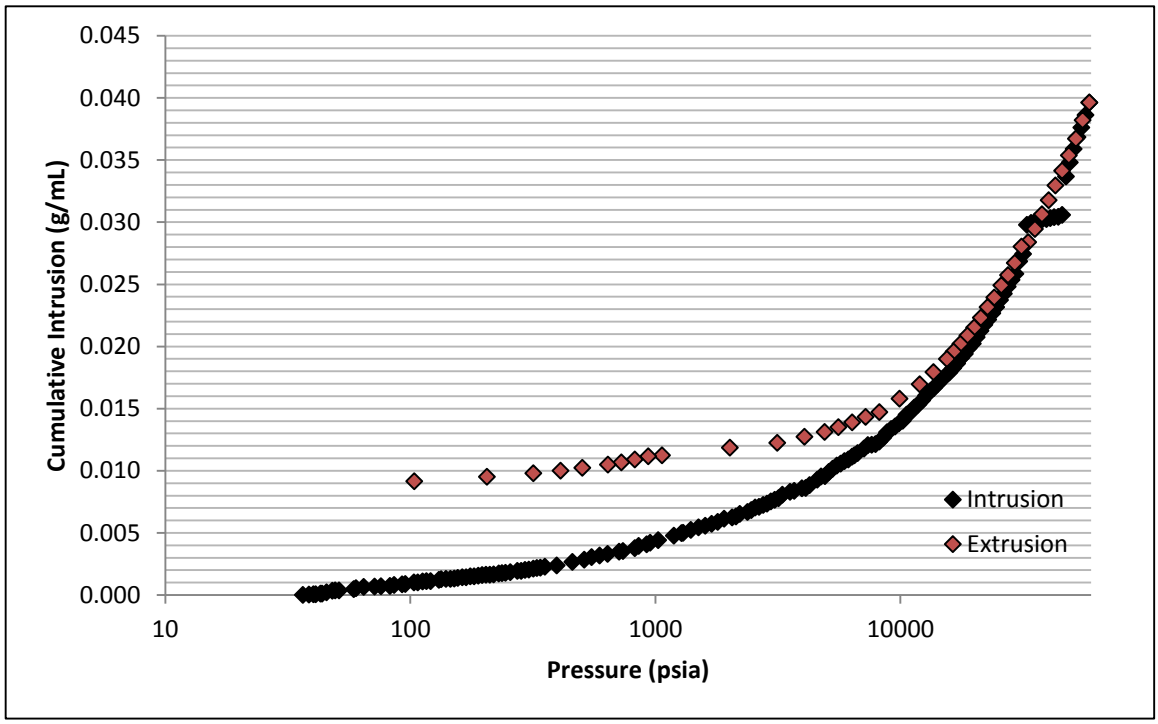

Figure 4.4: Cumulative intrusion/extrusion curve versus pressure for LV1.

Although the porosity data is more accurate than the equilibrium moisture data the PRN was still based on the ratio between volatile matter and equilibrium moisture as done by Dakič *et al.* (1989:913). In Table 4.5 the PRN values for the five coal samples are given.

Table 4.5: Pore resistance numbers for the different coal samples.

Coal origin	Equilibrium moisture (wt.%)[1]	Volatile Matter (equilibrium moisture wt.%)	Pore resistance number
LV1	3.0 ± 0.2	8.4	2.8
LV2	2.6 ± 0.3	12.7	4.9
HV1	4.1 ± 0.2	21.5	5.2
HV2	3.7 ± 0.3	24.9	6.7
HV Coking	1.8 ± 1.5	20.2	11.2

[1]Confidence interval based on a 95% confidence level

The PRN values were calculated with the initial coal volatile matter, converted to equilibrium moisture basis as shown in Equation 4.1, of the coal samples. For future studies it is recommended that the volatile loss percentages, as well as the developing pore structure at each temperature, should be obtained and used to attain a temperature dependant PRN.

$$Vm_{eq} = \frac{100\, Vm_{a.d.b}}{((100 - M_{a.d.b}) + M_{eq})} \qquad \textbf{\textit{Equation 4.1}}$$

Volatile matter (Vm) in wt.% air-dried basis (a.d.b) or equilibrium moisture basis (eq)

Moisture (M) in wt.% air-dried basis (a.d.b) or equilibrium moisture basis (eq)

From the PRN values in Table 4.5 it can be seen that the ratios between the volatile matter and porosity for the low volatile samples are smaller than for high volatile samples and would thus be affected to a lesser extent by volatile release stresses. From this table it can also be seen that the range of PRN values are relatively small. A recommendation for future studies is to test a broader range of PRN values.

To conclude these sections consider Table 4.6. The meso and macroporosities were calculated by using the pore diameter versus cumulative intrusion volume data. The intrusion volume smaller than 50 nm were divided by the total intrusion volume to get the mesoporosity fraction. The difference between total porosity and mesoporosity was then the macroporosity fraction. When considering the porosity percentages, mean pore diameters and average pore diameters it can be seen that all five coal samples are more mesoporous than macroporous. The pore diameters are all in the range of 2-50 nm, which is the IUPAC classification for mesopores, and the percentage mesoporosity is much higher than the macroporosity percentage for LV1, HV1 and HV2. It should however be noted that with MIP the mesoporous structure is sometimes overestimated due to hysteresis. The pore diameters, as well as the pore area results, correspond to that obtained by Du Preez (2012:51), Du Toit (2013:37), Hattingh (2012:136) and Hattingh (2009:70) for South African coal.

The true and apparent densities were also obtained during MIP. The apparent densities were used in heat transfer calculations to determine the temperature gradients in, and heating times for, the coal particles. In the section, dealing with the density results, the densities obtained with the mercury submersion technique are discussed and compared to those obtained by mercury intrusion.

Table 4.6: Mercury Intrusion Porosimetry results.

Analysis	LV1	LV2	HV1	HV2	HV Coking
Porosity (vol.%)					
Mesoporosity (vol.%)[1]	3.8	3.6	3.9	3.7	1.7
Macroporosity (vol.%)[2]	1.3	2.5	1.2	1.2	1.5
Median pore diameter (nm)					
Volume (nm)	10.0	15.6	10.7	8.8	12.2
Area (nm)	4.3	4.8	4.7	4.8	4.6
Average pore diameter (nm)	8.3	10.0	8.8	7.7	9.3
Total pore area (m^2/g)	19.4	19.8	19.1	21.0	9.1
Hysteresis	Moderate	High	Moderate	Moderate	Low
True density (kg/m^3)	1280	1226	1221	1296	1505
Apparent density (kg/m^3)	1349	1305	1287	1367	1555

[1]IUPAC standard: 2 –50 nm pores, [2]IUPAC standard: >50 nm pores

In Figure 4.5 an example of hysteresis for HV2 is given. It can be seen that the extrusion curve does not follow the intrusion curve. Some large pores were thus not taken into account during the intrusion process. According to Webb (2001:11) this is because the intrusion is hindered by the smaller pore throats connected to the large cavities which are only filled near the end of the intrusion process. The extrusion curve shows that the large pores were under-estimated during intrusion. In Table 4.6 hysteresis data was compared to each other and a classification was assigned. LV2 was more affected by hysteresis than LV1, HV1 and HV2. HV Coking was affected the least by hysteresis. This means that LV2 has more ink-shaped or irregular shaped pores than LV1, HV1 and HV2, which on their turn have more than HV Coking. If all pores were cylindrical-shaped volatiles would flow easier to the surface. HV Coking's volatiles would thus be transported more easily and LV2 the least through the pore network. This can have an influence on the fragmentation severity. Raw data obtained from the MIP and equilibrium moisture analyses is presented In Appendix C.

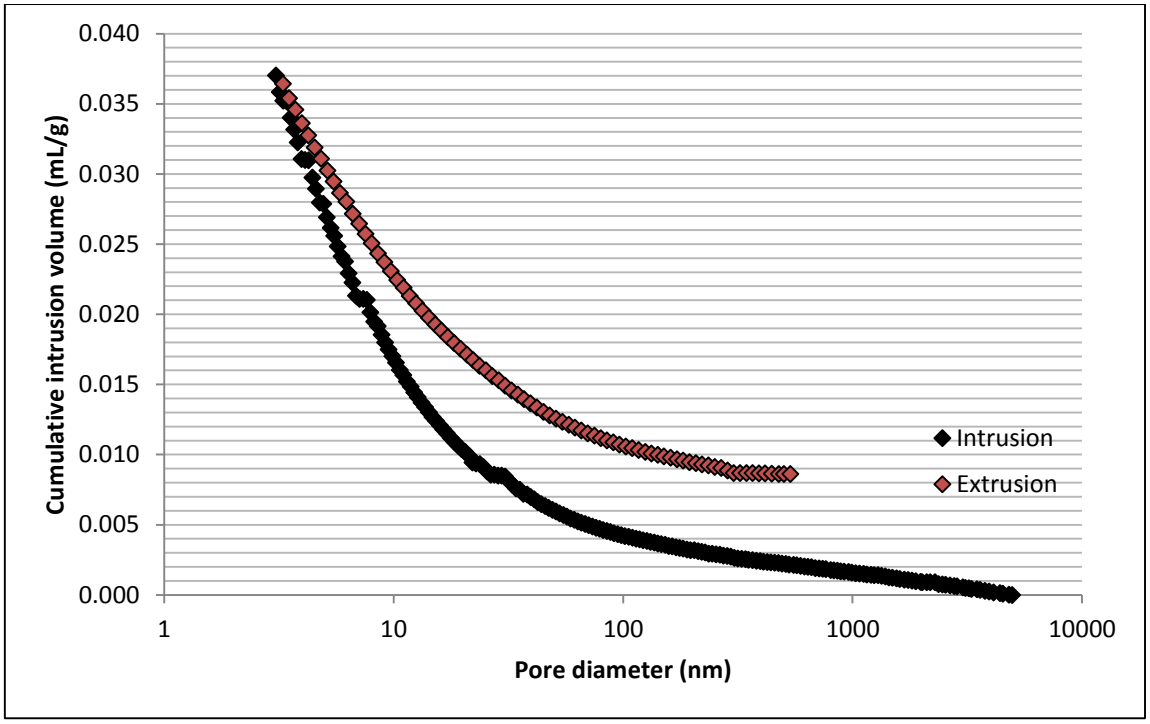

Figure 4.5: Cumulative intrusion/extrusion curve for HV2.

4.3 CRUCIBLE SWELLING NUMBER & ROGA INDEX ANALYSES

To determine the swelling and caking behaviour of the coal samples CSN and RI tests were conducted. In Table 4.7 the results for all five coals are given. Only HV2 and HV Coking showed the propensity to undergo swelling and caking. From the swelling numbers and Roga indices in the table it can be seen that HV2's swelling and caking tendency is much smaller than HV Coking's. The data for HV Coking is even lower than it should be when compared to typical South African coking coal, as reported by Coetzee (2014:83) and Jordan (2006:86). The deviations from literature can be due to the high heterogeneity of this coal's mineable seam. The particles used in fragmentation testing were thus first selected based on density before testing commenced.

Table 4.7: Crucible swelling numbers and Roga indices results for the different coal samples.

Analysis	LV1	LV2	HV1	HV2	HV Coking
Crucible swelling number	0.0	0.0	0.0	0.5	5.0
Roga index	-	-	-	9	25

In Figure 4.6 PRN versus CSN data is plotted. It can be seen that there is an increasing correlation between PRN and CSN. Dakič *et al.* (1989:914) made the same observation. Swelling rather than fragmentation would thus occur for coal with a large PRN. It should

however be noted that the CSN is not only a function of PRN, but also of other variables such as temperature. For future studies, it is recommended that the PRN should be found at different temperatures where swelling starts to influence the fragmentation behaviour of coal. From Figure 4.6 it can be seen that swelling started somewhere between a PRN of 5.2 to 6.7. This differs from observations made by Dakič *et al.* (1989:915) and Oka (2004:234) which found that swelling started at a PRN of 12 and between 15 and 17 respectively.

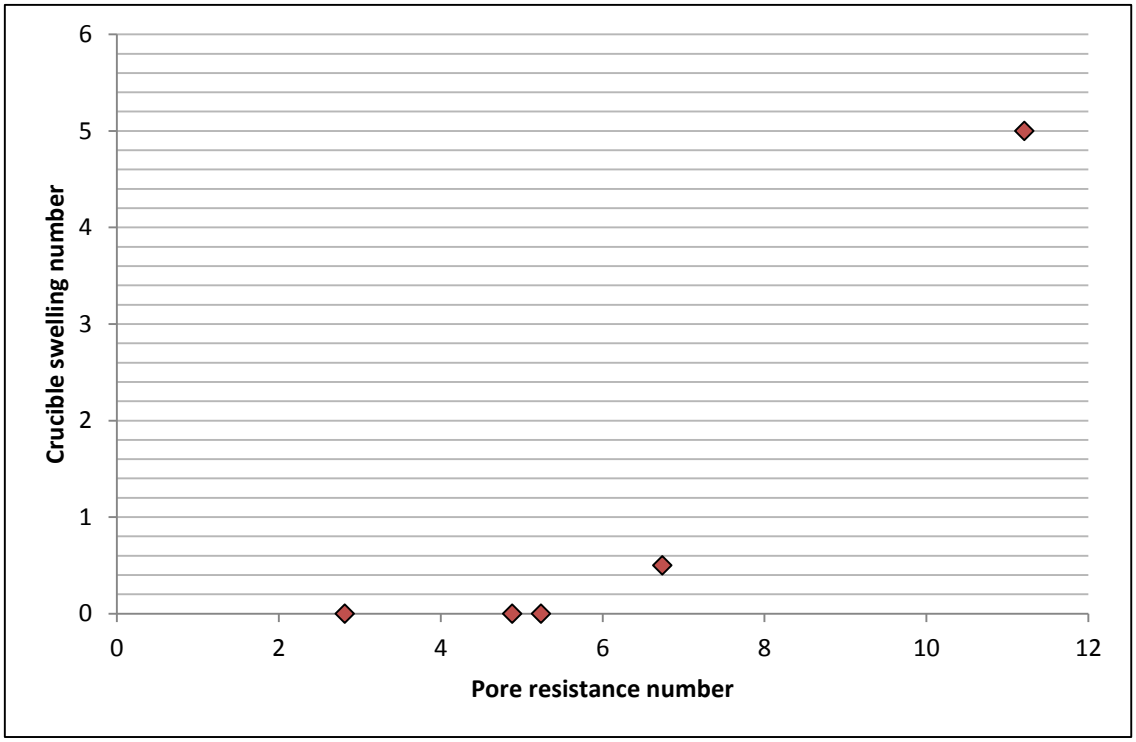

Figure 4.6: Pore resistance number versus crucible swelling number.

In Figure 4.7 a series of stills are shown in which the swelling for HV Coking with temperature is illustrated. The clips were taken by inserting a sample in an ash fusion temperature furnace equipped with a video camera. From Figure 4.7 it can be seen that swelling started at about 380 °C; then the particle melted and solidified before 500 °C was reached. The swelling will thus be more severe when heated to 400 and 600 than to 900 °C. Take note that the coal particle is the black object in the foreground while the white protruding object above it is the thermocouple.

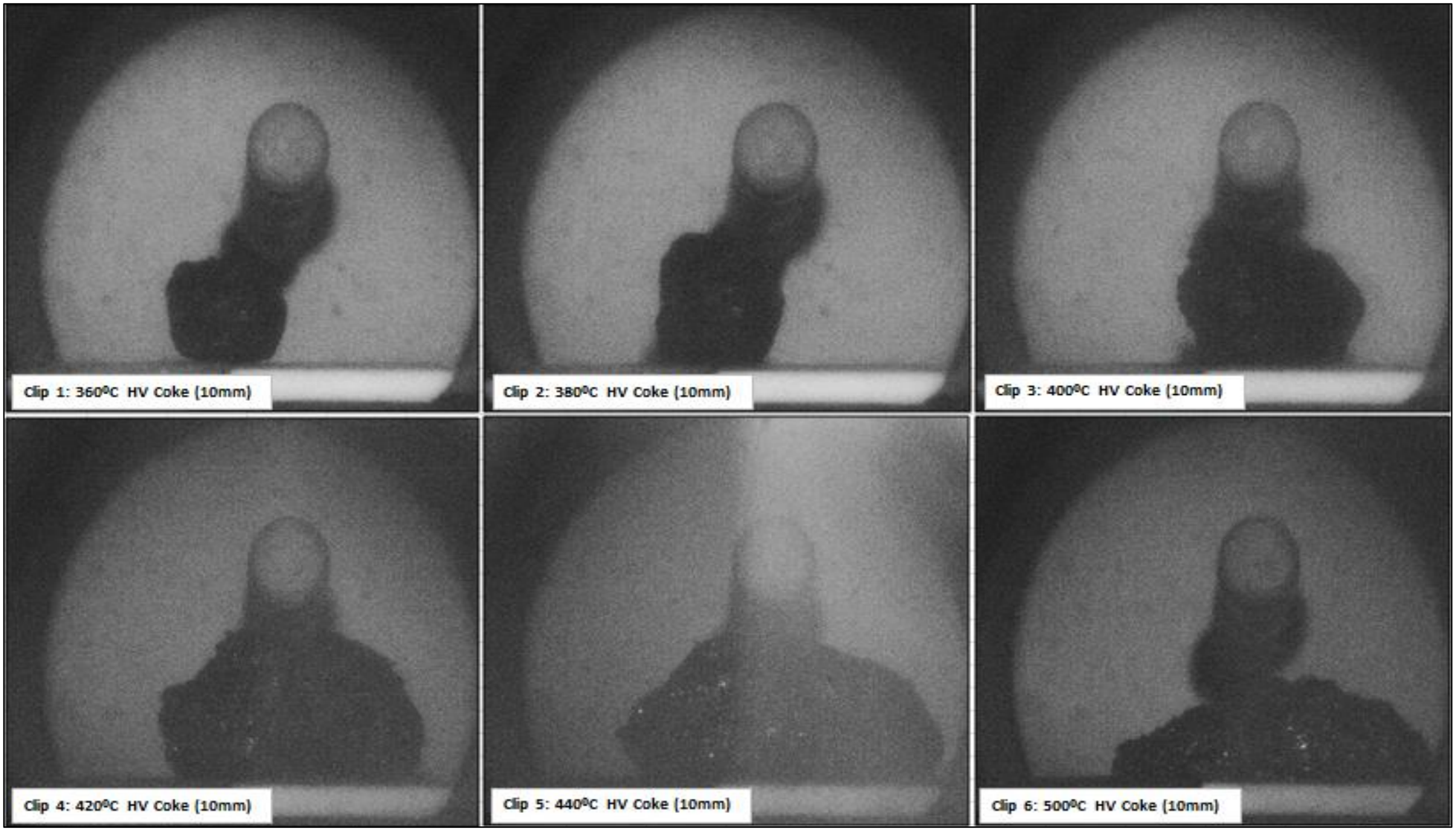

Figure 4.7: Stills showing swelling behaviour with temperature for a 10mm HV Coking sample.

4.4 DENSITY ANALYSIS

The mercury submersion technique was used to enable selection of individual particles based on their densities, ensuring some homogeneity in properties like mineral content and marcolithotype composition. The true densities were obtained from mercury submersion. MIP was used to determine the true and apparent densities of which the apparent densities were used in heat transfer calculations. The true densities in this dissertation refer to the densities obtained from the volume before any pores are filled, while the apparent densities are based on subtracting the volume of filled pores (Hayashi & Li, 2004:30; Webb & Orr, 1997:160-161).

In Table 4.8 the density results are given. The table shows that there is a difference between the true densities obtained through mercury submersion and those obtained from MIP. These differences can probably be ascribed to the fact that the densities via mercury submersion were measured on 20 mm samples, while those for the intrusion experiments were 1 mm particles. Van der Merwe (2010b:66) stated that coal particles with densities larger than 1600 kg/m^3 are more prone to primary fragmentation than particles with lower densities. All particles' densities in the table are smaller than 1600 kg/m^3 and density would thus not really have an influence on fragmentation. HV Coking might differ from the other samples but this can be ascribed to its high ash yield relative to the other samples.

Table 4.8: Density results from Mercury Intrusion Porosimetry and mercury submersion analyses respectively.

Analysis	LV1	LV2	HV1	HV2	HV Coking
True density (kg/m^3)[1]	1403	1384	1435	1414	1411
True density (kg/m^3)[2]	1280	1226	1221	1296	1505
Apparent density (kg/m^3)	1349	1305	1287	1367	1555

[1]Mercury submersion technique, [2]Mercury Intrusion Porosimetry technique

In Table 4.9 the mercury submersion density data is given. From Table 4.9 it can be seen that particles selected for HV Coking came from a broader range than the other samples. This is because of the heterogeneity of the seam where this coal is mined. Particles were selected in a lower range for the low volatile samples than for the high volatile samples. The standard deviations for these samples were also lower.

Table 4.9: Mercury submersion density data.

Analysis	LV1	LV2	HV1	HV2	HV Coking
Average density (kg/m^3)	1403	1384	1435	1414	1411
Standard deviation (kg/m^3)	66	56	78	72	80
Density range (kg/m^3)	1300-1450	1300-1450	1350-1500	1350-1500	1300-1500

The standard deviations, as well as the density distributions, were used to decide the cut points or density ranges of the samples. In Figure 4.8 an example of a density distribution is given. In Appendix C the raw data and distribution curves are given.

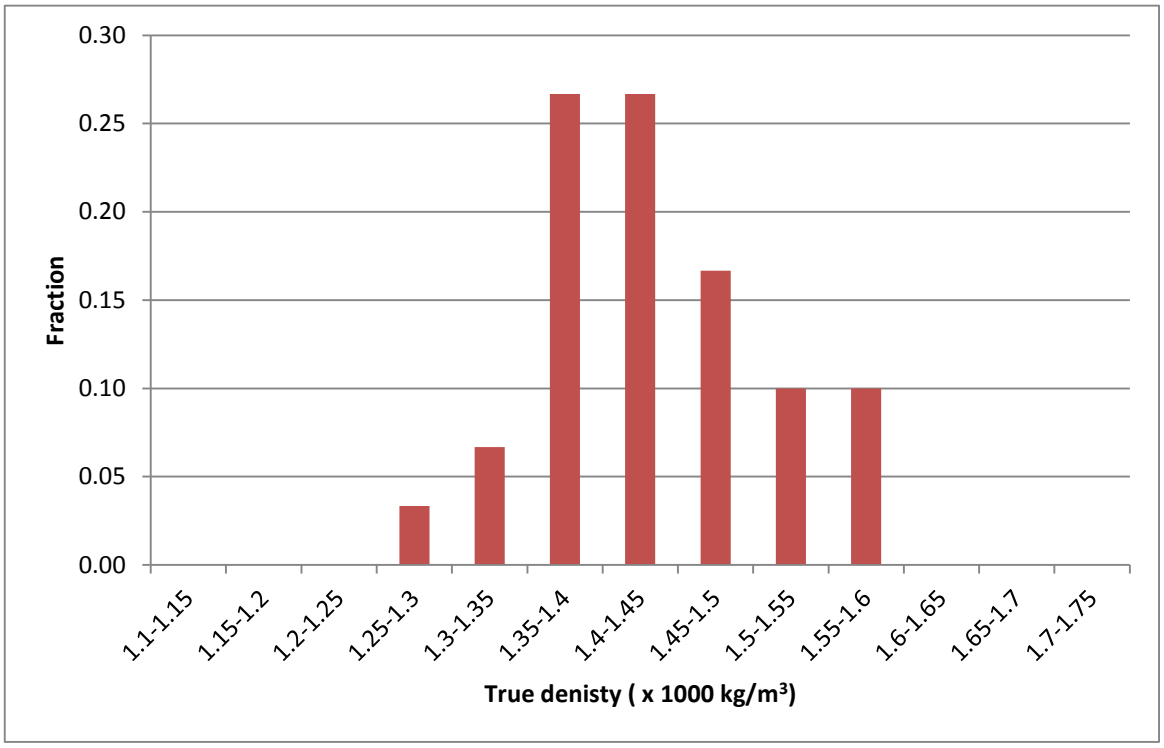

Figure 4.8: Density distribution curve for a 20 mm HV1 particle.

4.5 PETROGRAPHIC ANALYSIS

With the petrographic analysis, reflectance values and maceral composition were obtained for each sample. The maceral composition is of importance for this study. In Table 4.10 the maceral composition results are given.

Vitrinite is a very brittle maceral and has, according to Chen *et al.* (1994:137) and Stanmore *et al.* (1996:3272), an influence on the fragmentation behaviour due to thermal stresses. From Table 4.10 it can be seen that the two low volatile samples have medium vitrinite contents, while HV1 and HV2 have low vitrinite contents. HV2's content is however still close

to the low volatile samples' content. HV Coking, with the highest swelling extent, has the highest vitrinite content.

Table 4.10: Maceral composition results for the different coal samples.

Analysis	LV1	LV2	HV1	HV2	HV Coking
% Vitrinite	43.5	41.2	16.0	36.7	62.1
% Liptinite (Exinite)	0.0	0.0	0.0	2.9	0.0
% Reactive Semifusinite	0.0	0.0	29.8	30.9	0.4
% Inert Semifusinite	46.7	50.0	44.0	19.5	12.0
% Fusinite + Secretinite[1]	1.1	0.7	0.7	1.5	0.9
% Micrinite	0.0	0.0	0.4	0.4	0.0
% Mineral Matter[2]	8.7	8.1	9.1	8.1	24.6
% Total Reactives	-	-	45.8	70.5	62.5
% Total Inerts	-	-	54.2	29.5	37.5
Vitrinite Classification Content	Medium	Medium	Low	Low	Moderately High

[1]Secretinite: A highly reflective, inert maceral (Lyons *et al.,* 1986:1094), [2]Calculated

According to Chen *et al.* (1994:137) fusinite causes little or no fragmentation at all. Since vitrinite causes fragmentation and fusinite not, the ratio between these two contents might be able to give an indication of fragmentation. The ratios for the five samples are given in Table 4.11 and from here on will be termed the maceral ratios. The semifusinites, as well as the fusinites, were accounted for in this ratio. If the assumption is correct, then Table 4.11 shows that HV Coking will be the most influenced by a thermal shock and HV1 the least. Swelling should however not be excluded, and therefore LV1 might be influenced more than HV Coking by a thermal shock. In the chapter dealing with fragmentation results more on this will be given.

Table 4.11: Maceral ratios for all five coal samples.

Analysis	LV1	LV2	HV1	HV2	HV Coking
% Vitrinite	43.5	41.2	16.0	36.7	62.1
% Reactive Semifusinite	0.0	0.0	29.8	30.9	0.4
% Inert Semifusinite	46.7	50.0	44.0	19.5	12.0
% Fusinite + Secretinite	1.1	0.7	0.7	1.5	0.9
Maceral ratio between vitrinite and fusinites	0.9	0.8	0.2	0.7	4.7

4.6 RANK DETERMINATION

To determine the rank of the samples, the ASTM method was used as described in Chapter 3. In Table 4.12 the characteristics used in the Parr equation, as well as the final rank classification, are presented. From the table it can be seen that the coal rank ranged from semi anthracite to medium volatile bituminous.

Table 4.12: ASTM rank of coal samples.

Analysis	LV1	LV2	HV1	HV2	HV Coking
Ash yield (a.d.b wt.%)	15.1	12.1	12.6	15.9	25.3
Sulphur (a.d.b wt.%)	1.6	2.6	0.3	0.6	0.8
Mineral matter (a.d.b wt.%)	17.2	14.5	13.8	17.5	27.8
Volatiles (dmmf wt.%)	10.5	15.3	26.1	31.5	28.5
Carbon (dmmf wt.%)	92.0	87.5	75.2	70.6	75.1
Calorific value (mmf wt.%)	32.1	35.9	32.5	32.6	36.2
Rank	Semi Anthracite	Low volatile bituminous	Medium volatile bituminous	Medium volatile bituminous	Medium volatile bituminous

4.7 SUMMARY

The most important results obtained from this chapter are summarised below:

- Volatile release stresses will be more pronounced at higher temperatures;

- A linear correlation between equilibrium moisture and porosity exists for coal used in this dissertation;

- The PRN values for the coals range between 2.8 and 11.2;

- Mercury intrusion/extrusion showed that hysteresis in LV2 is the most and in HV Coking the least pronounced, meaning that more ink-pores are present in LV2 and more cylindrical pores in HV Coking;

- HV2 and HV Coking are two swelling samples;

- The maceral ratio (ratio between vitrinite and fusinite) for HV Coking is the highest and the lowest for HV1; and

- The coal rank ranged from semi anthracite to medium volatile bituminous.

CHAPTER 5: FRAGMENTATION RESULTS & DISCUSSION

In this chapter the location and extent of fractures formed and the impact and relationship that different factors (such as coal characteristics, temperature and particle size) have on the primary thermal fragmentation of coal is given.

5.1 CAUSES OF PRIMARY FRAGMENTATION

Two causes (as explained in Chapter 2) govern the thermal primary fragmentation of large coal particles. Thermal stresses present in a particle due to rapid heating and a pressure build-up of volatiles in the pores of a particle cause fragmentation. In this section, these two causes are investigated through crack extent, nature and placement observations obtained from the tomography scans.

5.1.1 CRACK EXTENT, NATURE AND PLACEMENT

Figure 5.1 shows tomography scans (reverse image, i.e. cracks are white and dense minerals black) of a particle before (left hand side) and after (right hand side) heating commenced. Reverse images were taken for clearer demonstrative. From the tomography scans taken of the coal particles before any heat treatment commenced small cracks can be seen throughout the particle volume. These small cracks can either be ascribed to natural cleats (A), or to fissures that formed during handling and preparation (B). The small and thin cracks that can be seen near the edges of the particles are probably due to handling, as stated by Hoffman (2012:91). Upon heating new cracks formed on these already existing cracks (C). This corresponds to Griffith's theory which stated that pre-cracks act as facilitators for new cracks to form on. New cracks also formed between coal-mineral interfaces (D) which are, according to Gajewski & Kijo-Kleczkowska (2006:12), the weak areas in the particles. Cracks still formed on already existing cracks in these interfaces but due to their "weakness" these new cracks are more abundant than in just e.g. a coal band. When comparing the crack at A and at C it can be seen that the pre-crack had widened and grown upon heating.

The cracks that formed upon heating were well structured and orientated either perpendicular or parallel to the bedding planes. Goehring (2003:7) found similar results for a thin, homogeneous film undergoing uniform drying. Although coal is a heterogeneous substance and heating commenced in a non-uniform manner, the same observations were still found.

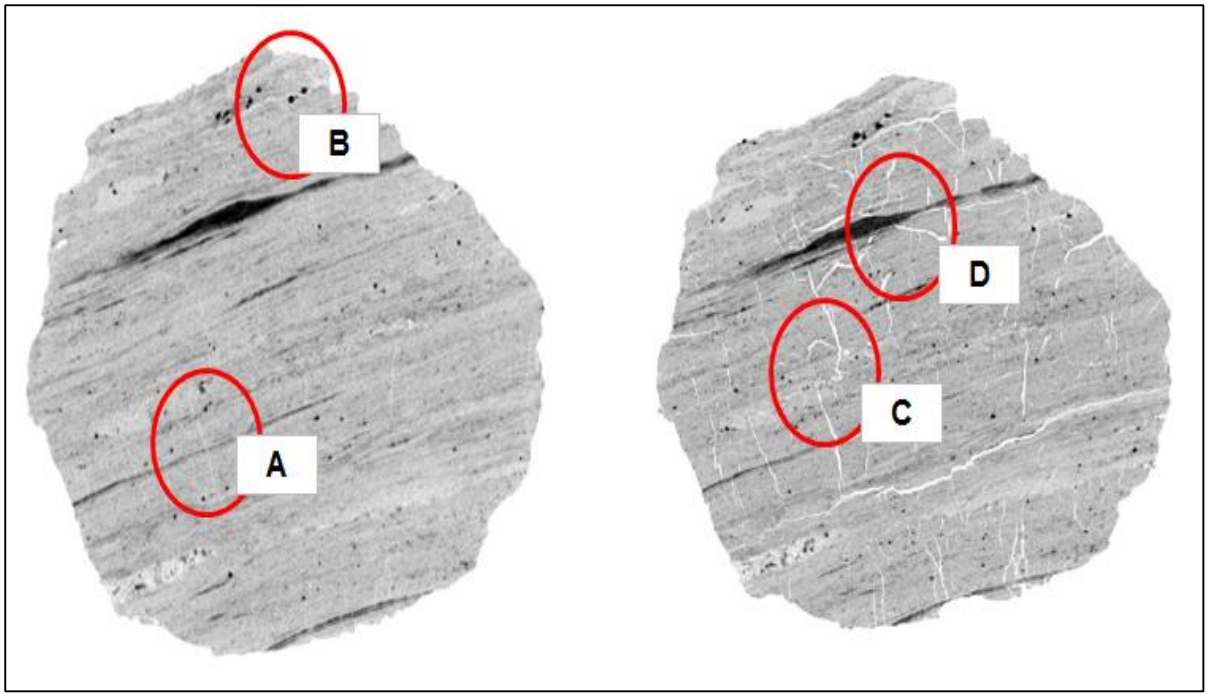

Figure 5.1: Cracks forming in a 10 mm LV2 particle heated to 600 °C (Before scan at left and after at right).

Figure 5.2 shows the fragmentation of low volatile samples (reverse image, i.e. cracks are white and dense minerals black). For the low volatile samples, many of these structured cracks were seen. A multitude of fragments then also formed from the outer core of these samples at high temperatures. This behaviour is associated with fragmentation caused by thermal stresses as described by Paprika *et al.* (2013:5489), Senneca *et al.* (2010a:3) and Senneca *et al.* (2013:255). Due to the low volatile matter and high thermal conductivities of these samples, fragmentation due to volatile release stresses will also be a minimum, and the observation that thermal stresses are the main cause of fragmentation is confirmed for these samples.

Consider Figure 5.3 (reverse image, i.e. cracks are white and dense minerals black). For the high volatile samples, cracks parallel to the bedding planes were mostly seen with small perpendicular cracks also present. Usually these parallel cracks were near the centre of the particle and reduced closer to the edges. According to Paprika *et al.* (2007:4) a pressure build-up of volatile matter is the most severe in the centre of the particle. The volatile matter in these particles is also relatively large when compared to the available pore structure and therefore it can be stated that this fragmentation behaviour is probably due to volatile release stresses. This strengthens conclusions from Chirone & Massimilla (1988:267-277). Particles then also fragmented into two coarse fragments or three and more slices. This is also an indication that fragmentation due to volatile release stresses is present (Lee & No, 1994:442; Ragland & Bryden, 2011:459; Sasongko & Stubington, 1996:3911).

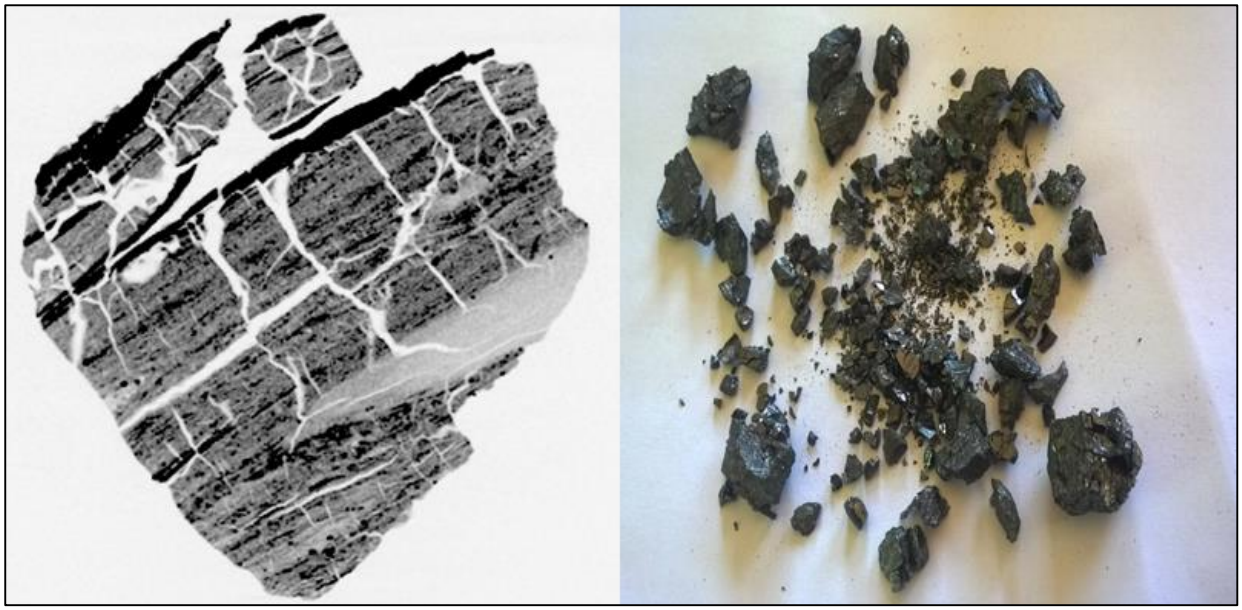

Figure 5.2: Fragmentation of low volatile samples heated to 900 °C (left hand side: tomogram after heating, right hand side: photograph after heating).

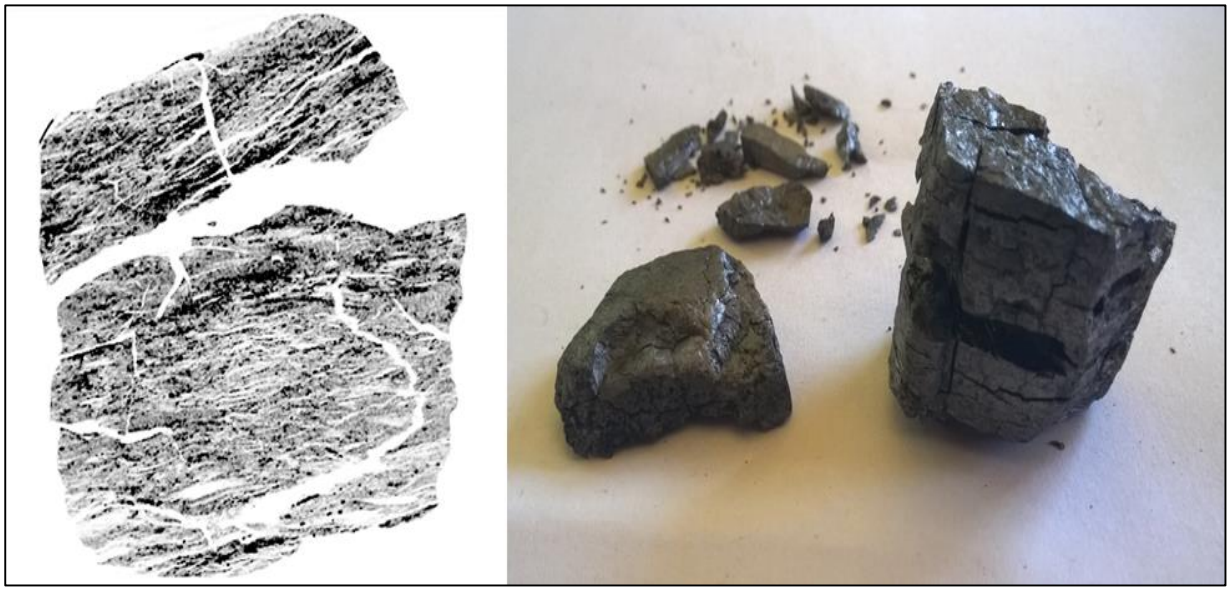

Figure 5.3: Fragmentation of high volatile samples heated to 900° C (Left hand side: tomogram after heating, right hand side: photograph after heating).

It can be assumed that the primary cause of fragmentation for the low volatile samples is thermal stresses and the primary cause for high volatile samples is volatile release stresses. The particle size, temperature and other coal characteristics beside volatile matter cannot be ignored as influential on the process. Their influence is considered in the next section in an attempt to establish a relationship between these factors and fragmentation parameters.

5.2 FACTORS INFLUENCING PRIMARY FRAGMENTATION

In Figure 5.4 the relationship between PRN and critical diameter for this study for particles heated to 900 °C is shown and compared to that from Dakič *et al.* (1989:916) for 850 °C. HV Coking was omitted from this relationship since the swelling of this sample caused large deviations in the data. It can be seen that there exists a good comparison between this study and that from Dakič *et al.* (1989:916) for PRN values ranging between 0 and 10. Due to the lack in variability of South African coalfields, PRN values larger than 10 could not be tested. The lower diameters for the low volatile samples are probably due to thermal stresses that are not accounted for in this relationship.

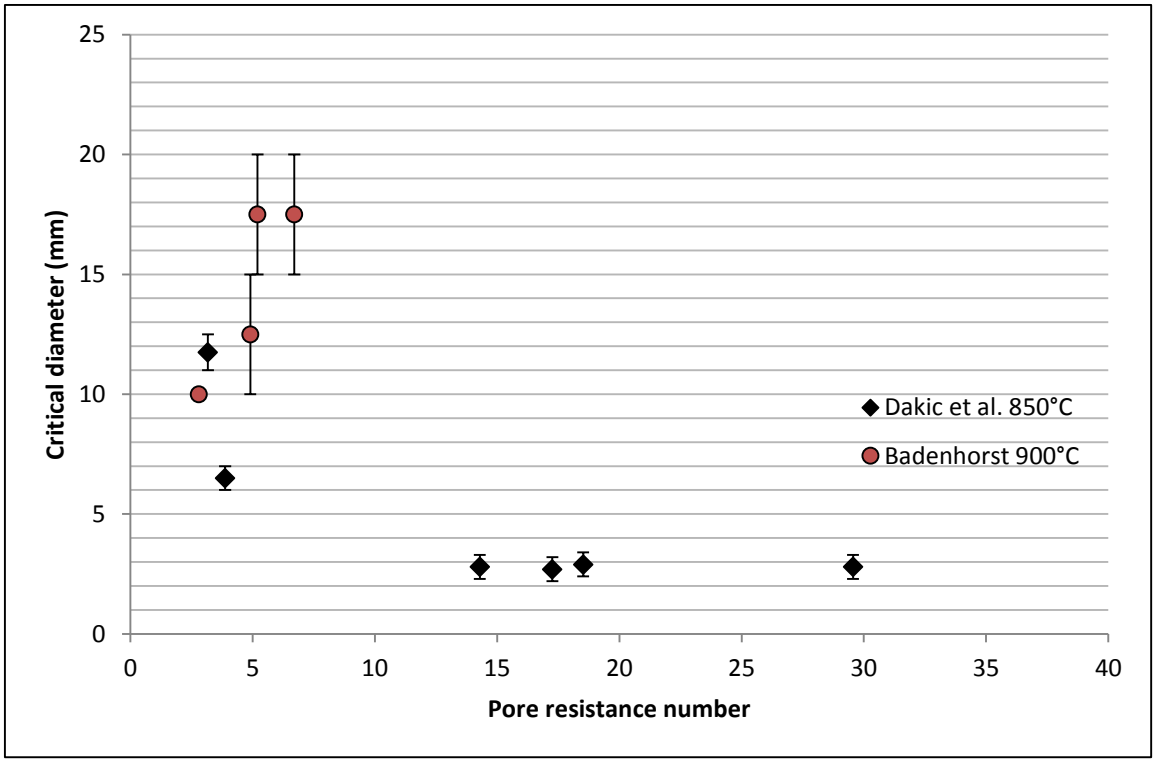

Figure 5.4: Critical diameter versus PRN for particles heated to 900 °C.

Overall, it can thus be concluded that the relationship proposed by Dakič *et al.* (1989:916) between PRN and critical diameter can be used to determine the critical diameters for South African coal samples at high temperatures. In the rest of this chapter the influence of coal characteristics, temperature and particle size on this relationship is discussed. Raw data and errors are given in Appendix D.

5.2.1 PARTICLE SIZE

In Table 5.1 the critical diameters are compared to literature values. The critical particle diameters for this study for 900 °C lay predominantly between 10 and 17.5 mm. In other words: 10 and 15 mm particles stayed intact while 20 mm and larger fragmented. This differs

from results obtained by Coetzee (2011:15) and Bunt & Waanders (2008:2856) which found a stable size of 25 mm. Coetzee (2011:46-48) tested South African bituminous coal heated to 900 °C and should thus have similar results than this study. The difference can be attributed to the fact that Coetzee (2011:46-48) followed a more visual approach when determining whether or not a particle fragmented, while for this study a more quantitative approach (in the form of breakage index) was followed. Shock heating can also be the reason for the differences. Chirone & Massimilla (1988:274) on the other hand tested non-swelling South African bituminous coal samples heated to 850 °C and found that all particles with sizes above 10 mm fragmented upon heating. For high volatile matter samples Dakič *et al.* (1989:913) found that the critical diameters of their samples (850 °C) are somewhere between 2 and 12 mm, and Peeler & Poynton (1992:429) stated that theirs (900 °C) are between 13 and 19 mm. The results of this study thus correspond to that of Chirone & Massimilla (1988:274), Peeler & Poynton (1992:429) and Dakič *et al.* (1989:913).

Table 5.1: Comparison between critical diameters for this study and those from literature.

Source	Temperature (°C)	Coal origin	Critical diameter (mm)
Badenhorst (2015)	900	SA high & low volatile	10-17.5
Coetzee (2011)	900	SA bituminous	25
Chirone & Massimilla (1988)	850	SA bituminous	3-10
Dakič *et al.* (1989)	850	Northern high volatile	2-12
Peeler & Poynton (1992)	900	High and low volatile	13-19
Bunt & Waanders (2008)	Turn-out sample	SA bituminous	25

Consider Figure 5.5. The average breakage indices for different size particles showed that an increase in particle size leads to an increase in fragmentation at all temperatures. It can be seen that, for LV1 particles heated to a temperature of 900 °C, a sudden decrease in breakage index (average) occurred between a size of 15 and 20 mm. Strangely enough this particular behaviour was seen for all five coals. A sudden decrease in breakage index was seen either between 15 and 20 mm or in some cases between 20 and 25 mm. This was not necessarily the critical diameter point but only the size where a drastic change in fragmentation was observed. Zhang *et al.* (2002:1838) made the same observation for their study between 4 and 5 mm particles, while Peeler & Poynton (1992:427) found that a sudden increase in fragments occurred at 19 mm. In Figure 5.6 a visual interpretation of this is shown. An increasing trend in fragmentation can be seen.

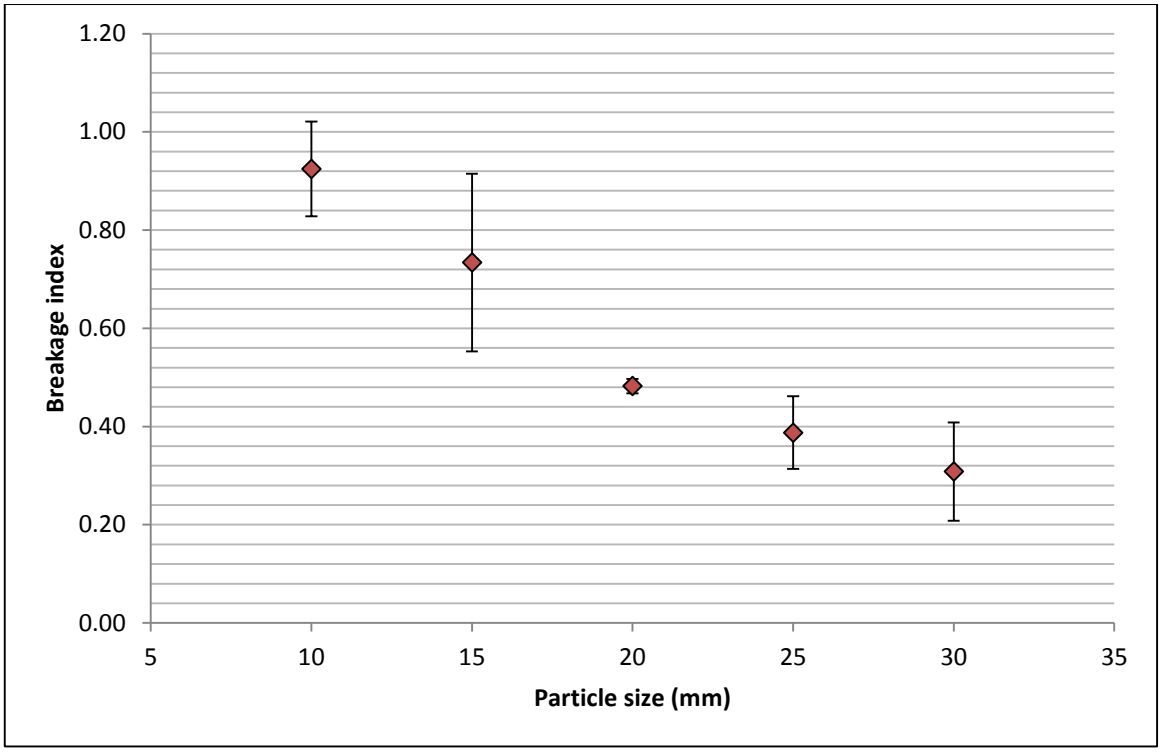

Figure 5.5: Influence of particle size on the breakage index for LV1 particles heated to 900 °C.

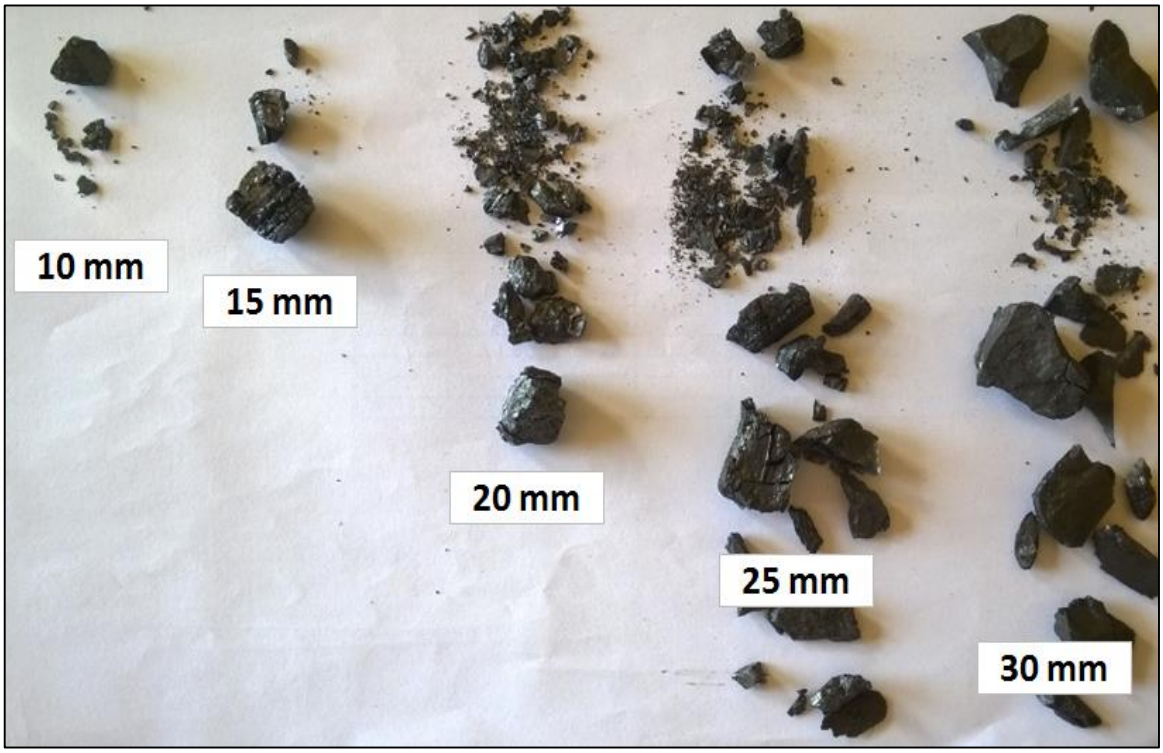

Figure 5.6: Influence of particle size on the breakage of LV2 samples heated to 900 °C.

5.2.2 COAL CHARACTERISTICS

In Table 5.2 the critical diameters at each temperature are given to aid in further discussion.

Table 5.2: Critical diameters at different temperatures for different coal samples.

	PRN			
Temperature (°C)	**2.8**	**4.9**	**5.2**	**6.7**
400	>30 mm	>30 mm	27.5 ± 2.5 mm	17.5 ± 2.5 mm
600	22.5 ± 2.5 mm	17.5 ± 2.5 mm	22.5 ± 2.5 mm	17.5 ± 2.5 mm
900	<10 mm	12.5 ± 2.5 mm	17.5 ± 2.5 mm	17.5 ± 2.5 mm

HV Coking was emitted since the excessive swelling of this sample led to large deviations in the data. The influence of volatile matter and porosity, moisture and ash yields, swelling behaviour and maceral composition on the fragmentation behaviour is investigated separately. Take also note that only five coal samples were tested and therefore there exists a great uncertainty in the results discussed in this section.

5.2.2.1 Volatile Matter & Porosity

From Table 5.2 it can be seen that, for particles heated to 400 °C a decrease in critical diameter exists with an increase in PRN. The decreasing trend can be explained when remembering that PRN represents the relationship between volatile matter and porosity. The larger the PRN the more volatile matter relative to pore space exists, and the pressure build-up of volatiles in the pore network would thus be more than for a sample with a low PRN, causing more fragmentation and thus a lower critical diameter. Fragmentation for particles heated to 400 °C is thus most probably caused by volatile release stresses for all the samples.

The smaller diameters for the low volatile samples heated to 600 and 900 °C can be attributed to thermal stresses and the decreasing relationship is thus not as evident as for the samples heated to 400 °C. In the study conducted by Dakič *et al.* (1989:911-916) coal samples with volatile matter ranging approximately between 23-45 equilibrium wt.% were heated to 850 °C. They did not test any low volatile (anthracite) samples as in this study and, according to Senneca *et al.* (2011:2936) coal with low volatile matter have rigid structures and high thermal conductivities and therefore the heating rates for these samples are much higher than for high volatile samples and the thermal induced stresses are thus more severe. The ratio of volatile matter to porosity is also small and volatile release stresses will be a minimum. He *et al.* (2007:159) also found that, for their anthracite samples, fragmentation

increased with a decrease in PRN and it can thus also be concluded that this is possibly due to a thermal shock. Combine this with the fact that the centre of these low volatile particles usually stayed intact, while a large portion of the outer core of the particles fragmented into a multitude of pieces, it is almost certain that a thermal shock induced fragmentation in these particles.

It was found that the type of pore structure had no influence whatsoever on the fragmentation behaviour (more samples should however be tested before this statement can be accepted). LV2 which have more ink shape or irregular pores should have fragmented more than HV Coking, which have a more open pore structure (see Chapter 4). This was however not always the case. For future studies, it is recommended that a more thorough investigation on the pore structure should be done to see what influence it will have on the fragmentation behaviour. It is also recommended that the pore structure developing with heat treatment, and not only the original pore structure, should be investigated since it can also have an influence on fragmentation behaviour.

5.2.2.2 Moisture Content & Ash Yield

No correlation between inherent moisture content and fragmentation was found for this study. This opposes observations made by Beukman (2009:46) and Van Dyk *et al.* (2001:6) but corresponds to that from Dacombe *et al.* (1999:1850). The reason for this can be that, in this study and the study conducted by Dacombe *et al.* (1999:1850) coal samples with low moisture contents were used, while Beukman (2009:46) used lignite coal. Van Dyk *et al.* (2001:6) also stated that the results they obtained included moisture trapped inside the pores of the samples. In Chapter 4, it was shown that the equilibrium moisture corresponds to the porosity and that it is the porosity, and not the moisture, which causes the fragmentation. An interesting future study will be to test the influence of moisture more thoroughly and to test if more fragmentation will take place when the samples are additionally wetted as attempted by Chirone *et al.* (2010:4). More samples should also be tested before any definite conclusions can be made.

There exists a relationship between the ash yield and density of coal. From Chapter 4 it can be seen that the ash yields (with the exception of HV Coking) are similar and low, and therefore not really a variable for this study. Van der Merwe (2010b:66) stated that coal with higher densities have a more dense pore network structure and are thus more prone to undergo fragmentation due to a pressure build-up. High densities in this case represent particles with densities above 1600 kg/m^3. Since all the coal samples in this study have densities below 1600 kg/m^3 it can be concluded that density will not have that great of an influence on the fragmentation behaviour for this study. More samples, however, should be

tested before any conclusions can be made. Finally, it can be concluded that if image analysis is done on ash samples some information on the size distribution can be obtained.

5.2.2.3 Swelling

HV2 and HV Coking have crucible swelling numbers of 0.5 and 5.0 respectively, while the other samples do not swell. At certain temperatures the swelling of these coal samples was able to relieve stresses caused by volatile release. The particles thus rather swelled than fragmented, leading to higher critical diameters than expected. This observation was also made by Stubington & Linjewile (1989:159). For HV2 it was seen that, for particles heated to 600 °C the breakage indices were higher than for 400 and 900 °C, while for HV Coking swelling was present at all three temperatures. The reason for swelling not having an influence for HV2 particles heated to 400 °C is that swelling has not really commenced yet and was not able to relieve pressure build-up. For particles heated to 900 °C swelling was not able to relieve volatile build-up and thermal stresses and fragmentation was present.

The fragments that did form in HV Coking particles heated to 900 °C were “boat”-shaped and shell-shaped as shown in Figure 5.7. Boëlle *et al.* (2002:13) stated that the plasticity behaviour of coal caused it to fragment like this. From the figure, it can also be seen that some fragments fused into each other. This is probably due to agglomeration. More on the influence of swelling on fragmentation is discussed in the section dealing with the influence of temperature.

Figure 5.7: Influence of fragmentation on HV Coking particles heated to 900 °C.

5.2.2.4 Petrography

According to Chen *et al.* (1994:137) the brittle nature of vitrinite enhances primary fragmentation due to thermal stresses, while fusinite constrains it. In Chapter 4, the ratio between these two properties (maceral ratio) was determined to see whether this ratio would explain fragmentation better than the PRN ratio. The only relationship found was for particles heated to 900 °C as seen from Figure 5.8 (HV Coking was omitted due to the large variation in data). In this figure, the critical diameters of the samples versus their maceral ratios are shown. It can be seen that a decreasing relationship is present. It was then also found that a multitude of fragments formed for the low volatile samples (maceral ratios of 0.8 and 0.9) and those particles that did not swell at 900 °C for HV2 (ratio of 0.7) also formed a lot more fragments than HV1 (ratio of 0.2). This multitude of fragments that formed can be ascribed to thermal stresses. The maceral ratios at high temperatures can thus be used partially to describe fragmentation due to thermal stresses. More research on this topic is, however, necessary, and it is recommended that it should be looked into for future studies.

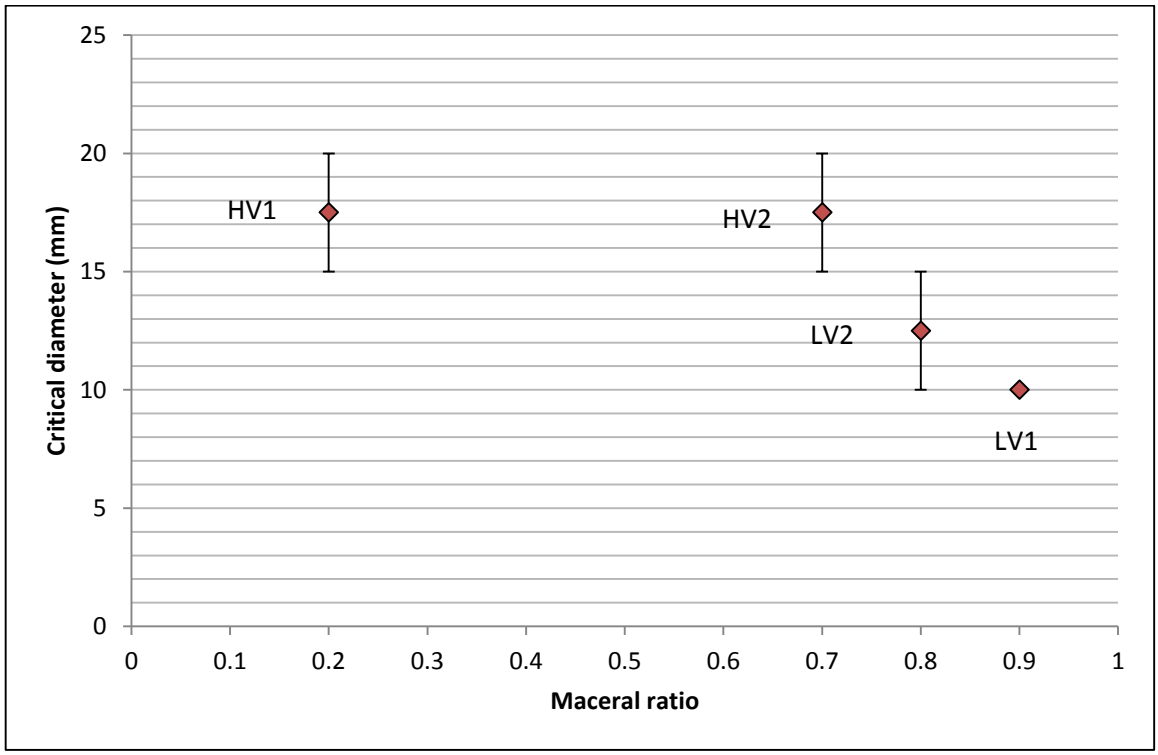

Figure 5.8: Critical diameters versus maceral ratios for samples heated to 900 °C.

For particles heated to 400 and 600 °C, no relationship was found between maceral ratio and critical diameter. A possible explanation for this is found from research done by Stanmore *et al.* (1996:3272). Stanmore *et al.* (1996:3272) stated that fragmentation increases with vitrinite content but also observed that the fissures that formed in the vitrinite bands, due to a thermal shock, were able to release pressure build-up since more openings

are created in which volatile matter can escape the particles. This makes sense seeing that the fissures formed in the vitrinite due to a thermal shock for particles heated to 400 and 600 °C is not that sever to fragment the particles on their own, but are still able to relieve the internal pressure of volatile matter that builds-up in a particle's pore network.

5.2.3 TEMPERATURE

In Figure 5.9 the relationship between PRN and critical diameter for Dakič *et al.* (1989:916) at 850 °C and this study at 400 °C is shown. From the figure, it can be seen that the relationship between critical diameter and PRN shifted upwards with a lowering in temperature. This corresponds to the prediction made by Liu *et al.* (2009:513) with their forecasting model for quartz particles in which it was found that the critical diameter is lower at higher temperatures. This makes sense when looking at the volatile loss quantities of the samples at the different temperatures (see Chapter 4). From Chapter 4 it is evident that, at higher temperatures, more volatile escapes from the samples. Therefore fragmentation due to a volatile pressure build-up will be more severe in these particles than particles exposed to lower temperatures. The thermal conductivities of coal samples also increase tremendously with temperature as proven by researches such as Kosowska-Golachowska *et al.* (2014:10) and Chen *et al.* (2012:93). The temperature gradients, and therefore the thermal stresses present in the particles at high temperatures, are thus more severe than at low temperatures and fragmentation increases greatly.

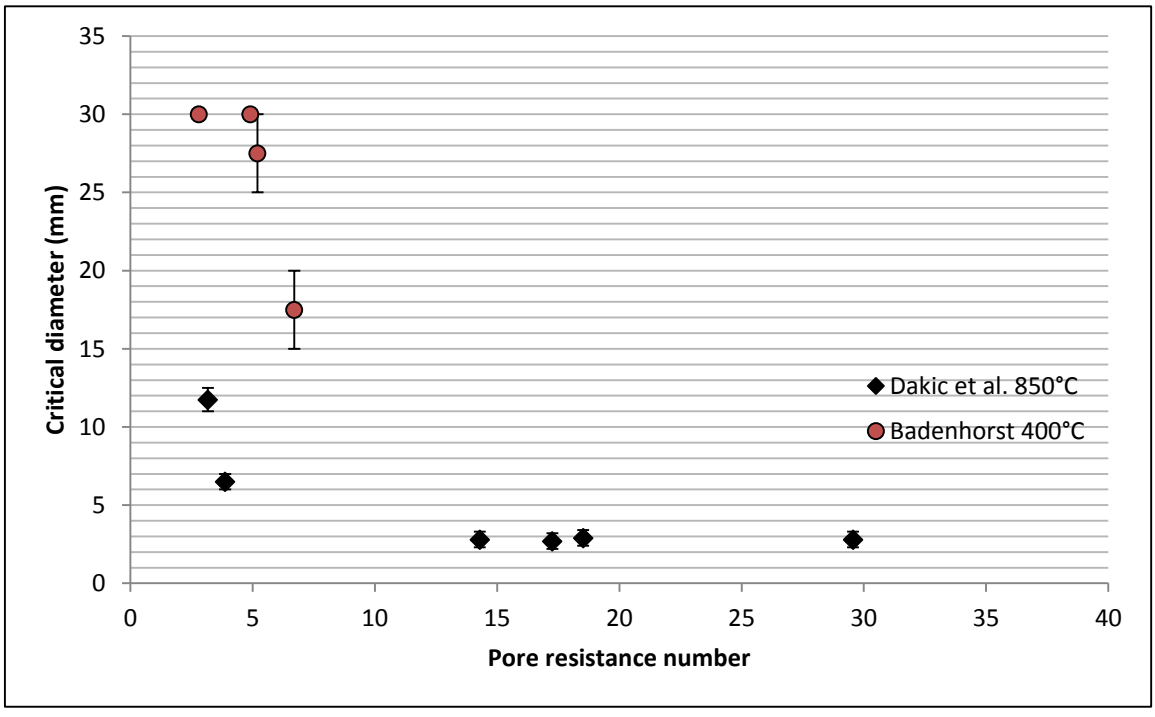

Figure 5.9: Critical diameter versus PRN for particles heated to 400 °C.

One should however be careful when describing the influence of temperature on fragmentation, especially for swelling coal samples. In Figure 5.10 the breakage index versus temperature data for a slightly swelling (HV2), as well as a non-swelling (HV1) sample is shown. It can be seen that, for the non-swelling sample, the average breakage index decreases with an increase in temperature, while for the swelling sample the breakage index increases from 400 to 600 °C and then decreases from 600 to 900 °C (take note, however, of the confidence intervals based on a 95% confidence level). The reason for this can be that, for the particles heated to 600 °C, swelling was able to relieve the pressure build-up of volatile matter in the pore network and therefore prevented or lowered fragmentation. This statement was confirmed by Stubington & Linjewile (1989:159) in their study. For particles heated to 900 °C the volatile release and thermal stresses were too harsh and swelling was not able to prevent excessive fragmentation. Boëlle *et al.* (2002:13) stated that this is due to the re-solidified layer formed during swelling, which is weak and fragments easily. Senneca *et al.* (2011:2937) believes it is the cenosphere type of structure of the swelling samples (with thin and weak walls) that enhances fragmentation. This is then also probably the reason why Dakič *et al.* (1989:916) found relative low critical diameters for their swelling samples heated to 850 °C.

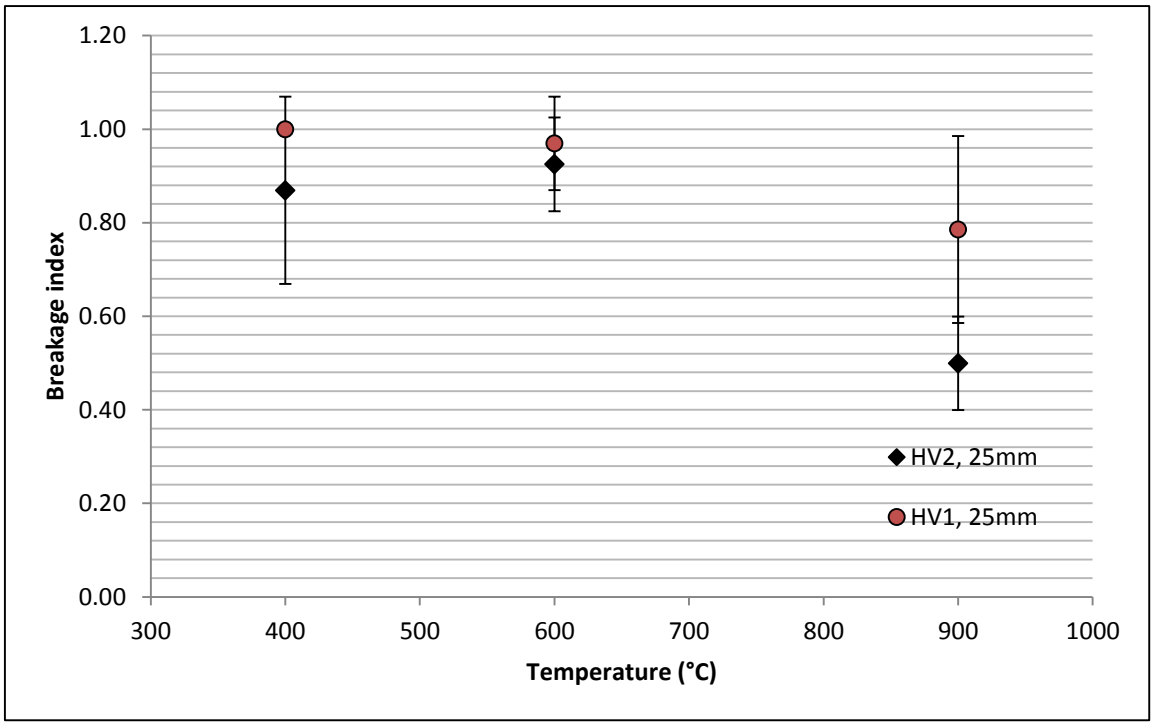

Figure 5.10: Breakage index versus temperature for a 25 mm non-swelling and swelling coal sample.

When viewing only the non-swelling samples a definite difference in fragmentation with temperature can be seen in the low volatile samples (LV1 and LV2). In Figure 5.11 the breakage typically obtained in low volatile samples at different temperatures is shown. For

particles heated to 400 °C little to no fragmentation was present. Even the 30 mm particles had breakage indices of 1.00 ± 0.00 for LV1 and 0.99 ± 0.02 for LV2. This is because at this temperature the samples lost only 0.8 and 3.1 wt.% volatiles respectively, which is very small when compared to the available pore structure. Fragmentation due to a pressure build-up was thus not an issue and temperature gradients at this temperature were not that severe to cause any noticeable breakage. At 600 °C, fragmentation increased a little with breakage indices for the 25 mm particles changing to 0.95 ± 0.07 and 0.87 ± 0.25 respectively for LV1 and LV2. This change can be ascribed to the increase in volatile release as well as the thermal stresses starting to take effect on the samples. For particles heated to 900 °C a sudden increase in fragmentation was observed with breakage indices as low as 0.22 ± 0.05. A multitude of small fragments formed from the outer core of the particle, while the inner core stayed partially intact. This behaviour is due to thermal stresses as stated by Senneca *et al.* (2013:254-257). The fact that low volatile coal samples usually have rigid structures and high thermal conductivities also contributes to this statement.

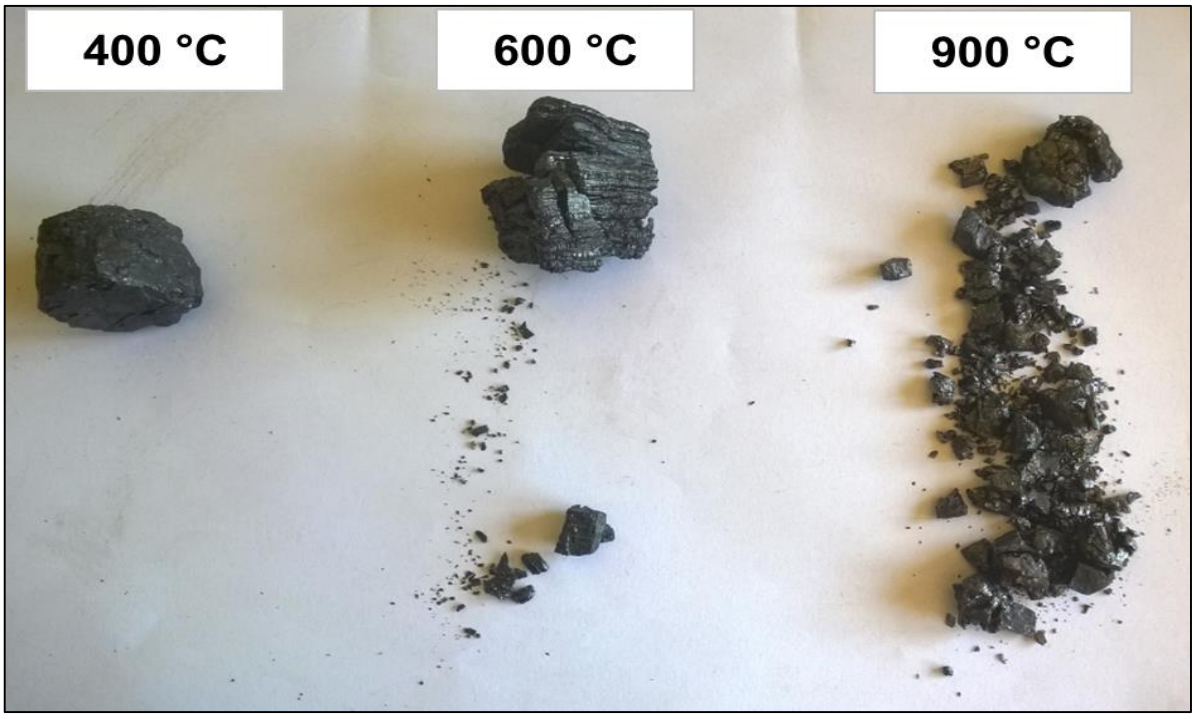

Figure 5.11: Typical breakage behaviour for low volatile samples at different temperatures.

In Figure 5.12 the breakage for HV1, which is the only non-swelling high volatile sample, is shown. It can be seen that fragmentation was present at all three temperatures. A small increase in fragmentation was seen with an increase in temperature with breakage indices of 1.00 ± 0.00, 0.97 ± 0.07 and 0.79 ± 0.16 at 400, 600 and 900 °C respectively for 25 mm particles. The fragmentation is most probably due to volatile release stresses since the

volatile loss percentages at the different temperatures are relatively high compared to the available pore network structure.

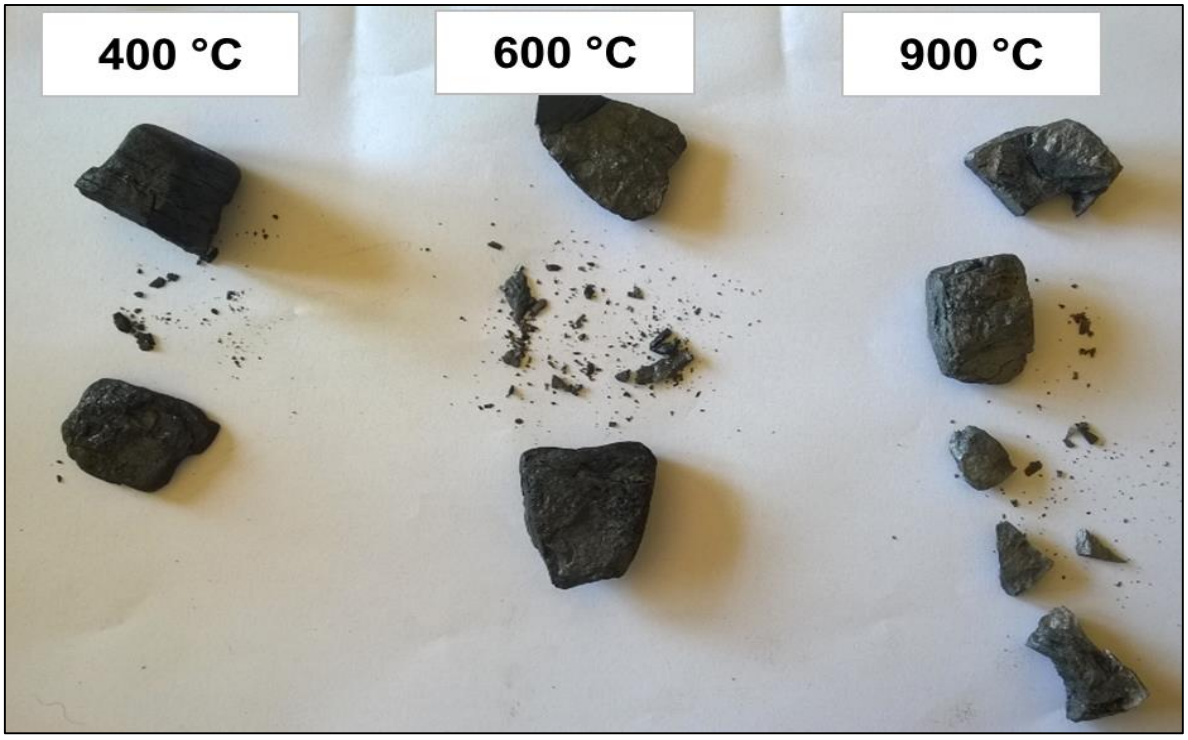

Figure 5.12: Typical breakage behaviour for HV1 heated to different temperatures.

5.3 SUMMARY

The most important results obtained from this chapter are summarised below:

- New cracks formed on already existing fissures, especially between coal-mineral interfaces;
- Fragmentation in low volatile samples are predominantly caused by thermal stresses;
- Fragmentation in high volatile samples are predominantly caused by volatile release stresses;
- A good correlation exists between the critical diameter relationship of Dakič *et al.* (1989:916) at 850 °C and this study at 900 °C (for PRN values ranging between 0 and 10), resulting in the conclusion that the proposed relationship can be used on South African coal samples close to these temperatures;
- The extent of breakage increases with an increase in particle size;

- The critical diameters found in this study correspond to literature results;

- Swelling for particles heated to 600 °C was able to relieve volatile release stresses and thus fragmentation in HV2 particles;

- Swelling was not able to relieve stresses, and thus fragmentation for particles heated to 900 °C;

- For particles heated to 900 °C the maceral ratio predicted the fragmentation in the coal particles relatively well, while at lower temperatures this was not the case;

- Fragmentation increased with an increase in temperature except for swelling samples were the swelling was able to relieve fragmentation at 600 °C;

- For particles heated to 400 °C the PRN versus critical diameter curve shifted upwards when compared to the curve at 900 °C;

- In Table 5.3 a summary is given to indicate what caused fragmentation (thermal stresses or volatile release stresses) at which temperature and why. The particle size was not incorporated into this table. The data for particles heated to 900 °C is important since, at this temperature, pyrolysis is almost complete.

Table 5.3: Summary of fragmentation for different coals at different temperatures.

Temperature (°C)	LV1	LV2	HV1	HV2	HV Coking
400	**No Fragmentation** Low volatile loss % Limited thermal stresses	**No Fragmentation** Low volatile loss % Limited thermal stresses	**Volatile release** High volatile loss % Limited thermal stresses	**Volatile release** High volatile loss % Limited thermal stresses	**Swelling & Volatile release** High volatile loss % Limited thermal stresses
600	**Thermal stresses** Rigid structure High thermal conductivity Low volatile loss % Exfoliation>fragments	**Thermal stresses** Rigid structure High thermal conductivity Low volatile loss % Exfoliation>fragments	**Volatile release** High volatile loss % Limited thermal stresses	**Swelling & Volatile release** High volatile loss % Limited thermal stresses	**Swelling & Volatile release** High volatile loss % Limited thermal stresses
900	**Thermal stresses** Rigid structure Inner core intact Multitude of fragments High thermal conductivity Low volatile loss % High vitrinite content	**Thermal stresses** Rigid structure Inner core intact Multitude of fragments High thermal conductivity Low volatile loss % High vitrinite content	**Volatile release** High volatile loss % Low vitrinite content	**Volatile & thermal stresses** High volatile loss % High vitrinite content	**Swelling, Volatile & thermal stresses** High volatile loss % High vitrinite content

CHAPTER 6: CONCLUSION & RECOMMENDATIONS

The aim of Chapter 6 is to summarise the study "*Primary fragmentation of large coal particles*". A conclusion is given and recommendations to improve the study are stated.

6.1 CONCLUSION

"What is the extent and nature of primary thermal fragmentation on large (5 to 30 mm) coal particles?" To answer this research question 10, 15, 20, 25 and 30 mm particles from five different South African coal origins were shock heated to 400, 600 and 900 °C respectively. The objectives were to determine crack extent, nature and placement behaviour, as well as determining the influence of different factors (size, temperature and origin) on the primary fragmentation of the coal particles. A relationship between particle size, temperature, origin and fragmentation was also pursued. An inert horizontal tube furnace and tomography were used as experimental equipment.

6.1.1 COAL CHARACTERISTICS

From the proximate results it was found that two low volatile and three high volatile samples were present in the chosen coal origins. Hence the name convention: LV1, LV2, HV1, HV2 and HV Coking. It was found that volatile loss percentages for particles heated to 600 and 900 °C were very close to the initial volatile matter, while for 400 °C very little volatiles escaped from the particles. It was thus expected that fragmentation due to a volatile release would be more severe at high temperatures than at low temperatures.

The porosity of each of the coals was compared to its equilibrium moisture content. It was found that a linear relationship between porosity and equilibrium moisture exists with a R^2 of 0.6 and a slope value of 1.1. Equilibrium moisture can thus be used instead of porosity when determining the available pore space for volatiles to transport through. The pore resistance numbers (ratio of volatile matter to equilibrium moisture) for this study where then determined as: 2.8 and 4.9 for the two low volatile samples, and 5.2, 6.7 and 11.2 for HV1, HV2 and HV Coking respectively.

From the CSN and RI tests, it was found that HV2 and HV Coking both showed the ability to swell. HV2 had a CSN of 0.5 and HV Coking a CSN of 5.0. The CSN increased with an increase in PRN. It was also found that swelling in particles heated to 900 °C was limited, while for 400 and 600 °C swelling was more pronounced.

From the petrography analysis, it was seen that the vitrinite contents and maceral ratios were high for the swelling samples, as well as the low volatile samples, while that for HV1

(non-swelling, high volatile sample) was relatively low. It was thus expected that thermal stresses will have a more pronounced influence on the low volatile samples than on the high volatile samples.

Lastly, the three high volatile samples were classified as medium volatile bituminous, while the low volatile samples were classified as semi-anthracite and low volatile bituminous respectively.

6.1.2 Causes of Primary Fragmentation

Micro-focus X-ray tomography was used to determine crack extent, nature and placement behaviour. From the tomography scans taken before any heat treatment was applied, small cracks can be seen throughout the particle volume. These cracks are either natural cleats or fissures formed due to handling. The latter can be distinguished as the small and thin cracks near the edges of the particle.

Upon heating, new cracks formed or propagated from these initial cracks. The cracks that formed were well structured and orientated either perpendicular or parallel to the bedding planes. Many of these structured cracks could be seen for the low volatile coal samples, while for the high volatile samples mainly cracks parallel to the bedding planes were seen with a few perpendicular cracks also present. The low volatile samples fragmented into a multitude of small pieces from the outer core of the particle due to thermal stresses. The high volatile samples fragmented into two or more coarse pieces due to volatile release stresses.

6.1.3 Factors Influencing Fragmentation

When comparing PRN versus critical diameter data for this study to that of Dakič *et al.* (1989:916) a good correlation was found for PRN values between 0 and 10. Overall it was concluded that the relationship proposed by Dakič *et al.* (1989:916) can be used to determine the critical diameters for South African coal samples at high temperatures. The low critical diameters for the low volatile samples were ascribed to thermal stresses.

When looking at the influence of size, it was found that fragmentation increased with an increase in particle size. For particles heated to 900 °C critical diameters between 10 and 17.5 mm (± 2.5 mm) were obtained, which corresponds to critical diameters obtained from literature. It was also found that, for particle sizes between 15 and 25 mm a change in fragmentation behaviour could be seen when heated to 900 °C for all five coal origins. This was not necessarily the critical particle diameter but just the point where fragmentation reduced or changed suddenly.

Coal origin had a very complex but significant influence on the breakage results. At high temperatures, thermal stresses controlled the fragmentation behaviour in the low volatile samples, while volatile release stresses were the main cause of breakage in high volatile samples. Moisture and ash yield had a limiting effect while swelling played a huge role in the fragmentation behaviour of the particles tested in this study. For HV2 particles heated to 600 °C swelling was able to relieve the pressure build-up of volatiles and thus prevent fragmentation. The stresses for particles heated to 900 °C were however too severe and swelling was not able to reduce fragmentation at this temperature. The fragments that formed when heated to 900 °C for HV Coking were largely “boat-shaped” and were ascribed to its plasticity nature. An important result obtained, and that should be further investigated, is the influence of petrography characteristics on the fragmentation behaviour. It was found that at low temperatures (400 and 600 °C) fractures that formed in the vitrinite bands due to thermal stresses facilitated volatile release and fragmentation was prevented to a certain extent. For particles heated to 900 °C thermal stresses were too severe and the brittle nature of the vitrinite bands enhanced rather than limited fragmentation. Therefore: at 900 °C an increase in vitrinite content led to an increase in fragmentation.

When looking at the influence of temperature it was found that a decrease in temperature leads to the PRN curve shifting upwards. A decrease in temperature thus leads to a decrease in fragmentation. This, however, pertains for non-swelling samples. For HV2 (a slightly swelling sample) fragmentation was less for 600 °C than for 400 and 900 °C due to swelling being able to relieve volatile release stresses at this temperature. When looking at the non-swelling samples only, it was concluded that for HV1 (a high volatile sample) volatile release stresses were the main cause of fragmentation at all three temperatures. For the two low volatile samples, fragmentation was absent or limited for particles heated to 400 and 600 °C, while for 900 °C thermal stresses dominated the fragmentation of these samples resulting in the particles fragmenting into a multitude of small pieces.

6.1.4 Applicability of Results

It can be stated that coal selection and particle size optimisation would reduce pressure losses in fixed-bed gasifiers. The information needed for coal and particle size optimisation can be obtained, or the building blocks to obtain it, from this dissertation. Information was obtained by:

a) Studying crack extent, nature and placement in a particle to obtain sufficient data to, at the end of the day, establish a model similar to that of Paprika *et al.* (2013:5488-5494) to predict fragmentation in a fixed bed-gasifier; and

b) Relating particle size, temperature and coal type with fragmentation, through PRN and critical diameter, to see if this can be used to optimise particle size and coal type selection in a South African fixed-bed gasifier.

It was found that cracks initiate from already existing cracks and are dominant between coal-mineral interfaces. For the high volatile samples cracks propagated parallel to the bedding planes and the particles fragmented into large, coarse pieces. For the low volatile samples thermal stresses prevailed in the outer core of the particles and a multitude of fragments formed from here while the inner core stayed partially intact. Although this information is not enough for a detailed model on fragmentation it still gives some building blocks for future work to be built on. It is recommended that for future studies crack propagation should be investigated more thoroughly (direction of growth, merging of cracks, quantifying etc.) and a model outline should be constructed.

A relationship was found between fragmentation, particle size, coal type and temperature (PRN versus critical diameter versus temperature) for South African coal particles. It is however suggested that more coal types should be tested since not enough samples were used to make definite conclusions. It was found that at 900 °C the critical diameters were relatively low for the low volatile samples resulting in a multitude of fragments forming for these particles (due to thermal stresses). Fragmentation problems will thus be severe in fixed-bed gasifiers if low volatile samples are implemented. For the high volatile samples fragmentation due to volatile release stresses was dominant and at 900 °C the critical diameters ranged between 15 and 20 mm for these samples. It was also found that a drastic change in the severity of fragmentation occurs between 15 and 25 mm. All particle sizes larger than 25 mm will thus probably fragment severely for high volatile samples. Since the maximum size tested in this study was 30 mm it is also suggested that sizes larger than this should be tested, especially since the typical maximum feed size for a fixed-bed gasifier is 65 mm (Bunt 7 Waanders, 2008: 2857).

6.2 RECOMMENDATIONS

Some ideas for future studies in thermal fragmentation, as well as improvements on the research conducted in this dissertation are now given:

- In Chapter 5 it was seen that vitrinite content and maceral ratio had an influence on thermal stress induced fragmentation. It is recommended that the influence of vitrinite and other petrographic properties on thermal fragmentation should be investigated in the future;

- The pore structure (ink-shaped pores, etc.) of a coal sample can aid in understanding fragmentation due to volatile release stresses. The PRN should also be obtained for different thermal conditions by considering the volatile loss and the developing pore structure at each temperature;

- In this study a narrow range of PRN values were tested and only a limited part of the PRN versus critical diameter correlation could be tested. For future studies it is recommended that a broader range of PRN values should be tested;

- In this dissertation, the MIP technique was used to determine the porous structure of the samples. MIP has many disadvantages as stated in Chapters 3 and 4. A better option to measure the porosity might be the Small Angel X-Ray Scattering (SAXS) technique, if available. This technique however can only be applied on thin coal slices of about a millimetre;

- It is recommended that smaller size particles, as well as larger size particles than used in this study, should be tested to narrow the critical particle diameters of the samples and predict the critical diameters more accurately;

- Since ash yield was not varied in this study, its influence on fragmentation is unknown. In the literature study a few observations regarding ash yield and fragmentation were made but still not investigated thoroughly;

- Chirone *et al.* (2010:4) observed that bituminous coal, when wetted, has a higher fragmentation severity than normal, while there is no difference between wet and normal anthracite. An interesting study will be to vary the saturation percentages of bituminous and anthracite samples respectively (and other rank samples for that matter) to determine the influence of moisture on the primary fragmentation of coal particles;

- Sreekanth (2014:505-507) used “time of fragmentation” to determine the thermal shock and volatile pressure build-up behaviour of their wood particles. Thermal shock would be dominant in the first time instances, while volatile release stresses will catch up later. Time of fragmentation can also be used to estimate the time period in which fragmentation occurs (Sreekanth, 2014:505);

- In this dissertation, spherical-like particles were used in experimentation. The shape of the particle will have an influence on the fragmentation behaviour as proven by Chirone & Massimilla (1988:273). Instead of spherical particles cylindrical and cubic particles (or any shape for that matter) can also be tested and compared to the fragmentation behaviour of the spherical particles;

- In the literature study, the influence that the type and concentration of different volatile gases in a coal particle have on fragmentation was discussed. Further experimentation can be done in which the influence of these gases can be tested;

- An in depth study can be done in which the influence of the minerals and macerals on fragmentation can be tested, as done by Tian (2011:82-85). He *et al.* (2007:157-162) also determined the influence of different lithotypes on fragmentation;

- Research on secondary fragmentation is even scarcer than research on primary fragmentation. Some studies on secondary fragmentation include those done by Liu *et al.* (2000:627-633); Mitchell & Akanetuk (1996:3137-3144); Pinho (2006:147-155); and Tilghman & Mitchell (2013:2461-2469);

- For future studies it is recommended that the PRN should be obtained at different temperatures where swelling starts to influence the fragmentation behaviour of coal;

- A gap in fragmentation research (both primary and secondary fragmentation, as well as mechanical fragmentation) exists regarding the modelling of fragmentation during gasification. This research is industrially relevant and is the focus of most papers. The crack extent, nature and placement results obtained from this study can be used in a similar manner as done by Paprika *et al.* (2013:5488-5494) to model primary fragmentation of South African coal in a fixed-bed gasifier;

- For future studies crack propagation should be investigated more thoroughly (direction of growth, merging of cracks etc.); and

- Particle size distribution after fragmentation is also important and it should be examined in future.

REFERENCES

Ammendola, P., Chirone, R., Miccio, F., Ruoppolo, G. & Scala, F. 2010. Attrition of bed materials and fuel pellets for fluidized bed gasification application. Paper presented at The 13th International Conference on Fluidization – new Paradigm in Fluidization Engineering, Gyeong-ju, 16-21 May. Date of access: 28 September 2015.

Badenhorst, C.J. 2013. Study on the thermal fragmentation behaviour of coal by using tomography. Potchefstroom: North-West University. (Mini dissertation – Honours).

Beukman, M.T. 2009. Coal pyrolysis modelling and the influence of pyrolysis conditions on char reactivity for large particles. Potchefstroom: North-West University. (Dissertation – Masters).

Boëlle, A., Qian, M., Jaud, P., Chirone, R., Salatino, P., Winter, F., Liu, X., Olsson, D., Amand, L., Leckner, B., Brunello, S., Na, Y. & Yue, G. 2002. Coal comminution characterization for industrial scale circulating fluidized bed. (A research program in the frame of the International Energy Agency implementing agreement for co-operation in the field of fluidized bed conversion of fuels applied to clean energy production. EDF Research & Development department).

Bunt, J.R. 2006. A new dissection methodology and investigation into coal property transformational behaviour impacting on a commercial-scale Sasol-Lurgi MK IV fixed-bed gasifier. Potchefstroom: North-West University. (Thesis – PhD).

Bunt, J.R. 2014. Coal heterogeneity. Potchefstroom: NWU, Potchefstroom Campus. (Coal Chemistry Course).

Bunt, J.R. & Waanders, F.B. 2008. An understanding of lump coal physical property behaviour (density and particle size effects) impacting on a commercial-scale Sasol-Lurgi FBDB gasifier. *Fuel,* 87 (2008): 2856-2865.

Campbell, Q.P., Viljoen, J., Le Roux, M. & Matthews, J.P. Micro-focus X-Ray computed tomography. *Inside Mining,* 2 (2014): 22-25.

Chen, W., Nagarajan, G. & Zhang, Z. 1994. Stochastic modeling of devolatilization-induced coal fragmentation during fluidized-bed combustion. *Ind. Eng. Chem.,* 33 (1994): 137–145.

Chen, Q., Dai, G., Zhang, G., Fan, X. & Qin, R. 2012. Experimental study on thermo physical parameter of loose coal bulk. *AGH Journal of Mining and Geoengineering,* 36 (3): 89-98.

Chirone, R. & Massimilla, L. 1988. Primary fragmentation of a coal in fluidized bed combustion. Paper presented at the Twenty-Second Symposium (International) on Combustion/The Combustion Institute, Seattle, Washington, 14-19 August.

Chirone, R., Senneca, O., Cumbo, D. & Russo, S. 2010. Relevance of primary fragmentation of coal particles during isotherm combustion conditions. (Unpublished).

Coetzee, G.H. 2011. The influence of particle size on the steam gasification kinetics of coal. Potchefstroom: North-West University. (Dissertation – Masters).

Coetzee, S., Neomagus, H.W.J.P., Bunt, J.R., Strydom, C.A. & Schobert, H.H. 2014. The transient swelling behaviour of large (-20 + 16mm) South African coal particles during low-temperature devolatilisation. *Fuel,* 136 (2014): 79-88.

Cui, Y. & Stubington, J.F. 2001. In-bed char combustion of Australian coals in PFBC. 3. Secondary fragmentation. *Fuel,* 80 (2001): 2245-2251.

Cui, Z., Han, X., Jiang, X. & Liu, J. 2009. Experiment and neural network model of primary fragmentation of oil shale in fluidized bed. *Oil Shale,* 26 (2): 114-124.

Cui, T., Zhou, Z., Dai, Z., Li, C., Yu, G. & Wanf, F. 2015? Primary fragmentation characteristics of coal particles during rapid pyrolysis. *Energy Fuels* (In press).

Dacombe, P., Pourkashanian, M., Williams, A. & Yap, L. 1999. Combustion-induced fragmentation behaviour of isolated coal particles. *Fuel,* 78 (1999):1847-1857.

Dakič, D., Van der Honing, G. & Valk, M. 1989. Fragmentation and swelling of various coals during devolatilization in a fluidized bed. *Fuel,* 68 (1989): 911-916.

De Korte, G.J. 2000. Moisture in coal: Its occurrence, its implications and some of the problems met in practice. (Report No. 16 of 1969 edited on 13 July 2000. Fuel Research Institute of South Africa).

Department of energy see South Africa.

Du Preez, S.M. 2012. The influence of minerals on the moisture adsorption and desorption properties of South African fine coal. Potchefstroom: North-West University. (Dissertation-Masters).

Du Toit, GJD. 2013. The influence of CO_2 on the steam gasification rate of a typical South African coal. Potchefstroom: North-West University. (Dissertation – Masters).

Everson, R., Koekemoer, A., Bunt, J., Neomagus, H. & Schwarz, C. 2013. Detailed characterization of South African high mineral matter inertinite-rich coals and density fractions and effect on reaction rates with carbon dioxide: Macerals, microlithotypes, carbominerites and minerals. *South African Journal of Chemical Engineering,* 18 (1): 1-16.

Felder, R.M. & Rousseau, R.W. 2005. Elementary Principles of Chemical Processes. 3rd edition. Hoboken, NJ: John Wiley & Sons, Inc.

Gajewski, W., Koswoska, M., Otwinowski, H. & Szymanek, J. 2003. The influence of physical properties of coal on the thermal fragmentation . Paper presented at the 30th International Conference of SSCHE, Tatranské Matliare, 26-30 May.

Gajewski, W. & Kijo-Kleczkowska, A. 2006. Solid fuels particles fragmentation during the periodic combustion. (Unpublished).

Giesche, H. 2006. Mercury porosimetry: A general (practical) overview. *Part. Part. Syst. Charact.,* 23 (2006): 1-11.

Goehring, L. 2003. A study of 3D crack patterns and columnar jointing in corn starch. Toronto: University of Toronto. (Thesis – Masters).

Hattingh, B. 2009. The determination of the reaction mechanisms involved in the CO_2 gasification of inertinite-rich, high ash coal. Potchefstroom: North-West University. (Dissertation – Masters).

Hattingh, B. 2012. Product evaluation and reaction modelling for the devolatilization of large coal particles. Potchefstroom: North-West University. (Thesis – PhD).

Hayashi, J. & Li, C. 2004. Structure and Properties of Victorian Brown Coal. (*In* Li, C., *ed.* Advances in the science of victorian brown coal. Oxford: Elsevier. p.11-84).

He, H., Luo, Z. & Cen, K. 2007. Experimental research on the fragmentation of Long-Yan anthracite with different lithotypes in fluidized bed combustion. Paper presented at the International Conference on Power Engineering, Hangzhou, 23 – 27 October. Date of access: 10 July 2014.

Hoffman, J.W. 2012. Ionizing radiation as imaging tool for coal characterization and gasification research. Potchefstroom: North-West University. (Dissertation – Masters).

Hoffman, J.W. & De Beer, F.C. 2012. Characteristics of the Micro-Focus X-ray Tomography Facility (MIXRAD) at Necsa in South Africa. Paper presented at the 18th World Conference on Nondestructive Testing, Durban, 16-20 April. Date of access: 31 July 2013.

Holdich, R.G. 2002. Fundamentals of Particle Technology. Leicestereshire: Midland Information and Technology Publishing.

Höök, M. & Aleklett, K. 2009. A review on coal to liquid fuels and its coal consumption. *International Journal of Energy Research,* (2009): 1-17.

Incropera, F.P., Dewitt, D.P., Bergman, T.L. & Lavine, A.S. 2007. Fundamentals of Heat and Mass Transfer. 6th edition. USA: John Wiley & Sons.

Johansson, M. 2012. Dynamic model of a bubbling fluidized bed boiler. Göteborg: Chalmers University of Technology. (Thesis – Masters).

Jordan, P. 2006. Characterising coals for coke production and assessing coal – Predicting coke quality based on coal petrography, rheology and coke petrography. Johannesburg: University of the Witwatersrand. (Project Report – Masters).

Kelly, E.G. & Spottiswood, D.J. 1982. Introduction to Mineral Processing. USA: Wiley & Sons.

Kijo-Klecskowska, A. 2012. Research on coal-water fuel combustion in a circulating fluidized bed. *Arch. Min. Sci.,* 75 (1): 79 – 92.

Kosowska-Galachowska, M. & Luckos, A. 2010. An experimental investigation into the fragmentation of coal particles in a fluidized-bed combustor. Paper presented at the 20th International Conference on Fluidized Bed Combustion, Xi'an, 18-20 May. Date of access: 3 April 2014.

Kosowska-Galachowska, M., Gajewski, W. & Musial, T. 2014. Determination of the effective thermal conductivity of solid fuels by the laser flash method. *Archives of thermodynamics,* 35 (2014): 3-16.

Laubach, S.E., Marrett, R.A., Olson, J.E. & Scott, A.R. Characteristics and origins of coal cleat: A review. *International Journal of Coal Geology,* 35 (1998): 175-207.

Lee, C.H. & No, S.Y. 1994. Observation of coal fragmentation in early stages of combustion. *KSME Journal,* 8 (4): 436 – 443.

Lee, J.M., Kim, J.S., Kim, J.J. & Kim, S.D. 2001. Observation of comminution characteristics of Korean anthracite in a CFB reactor. Presentation presented at the 43rd

International Energy Agency-Fluidized Bed Conversion, Lisbon, 22-24 Nov. Date of access: 8 July 2014.

Lee, S.H., Kim, S.D. & Lee, D.H. 2002. Particle size reduction of anthracite coals during devolatilization in a thermobalance reactor. *Fuel,* 81 (2002): 1633 – 1639.

León y León, C.A. New perspectives in mercury porosimetry. 1998. *Advances in Colloid and Interface Science,* 76-77 (1998): 341-372.

Liu, G., Wu, H., Gupta, R.P., Lucas, J.A., Tate, A.G. & Wall, T.F. 2000. Modeling of the fragmentation of non-uniform porous particles during pulverized coal combustion. *Fuel,* 79 (2000): 627-633.

Liu, J., Jiang, X., Zhou, L., Wang, H. & Han, X. 2009. Thermal stress-induced fragmentation of quartzite particles in a hot fluidized bed. *Chemical Engineering and Processing,* 48 (2009): 507-514.

Lyons, P.C., Hatcher, P.G. & Brown, F.W. 1986. Secretinite: a proposed new maceral of the inertinite maceral group. *Fuel,* 65 (8): 1094-1098.

Mandal, D., Rautela, M.S. & Tewari, D.C. 2004. Analysis of micro-fractures in coal for coal bed methane exploitation in Jharia coal field. Paper presented at the 5th Conference & Exposition on Petroleum Geophysics, Hyderabad, 15-17 January. Date of access: 20 July 2013.

Mathews, J.P., Pone, J.D.N., Mitchell, G.D. & Halóck, P. 2011. High-resolution X-ray computed tomography observations of the thermal drying of lump-sized subbituminous coal. *Fuel Processing Technology,* 92 (2011): 58-64.

Mazumder, S., Wolf, K.-H.A.A., Elewaut, K., Ephraim, R. 2006. Application of X-ray computed tomography for analyzing cleat spacing and cleat aperture in coal samples. *International Journal of Coal Geology,* 68 (2006): 205-222.

Mitchell, R.E. & Akanetuk, E.J. 1996. The impact of fragmentation on char conversion during pulverized coal combustion. Paper presented at the Twenty-Sixth Symposium (International) on Combustion/The Combustion Institute, Naples, 28 July-2 Augustus.

Morcote, A., Mavko, G. & Prasad, M. 2010. Dynamic elastic properties of coal. *Geophysics,* 75 (6): E227 – E234.

Mostert, P.J. 2010. Investigation of the influence of heating rate and isothermal temperature on the pyrolysis behaviour of South African coals: Highveld coal XA. Potchefstroom: North-West University. (Dissertation – Honours).

Oboirien, B.O. 2011. Gasification of high ash coal and chars from South African coals. Johannesburg: University of the Witwatersrand. (Thesis – PhD).

Oka, S.N. 2004. Fluidized Bed Combustion. New York: Marcel Dekker, Inc.

Paprika, M., Winter, F., Komatina, M. & Dakič, D. 2007. Influence of FB conditions on processes within a large fuel particle during initial phases of conversion. Paper presented at The 12th International Conference on Fluidization – New Horizons in Fluidization Engineering, Vancouver, 13 – 17 May.

Paprika, M.J., Komatina, M.S., Dakič, D.V. & Nemoda, S.D. 2013. Prediction of coal primary fragmentation and char particle size distribution in fluidized bed. *Energy & Fuels,* 27 (2013): 5488-5494.

Paprika, M.; Komatina, M.; Dakić, D.; Živković, G.; Mladenović, M., 2015. Experimental and numerical investigation of the primary fragmentation of a lignite during fluidized-bed (FB) devolatilization. *Energy & Fuels 29* (5), 3394-3398.

Patadiya, D.M., Jaisankar, S. & Sheshadri, T.S. 2014. Computational model for thermal and volatilization induced spontaneous fragmentation of coal particle. Proceedings of the Second International Conference on Advances in Mechanical and Robotics Engineering, Zurich, 25-26 October.

Peeler, J.P.K. & Poynton, H.J. 1992. Devolatilization of large coal particles under fluidized bed conditions. *Fuel,* 71 (1992): 425-430.

Pinho, C. 2006. Fragmentation on batches of coke or char particles during fluidized bed combustion. *Chemical Engineering Journal,* 115 (2006): 147-155.

Pretorius, C.C., Boshoff, H.P. & Pinheiro, H.J. 2002. Analyses of coal product samples of South African collieries 2001-2002. (In Bulletin 114. SABS: Pretoria).

Ragland, K.W. & Bryden, K.M. 2011. Combustion Engineering. 2nd edition. USA: CRC Press Taylor & Francis Group.

Ryan, B. 2006. A discussion on moisture in coal implications for coalbed gas and coal utilization. (Summary of Activities. BC Ministry of Energy, Mines and Petroleum Resources: Victoria).

Sasongko, D. & Stubington, J.F. 1996. Significant factors affecting devolatilization of fragmenting, non-swelling coals in fluidized bed combustion. *Chemical Engineering Science,* 51 (16): 3909 – 3918.

Senneca, O. & Chirone, R. 2009. Fragmentation of biomass particles under severe heating conditions. Paper presented at Proceedings of the European Combustion Meeting 2009, Vienna, 14-17 Apr.

Senneca, O., Russo, S. & Chirone, R. 2009. Primary fragmentation of coal particles at high heating rate. *Chemical Engineering Transaction,* 18 (2009): 569-574.

Senneca, O., Russo, S., Urcuiolo, M. & Chirone, R. 2010a. Fragmentation of solid fuels under severe heating conditions. Paper presented at Process and Technologies for a Sustainable Energy, Ischia, 27 – 30 June. Date of access: 9 July 2014.

Senneca, O., Allouis, C., Chirone, R. & Russo, S. 2010b. Set up of an experimental apparatus for the study of fragmentation of solid fuels upon severe heating. *Experimental Thermal and Fluid Science,* 34 (2010): 366 – 372.

Senneca, O., Urciuolo, M., Chirone, R. & Cumbo, D. 2011. An experimental study of fragmentation of coals during fast pyrolysis at high temperature and pressure. *Fuel,* 90 (2011): 2931-2938.

Senneca, O., Urciuolo, M. & Chirone, R. 2013. A semidetailed model of primary fragmentation of coal. *Fuel,* 104 (2013):253-261.

Sharma, N., Gupta, B. & Chauhan, R.P.S. 2012. Analysis of Exergy and Energy of Gasifier Systems for Coal-to-Fuel. *International Journal of Mechanical and Industrial Engineering,* 1 (3): 55-61.

Sinha, A. Oct. 2007. Advances in X-ray and neutron imaging and its applications. Newsgroup: http://barc.ernet.in/publications/nl. Date of access: 11 Aug 2013.

Smith, W.F. & Hashemi, J. 2010. Foundations of Materials Science and Engineering. 5th edition. USA: McGraw-Hill.

South Africa. Department of Energy. 2015. Coal resources. Pretoria.

Speight, J.G. 2005. Handbook of Coal Analysis. Hoboken: John Wiley & Sons Inc. (Chemical Analysis: A series of Monographs on Analytical Chemistry and its Applications, 166).

Sreekanth, M. 2014. Primary fragmentation of wood in a fluidized bed combustor – An experimental investigation. *International Journal of Innovation and Scientific Research,* 9 (2): 502-510.

Sreekant, M., Kolar, A.J. & Leckner, B. 2008. A semi-analytical model to predict primary fragmentation of wood in a bubbling fluidized bed combustor. *Journal of Analytical and Applied Pyrolysis,* 83 (2008): 88-100.

Stanmore, B.R., Brillard, A., Gilot, P. & Delfosse, L. 1996. Fragmentation of small coal particles under fluidized-bed combustor conditions. Paper presented at the Twenty-Sixth Symposium (International) on Combustion/ The Combustion Institute, Naples, 28 July – 2 Augustus. Date of access: 9 July 2014.

Stubington, J.F. & Linjewile, T.M. 1989. The effects of fragmentation on devolatilization of large coal particles. *Fuel,* 68 (1989): 155-160.

Suárez-Ruiz, I. & Crelling, J.C. 2008. Applied Coal Petrology: The Role of Petrology in Coal Utilization. USA: Elsevier Ltd.

The Southern African Coal Processing Society. 2015. Coal Preparation in Southern Africa. 5th edition. South Africa: The Southern African Coal Processing Society.

Thomas, J.T. & Damberger, H.H. 1976. Internal surface area, moisture content, and porosity of Illinois coals: Variations with coal rank. (In Illinois State Geological Survey. State of Illinois Department of Registration and Education: Illinois).

Tian, S. 2011. Fragmentation of large coal particles at high temperature in a drop tube furnace. Edmonton: University of Alberta. (Thesis – Masters).

Tilghman, M.B. & Mitchell, R.E. 2013. Characterizing char particle fragmentation during pulverized coal combustion. *Proceedings of the Combustion Institute,* 34 (3): 2461-2469.

Van der Merwe, G.L. 2010a. The influence of particle size and devolatilisation conditions on the CO_2 gasification of Highveld coal. Potchefstroom: North-West University. (Dissertation – Masters).

Van der Merwe, G.W. 2010b. The influence of particle size and density on the combustion of Highveld coal. Potchefstroom: North-West University. (Dissertation – Masters).

Van der Merwe, R. 2014. Mercury Intrusion Porosimetry [correspondence]. 8-12 Sept., Necsa.

Van Dyk, J.C. 2001. Development of an alternative laboratory method to determine thermal fragmentation of coal sources during pyrolysis in the gasification process. *Fuel,* 80 (2001): 245-249.

Van Dyk, J.C., Keyser, M.J. & Van Zyl, J.W. 2001. Suitability of feedstocks for the Sasol-Lurgi fixed bed dry bottom gasification process. Paper presented at Gasification Technologies 2001, San Francisco , 7-10 October. Date of access: 12 April 2014.

Waples, D.W. & Waples, J.S. A review and evaluation of specific heat capacities of rocks, minerals, and subsurface fluids. Part 1: Minerals and Nonporous Rocks. *Natural Resources Research,* 13 (2): 97-122.

Webb, P.A. & Orr, C. 1997. Analytical Methods in Fine Particle technology. USA: Micrometrics Instrument Corporation.

Webb, P.A. 2001. An introduction to the physical characterization of materials by mercury intrusion porosimetry with emphasis on reduction and presentation of experimental data. (For the Micrometrics Instrument Corp. Micrometrics Instrument Corp: Georgia).

Westermarck, S. 2000. Use of mercury porosimetry and nitrogen adsorption in characterisation of the pore structure of mannitol and microcrystalline cellulose powders, granules and tablets. Helsinki: University of Helsinki. (Dissertation - Masters).

Zhang, H., Cen, K., Yan, J. & Ni, M. 2002. The fragmentation of coal particles during the coal combustion in a fluidized bed. *Fuel,* 81 (2002): 1835-1840.

APPENDIX A: EXPERIMENTAL EQUIPMENT & ERROR CALCULATIONS

In this Appendix more information regarding the experimental equipment is given. The gas calibration data, temperature profiles across the furnace and the X-ray scanner specifications are presented respectively. The experimental error calculations are also given.

A.1 GAS CALIBRATION DATA

A bubble flow meter was used to calibrate the rotameter. In Table A.1 the data is given. From the table it can be seen that the normal flow measured by the rotameter is relatively inaccurate when compared to that of the normal flow measured by the bubble flow meter. A set point of 0.3 L/min (actual) was needed for an inert atmosphere which means that the rotameter was set to 86 L/h (normal).

Table A.1: Gas calibration data.

Rota (L_{normal}/h)	8.0	20.0	40.0	60.0	80.0	86.0
Bubble (L_{normal}/h)	1.9	4.0	7.6	11.2	13.1	15.9
Bubble (L_{actual}/min)	0.0	0.1	0.1	0.2	0.3	0.3

A.2 TEMPERATURE PROFILES

The temperature profiles across the furnace were measured with controller set points of 400, 600 and 900 °C respectively. This was done in order to determine the distance, from the side, where the sample holder should be placed to ensure that the samples are shocked to the correct temperatures. In Figures A.1 to A.3 the temperature profiles are given. For 400 °C experiments, the samples were placed anywhere between 260 and 410 mm resulting in the samples being exposed to temperatures between 390 and 410 °C. For 600 °C experiments, the samples were also placed between 260 and 410 mm. The samples were then exposed to temperatures ranging between 580 and 610 °C. Lastly it was found that for 900 °C samples should also be placed between 260 and 410 mm. The exposure temperatures then ranged between 880 and 910 °C. Due to the large differences between the different temperatures the variations were tolerable.

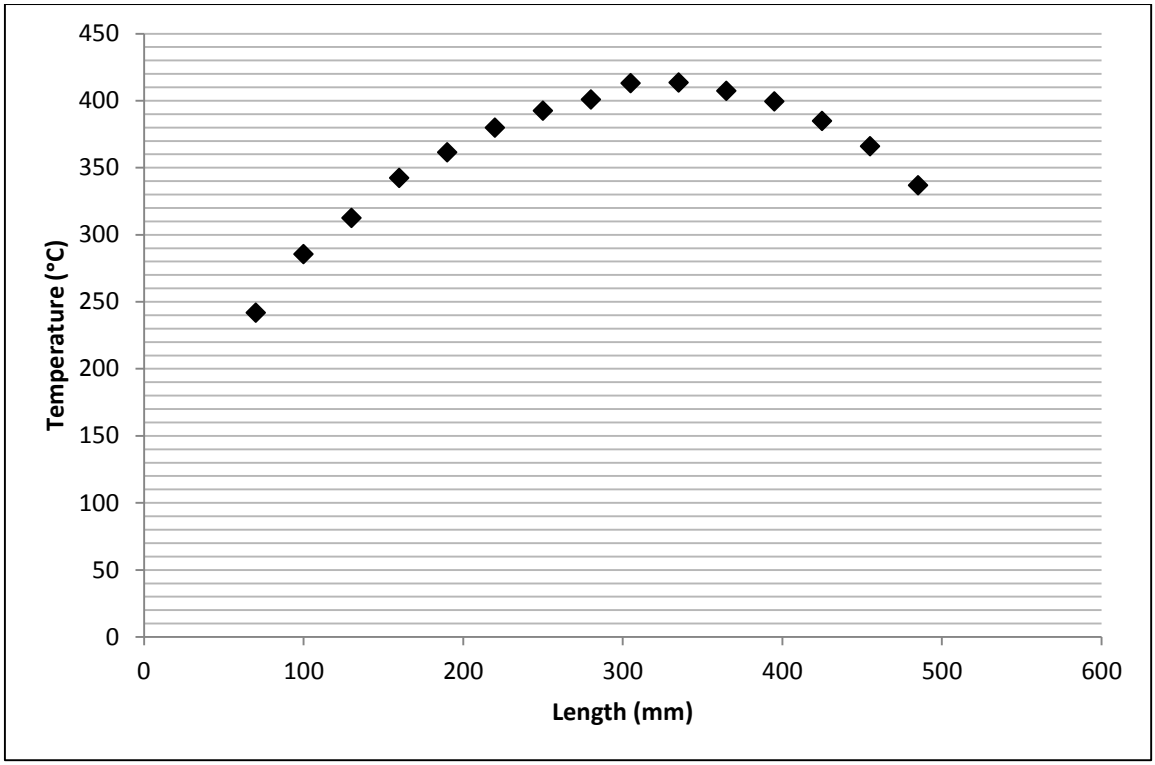

Figure A.1: Temperature profile across furnace for 400°C.

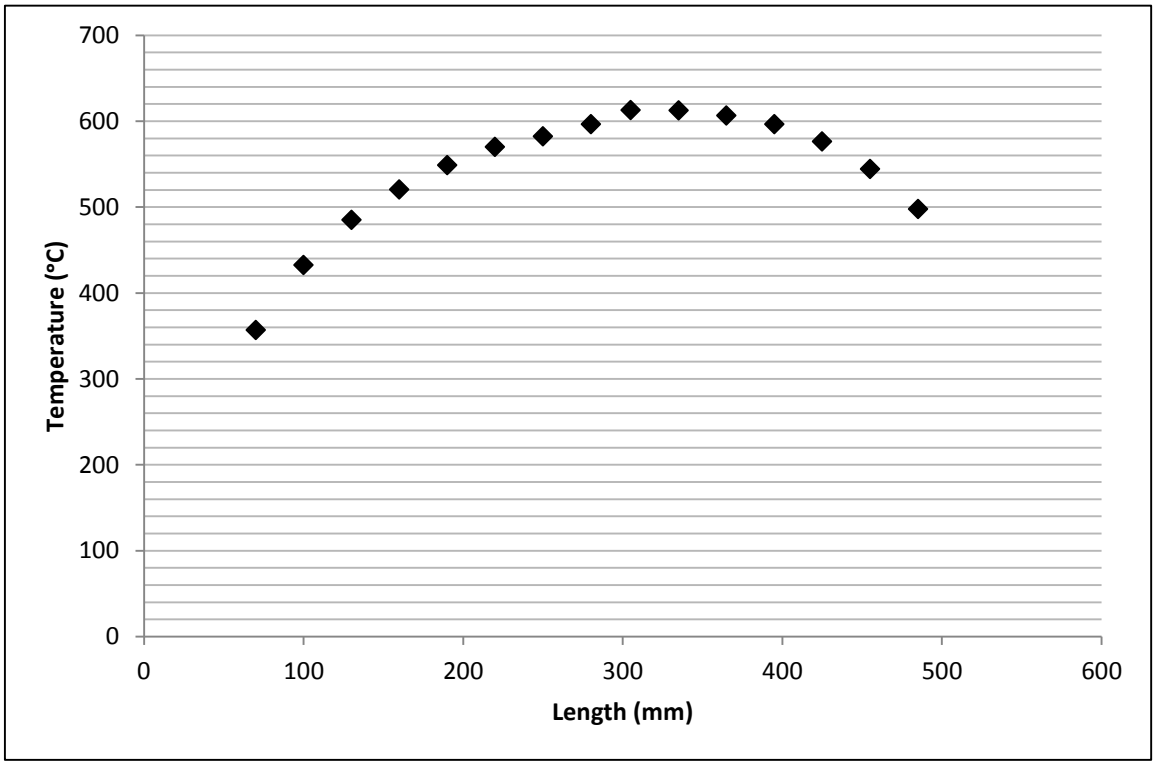

Figure A.2: Temperature profile across furnace for 600°C.

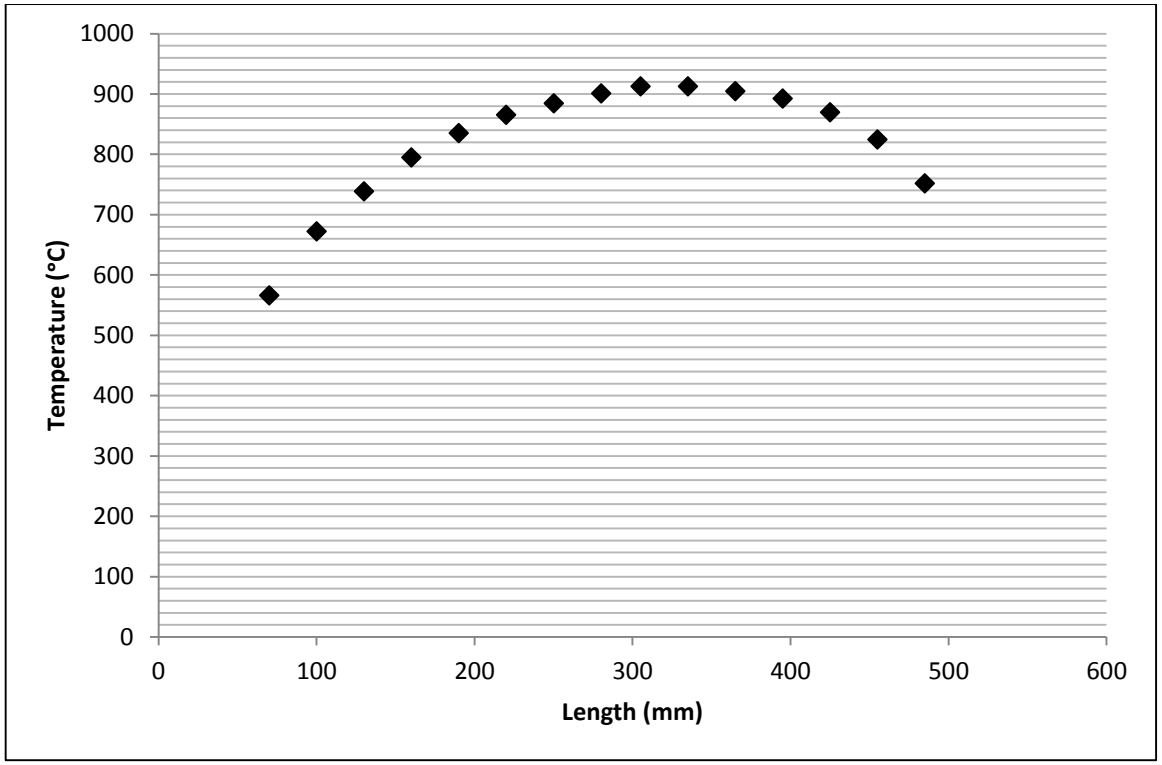

Figure A.3: Temperature profile across furnace for 900°C.

A.3 X-RAY SCANNER SPECIFICATIONS

In Table A.2 additional information on the Micro-focus X-Ray tomography system is given.

Table A.2: X-ray Scanner specifications (Adapted from Hoffman & De Beer, 2012:3).

X-Ray Source	
Voltage (kV)	30-225
Current (mA)	0-1
Spot size (μm)	~1-3
Beam angles (°)	25
Multi target	Mo; Cu; W; Ag
Filter kit with a range of thickness of foils	Cu; Al; Sn; Ag
Translation Table	
Axis movement (directions)	5
Sample movement in horizontal plane (mm)	200
Sample movement in vertical plane (mm)	300
Sample movement in beam direction (mm)	610
Rotation accuracy	1/1000th of a degree
Tilt	45
Movement	Ultra slow; Slow; Medium; Fast
Detector	
Type	Perkin Elmer
Dynamic range	16 bit
Physical size (mm)	400x400
Pixel size (μm)	200x200

A.4 EXPERIMENTAL ERROR

To calculate the experimental errors, confidence interval based on a 95% confidence level, excel was used. The functions and steps were as follows:

Step 1: Determine the average of your data; =Average (range)

Step 2: Determine the standard deviation; =Stdev (range)

Step 3: Determine the confidence level based on a t-distribution (less than 30 repeats); =Confidence.t (0.05, stdev, amount of repeats)

APPENDIX B: HEAT TRANSFER

B.1 CALCULATIONS

Heat transfer calculations were conducted in order to describe the change in temperature with time, at different positions in the coal particles, as well as to determine the heating times for the different particles at the relevant conditions. The following assumptions were made when implementing these calculations:

- Particles have a spherical geometry;
- Particles are heated and devolatilised in an inert atmosphere with nitrogen as the contact fluid;
- Only heat transfer in the radial direction takes place (one-dimensional transfer);
- Heat transfer takes place due to convection and conduction only;
- Energy generation is assumed to be negligible; and
- The influence of the sample holder was neglected by assuming that its influence is minimum on the heat transfer process

Taking the above assumptions into consideration the second order non-linear heat transfer model, given in Equation B.1, was derived from the general heat equation (Incropera *et al.,* 2007:74, Paprika *et al.,* 2007:987, Sasongko & Stubington, 1996:3910, Senneca *et al.,* 2013:254):

$$\frac{\partial T}{\partial t} = \frac{k_s}{\rho r^2 C_p}\frac{\partial}{\partial r}\left(r^2\frac{\partial T}{\partial r}\right) \qquad \textbf{\textit{Equation B.1}}$$

Solid thermal conductivity (k_s) in W/mK

Density (ρ) in kg/m^3

Radius (r) in m

Heat Capacity (C_p) in J/kgK

Temperature (T) in K

Time (t) in s

With initial condition (Incropera *et al.,* 2007:270, Paprika *et al.,* 2007:987, Patadiya *et al.* 2014:44, Sasongko & Stubington, 1996:3910, Senneca *et al.,* 2013:255):

$$T = T_i \; at \; t = 0 \qquad \textbf{Equation B.2}$$

and boundary conditions (Incropera *et al.,* 2007:270-271, Paprika *et al.,* 2007:987, Sasongko & Stubington, 1996:3911, Senneca *et al.,* 2013:255):

$$\frac{\partial T}{\partial r} = \frac{h(T_\infty - T)}{k_s} \; at \; t > 0 \; and \; r = R \qquad \textbf{Equation B.3}$$

$$\frac{\partial T}{\partial r} = 0 \; at \; t > 0 \; and \; r = 0 \qquad \textbf{Equation B.4}$$

Convection coefficient (h) in W/m^{2}K

The first boundary condition is known as the convection at surface condition while the second one is known as the symmetry at mid-plane condition (Incropera *et al.,* 2007:270–271).

In order to solve Equations B.1 to B.4 the approximate solution method as given by Incropera *et al.* (2007:277) was implemented. There is however a constraint when using the approximate solution method in the form of the Fourier number (Fo), as shown in Equation B.5, and one should thus be careful when implementing this method (Incropera *et al.,* 2007:277):

$$Fo = \frac{tk_s}{r^2 \rho C_p} > 0.2 \qquad \textbf{Equation B.5}$$

Fourier number (Fo) is dimensionless

The approximate solution for the temperature history at the centre of a spherical particle is given in Equation B.6, while the temperature history at any other point in the particle is given in Equation B.7 (Incropera *et al.,* 2007:277):

$$T = T_\infty + \left(C_1 (T_i - T_\infty) exp^{-Fo\zeta_1{}^2}\right) \qquad \textbf{Equation B.6}$$

$$T = T_\infty + (T_i - T_\infty)(\frac{C_1 exp^{-Fo\zeta^2}}{\zeta_1 r^*}\sin\zeta_1 r^*)$$ ***Equation B.7***

In these two equations r^* represents a dimensionless spatial coordinate and may be defined as (Incropera *et al.,* 2007:273):

$$\frac{r_n}{r}$$ ***Equation B.8***

With: r_n the radius at point n. The approximate solution constants ζ_1 and C_1 can be found from literature (Incropera *et al.,* 2007:274).

In Equation B.3 the convective coefficient (h) was used. To calculate the convective coefficient Equation B.9 should be implemented (Incropera *et al.,* 2007:371):

$$h = \frac{Nuk_f}{2r}$$ ***Equation B.9***

Fluid thermal conductivity (kf) in W/mK

Nusselt number (Nu) is dimensionless

The Nusselt number (Nu) was calculated with Equation B.10 (Incropera *et al.,* 2007:434):

$$Nu = 2 + (0.4Re^{0.5} + 0.06Re^{0.67})Pr^{0.4}(\frac{\mu}{\mu_s})^{0.25}$$ ***Equation B.10***

With the following three constraints (Incropera *et al.,* 2007:434):

$$0.71 \lesssim Pr \lesssim 380$$

$$3.5 \lesssim Re \lesssim 7.6 \times 10^4$$

$$1.0 \lesssim \left(\frac{\mu}{\mu_s}\right) \lesssim 3.2$$

Prandtl number (Pr) is dimensionless

Viscosity at temperature T (μ) in Ns/m^2

Viscosity at temperature $\frac{T_i+T_\infty}{2}$ (μ_s) in Ns/m^2

The Reynolds number (Re) was calculated as follows (Incropera *et al.,* 2007:424):

$$Re = \frac{2Vr}{v}$$ ***Equation B.11***

The kinematic viscosity (v) in m^2/s

Velocity (V) in m/s

In Table B.1 the experimental conditions used are given. The velocities in the table were calculated with the ***actual*** volumetric flow rates ($\dot{V}$) at the different temperatures and the tube diameter (D) of the furnace.

Table B.1: Experimental conditions used in heat transfer calculations.

Parameter	**Quantity**
T_i (°C)	25
T∞ (°C)	400, 600, 900
***$\dot{V}$*(L/min)**	0.3
D (mm)	50
V (m/s)	
400 °C	0.007
600 °C	0.010
900 °C	0.013
r (mm)	5, 7.5, 10, 12.5, 15
Coal origin	LV1, LV2, HV1, HV2, HV Coking

In Table B.2 the solid properties are given. The apparent densities obtained from MIP and the thermal conductivities obtained from Kosowska-Golachowska *et al.* (2014: 10) were used.

Table B.2: Solid properties used in heat transfer calculations.

Parameter	k_s (W/mK)	C_p (J/kgK)	ρ (kg/m^3)
LV1			1349
400 °C	0.5	2362	
600 °C	0.9	3099	
900 °C	2.1	4203	
LV2			1305
400 °C	0.5	2391	
600 °C	0.9	3127	
900 °C	2.1	4231	
HV1			1287
400 °C	0.4	2446	
600 °C	0.8	3183	
900 °C	1.8	4287	
HV2			1367
400 °C	0.4	2468	
600 °C	0.8	3204	
900 °C	1.8	4309	
HV Coking			1555
400 °C	0.4	2438	
600 °C	0.8	3147	
900 °C	1.8	4279	

To calculate the heat capacities the volatile-based method proposed by Waples & Waples (2004:106) were used. In Equation B.12 this method is given.

$$C_p = 4184 \times (0.2 + 0.00088T + 0.0015Vm) \qquad \textit{Equation B.12}$$

Volatile matter (Vm) in wt.% air-dried basis

Temperature (T) in °C

In Table B.3 the nitrogen properties are given. All values in the table were obtained from Incropera *et al.* (2007:944). The heating times were taken as 95% of the total time taken to reach isothermal conditions.

Table B.3: Nitrogen properties used in heat transfer calculations.

Temperature (°C)	k (W/mK)	Pr	μ (Ns/m^2)	μ_s (Ns/m^2)	v (m^2/s)
400	0.048	0.705	3.129×10^{-5}	-	6.270×10^{-5}
600	0.058	0.719	3.683×10^{-5}	-	9.563×10^{-5}
900	0.074	0.715	4.394×10^{-5}	-	1.531×10^{-6}
213	-	-	-	2.525×10^{-5}	-
312	-	-	-	2.862×10^{-5}	-
462	-	-	-	3.310×10^{-5}	-

B.2 RESULTS

The size of a coal particle plays a role in the amount of breakage occurring due to thermal stresses. When considering Figure B.1 this observation can be confirmed. Figure B.1 illustrates the difference between the centre and surface temperature, for a HV1 particle at 900 °C, with time. The temperature difference between the centre and surface of a large particle is larger for most of the time than for a small particle. Thermal stresses, and thus fragmentation due to thermal stresses, are more pronounced in larger particles than in smaller particles.

In Figure B.2 the thermal conductivities for the low volatile samples versus the high volatile samples, at different temperatures, are shown. From this figure it can be seen that the conductivities are relatively close for 400 and 600 but for 900 °C the conductivity of the low

volatile samples suddenly surpasses that of the high volatile samples. It is thus suspected that at 900 °C thermal stress fragmentation in the low volatile samples will increase tremendously and will differ from that in the high volatile samples.

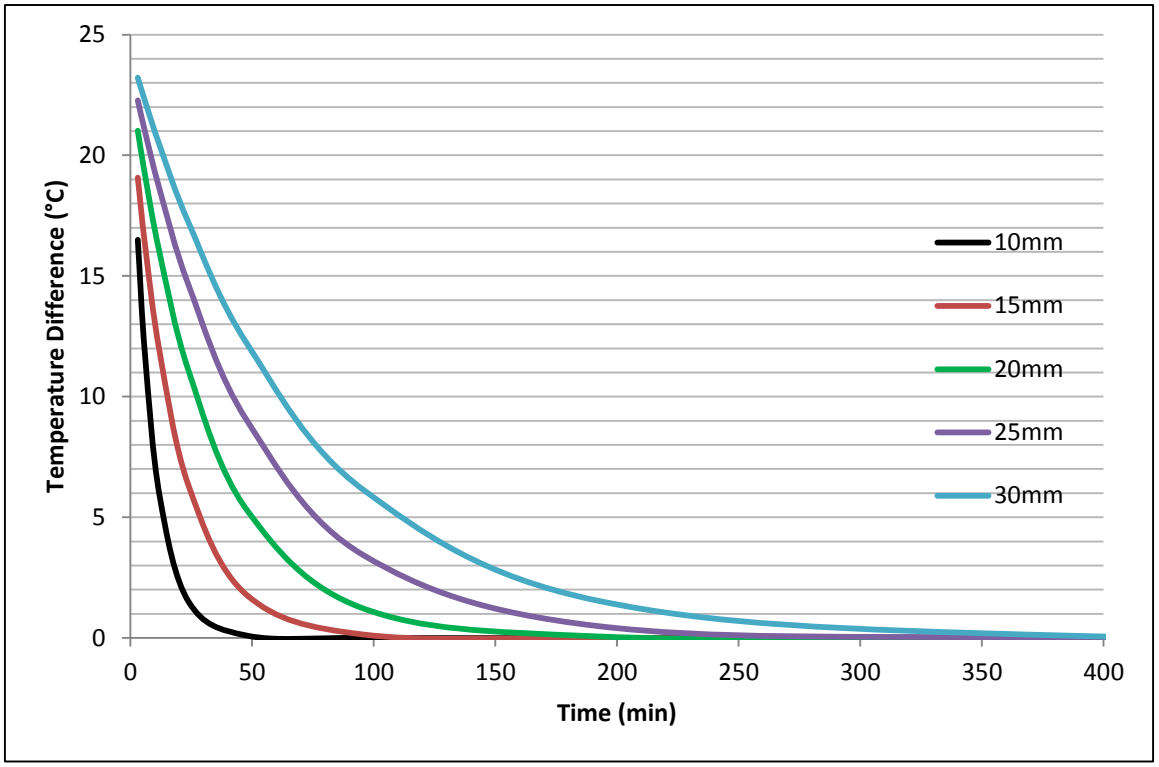

Figure B.1: Temperature difference versus time for different size, HV1 particles heated to 900 °C.

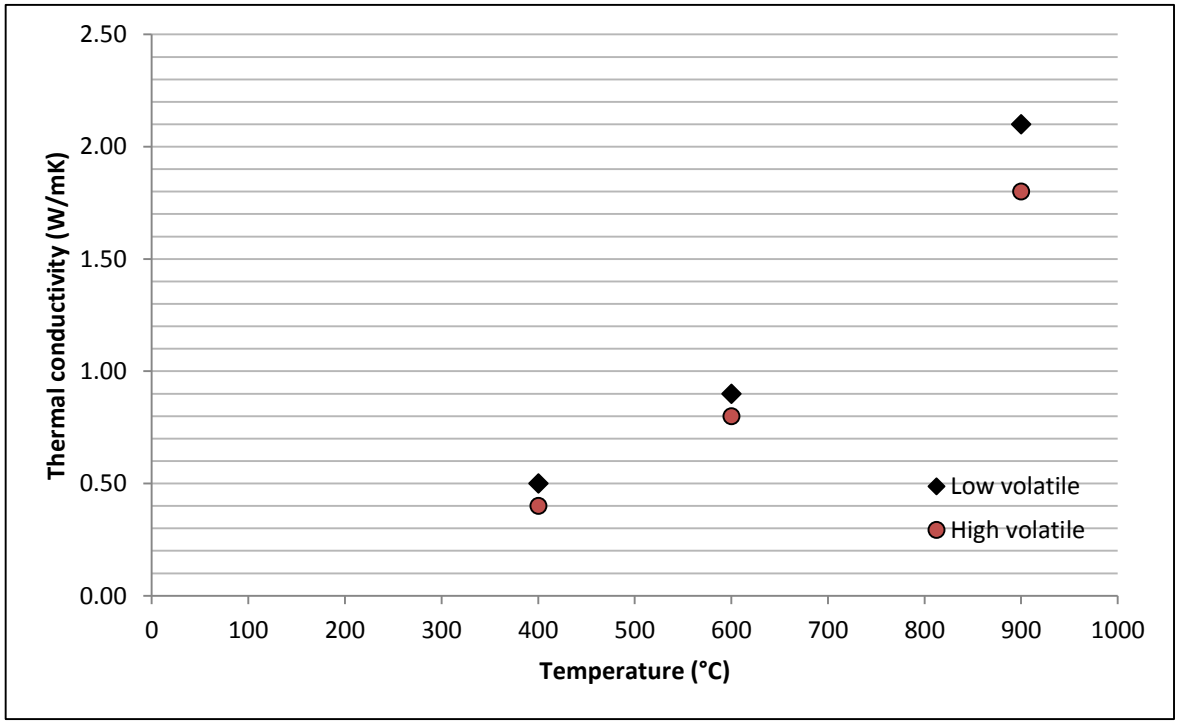

Figure B.2: Thermal conductivities at different temperatures for the different coal origins.

According to Senneca *et al.* (2013:255) thermal stresses result in a multitude of fragments forming from the outer core of the particle. This can probably be explained by considering Figure B.3. In Figure B.3 the temperature difference between the surface and a random point, located exactly between the surface and centre of the particle, and the temperature difference between the centre and this random point is illustrated. It can be seen that although the distance between these two cases are exactly the same, the temperature difference for case one is much larger than for case two. This confirms why fragmentation in the outer core is more pronounced due to thermal stresses.

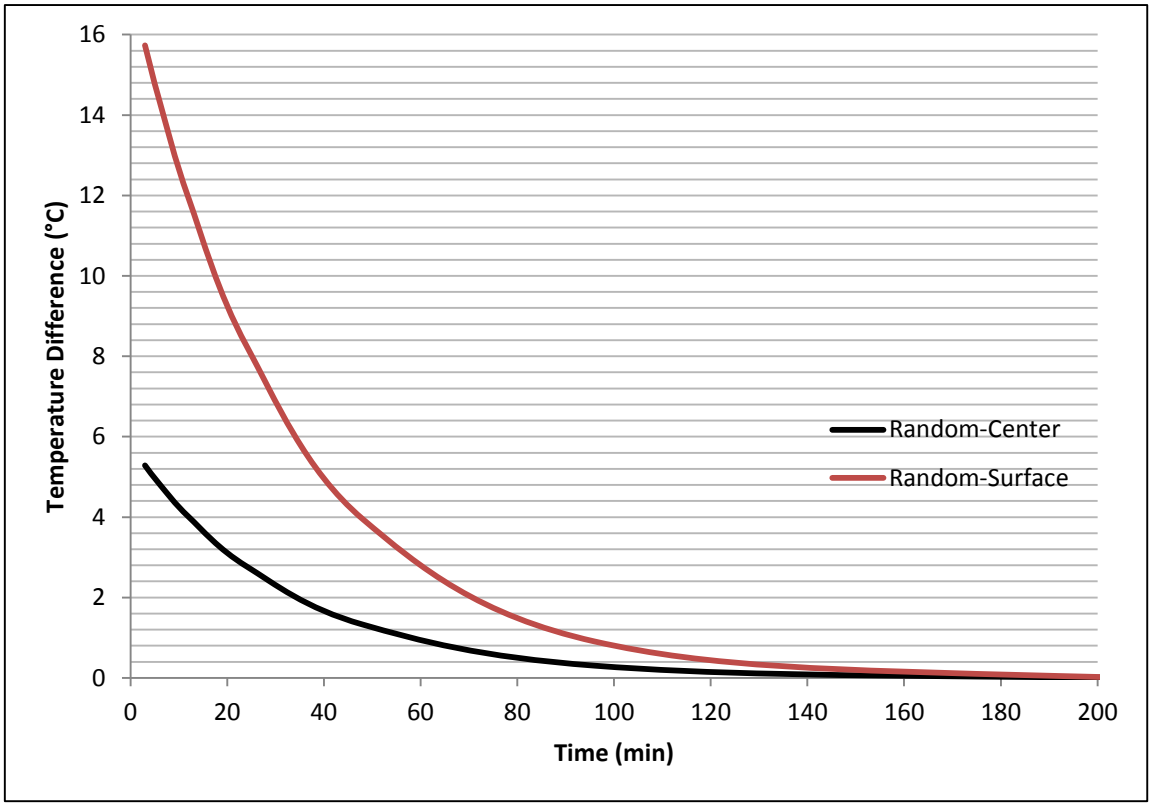

Figure B.3: Temperature difference in the outer and inner core of a particle respectively for a 20 mm high volatile sample heated to 900 °C.

From the heat transfer calculations the heating times were also obtained. The calculated heating times (95% from isothermal time) varied between 30 minutes up to four hours. Due to the fact that thermal stresses, as well as volatile release stresses, are only present in the first instances of the heating process, these times were reduced to between 30 and 90 minutes. Van Dyk (2001:346) then also stated that most fragmentation occurs in the first hour and further heating is unnecessary.

APPENDIX C: COAL CHARACTERISATION RAW DATA

In this Appendix the raw data for the equilibrium moisture, char proximate as well as the Mercury Intrusion Porosimetry analyses are given.

C.1 EQUILIBRIUM MOISTURE RAW DATA

In Table C.1 the raw equilibrium moisture data is given. The average was calculated and the confidence interval, based on a 95% confidence level, taken as error. From the table it can be seen that the errors are relatively small except for HV Coking.

Table C.1: Equilibrium moisture raw data.

Run	LV1	LV2	HV1	HV2	HV Coking
Run 1 (wt.%)	3.1	2.9	4.2	3.6	3.0
Run 2 (wt.%)	2.9	2.3	4.0	3.7	2.2
Run 3 (wt.%)	2.9	2.5	4.2	4.0	1.1
Run 4 (wt.%)	2.7	2.9	3.9	3.7	1.0
Run 5 (wt.%)	3.2	2.6			
Average (wt.%)	3.0	2.6	4.1	3.7	1.0
Error (wt.%)	0.2	0.3	0.2	0.3	1.5

C.2 MERCURY INTRUSION POROSIMETRY RAW DATA

In Table C.2 raw data for MIP analyses are given. It can be seen that the errors (confidence level based on 95% confidence level) for the porosities are relatively small except for HV2.

Table C.2: Mercury Intrusion Porosimetry raw data.

RUN 1					
Analysis	**LV1**	**LV2**	**HV1**	**HV2**	**HV Coking**
Porosity (vol.%)	5.3	6.0	5.1	4.3	3.2
Median pore diameter (nm)					
Volume (nm)	10.3	16.1	10.9	8.9	14.7
Area (nm)	4.6	4.8	4.7	4.7	4.6
Average pore diameter (nm)	8.5	10.3	8.9	7.8	9.7
Total pore area (m^2/g)	19.3	19.0	18.5	19.0	8.8
Bulk density (kg/m^3)	1305	1232	1237	1310	1512
Apparent density (kg/m^3)	1379	1311	1303	1377	1562
RUN 2					
Porosity (vol.%)	5.0	6.2	5.2	5.5	3.1
Median pore diameter (nm)					
Volume (nm)	9.6	15.1	10.5	8.7	9.6
Area (nm)	3.9	4.8	4.6	4.8	4.6
Average pore diameter (nm)	8.1	9.8	8.7	7.5	8.9
Total pore area (m^2/g)	19.6	20.6	19.8	22.8	9.4
Bulk density (kg/m^3)	1254	1219	1205	1282	1498
Apparent density (kg/m^3)	1320	1300	1271	1357	1547
AVERAGE/ERROR					
Porosity (vol.%)	5.1/2.7	6.1/0.9	5.1/0.9	4.9/8.1	3.2/0.9
Median pore diameter (nm)					
Volume (nm)	10.0	15.6	10.7	8.8	12.2
Area (nm)	4.3	4.8	4.7	4.8	4.6
Average pore diameter (nm)	8.3	10.1	8.8	7.7	9.3
Total pore area (m^2/g)	19.5	19.8	19.2	20.9	9.1
Bulk density (kg/m^3)	1280	1226	1221	1296	1506
Apparent density (kg/m^3)	1349	1305	1287	1367	1555

C.3 CHAR PROXIMATE ANALYSIS

In Table C.3 the char proximate analysis results for 400 °C are given:

Table C.3: Proximate analysis results for 400 °C chars.

Analysis	LV1	LV2	HV1	HV2	HV Coking
Inherent moisture (a.d.b wt.%)	1.1	0.9	1.2	1.0	0.1
Volatile Matter (a.d.b wt.%)	7.8	9.8	16.7	16.8	16.3
Ash yield (a.d.b wt.%)	9.9	11.0	16.1	16.8	26.9
Fixed carbon (a.d.b wt.%)	81.1	78.3	66.0	65.4	56.6
Total (wt.%)	**100**	**100**	**100**	**100**	**100**

In Table C.4 the char proximate analysis results for 600 °C are given:

Table C.4: Proximate analysis results for 600 °C chars.

Analysis	LV1	LV2	HV1	HV2	HV Coking
Inherent moisture (a.d.b wt.%)	1.5	1.5	1.4	1.5	1.2
Volatile Matter (a.d.b wt.%)	5.4	5.6	6.8	6.8	5.6
Ash yield (a.d.b wt.%)	10.7	11.4	20.9	19.8	23.7
Fixed carbon (a.d.b wt.%)	82.4	81.4	70.9	71.9	69.5
Total (wt.%)	**100**	**100**	**100**	**100**	**100**

In Table C.5 the char proximate analysis results for 900 °C are given:

Table C.5: Proximate analysis results for 900 °C chars.

Analysis	LV1	LV2	HV1	HV2	HV Coking
Inherent moisture (a.d.b wt.%)	1.8	2.1	2.6	1.8	1.2
Volatile Matter (a.d.b wt.%)	2.7	1.4	1.6	2.5	3.9
Ash yield (a.d.b wt.%)	13.2	16.9	17.9	17.1	23.6
Fixed carbon (a.d.b wt.%)	82.3	79.6	77.9	78.6	79.6
Total (wt.%)	**100**	**100**	**100**	**100**	**100**

C.4 DENSITY DISTRIBUTION CURVES & RAW DATA

In this section the raw density data, obtained from mercury submersion analysis, as well as the distribution curves are given for the 20mm particles. In Table C.6 the densities obtained for the particles from the different coal origins are given.

Table C.6: Raw mercury submersion density data for the 20mm particles of the different coal samples.

Particle number	LV1	LV2	HV1	HV2	HV Coking
Particle 1	1432	1406	1447	1461	1378
Particle 2	1303	1367	1398	1482	1357
Particle 3	1408	1307	1366	1312	1300
Particle 4	1437	1376	1586	1490	1360
Particle 5	1300	1446	1434	1341	1340
Particle 6	1261	1338	1393	1353	1467
Particle 7	1399	1424	1469	1580	1434
Particle 8	1356	1355	1474	1330	1430
Particle 9	1403	1346	1597	1537	1335
Particle 10	1398	1330	1533	1430	1409
Particle 11	1373	1434	1405	1458	1334
Particle 12	1394	1439	1274	1361	1441
Particle 13	1481	1453	1400	1465	1590
Particle 14	1384	1448	1455	1441	1504
Particle 15	1409	1375	1438	1385	1394
Particle 16	1413	1355	1422	1296	1448
Particle 17	1432	1373	1416	1452	1509
Particle 18	1401	1272	1457	1421	1385
Particle 19	1475	1499	1570	1355	1399
Particle 20	1309	1414	1372	1321	1295
Particle 21	1424	1357	1311	1288	1546
Particle 22	1370	1295	1448	1493	1520
Particle 23	1377	1447	1517	1406	1384
Particle 24	1381	1463	1389	1432	1271
Particle 25	1392	1386	1498	1431	1387
Particle 26	1586	1387	1505	1379	1348
Particle 27	1415	1343	1323	1405	1392

Particle 28	1397	1377	1397	1477	1392
Particle 29	1549	1411	1357	1382	1552
Particle 30	1435	1289	1394	1465	1441
Average density (kg/m^3)	1403	1384	1435	1414	1411
Standard deviation (kg/m^3)	66	56	72	72	80

In Figure C.1 the distribution curve for the 20mm LV1 particles are given.

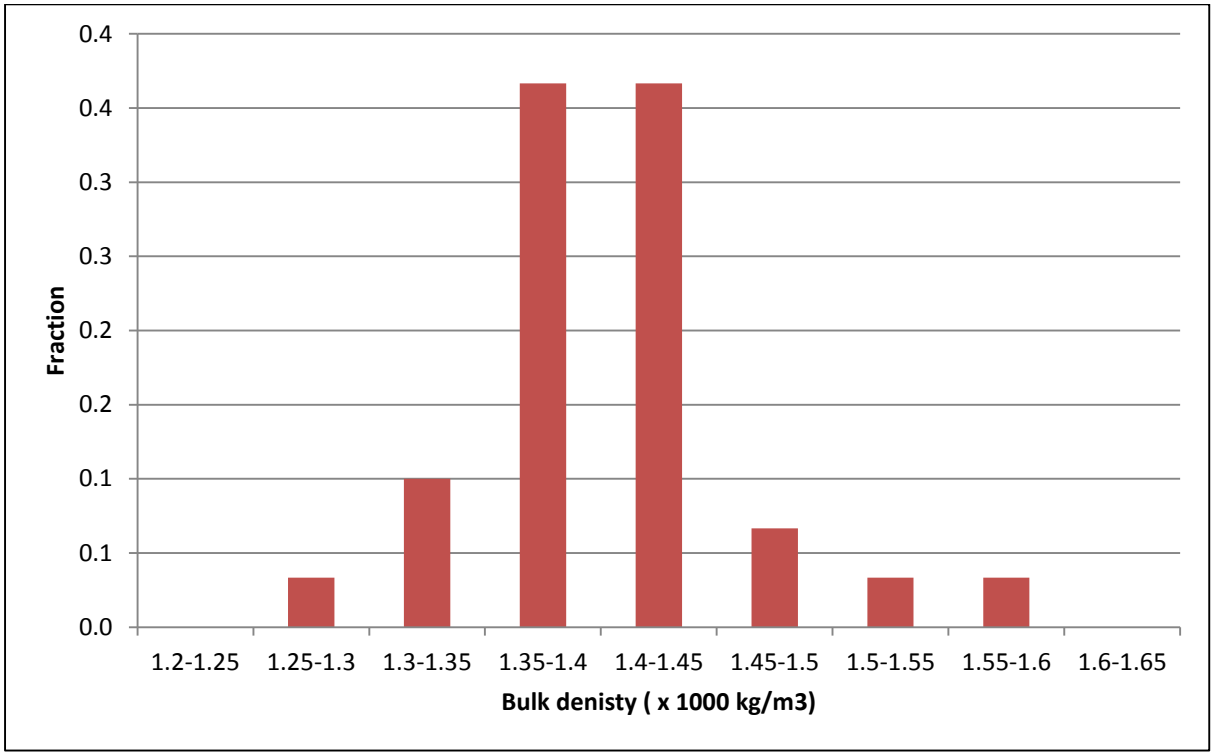

Figure C.1: Density distribution for 20mm LV1 particles.

In Figure C.2 the distribution curve for the 20mm LV2 particles are given.

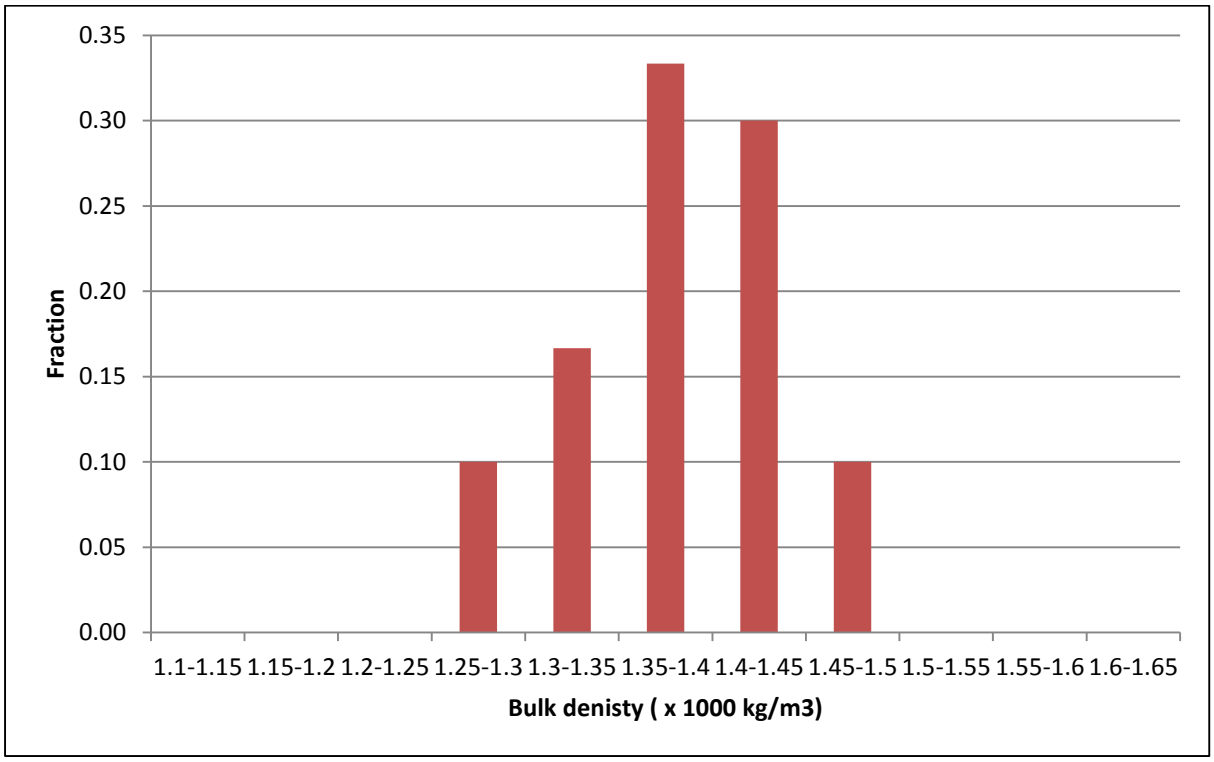

Figure C.2: Density distribution for 20mm LV2 particles.

In Figure C.3 the distribution curve for the 20mm HV1 particles are given.

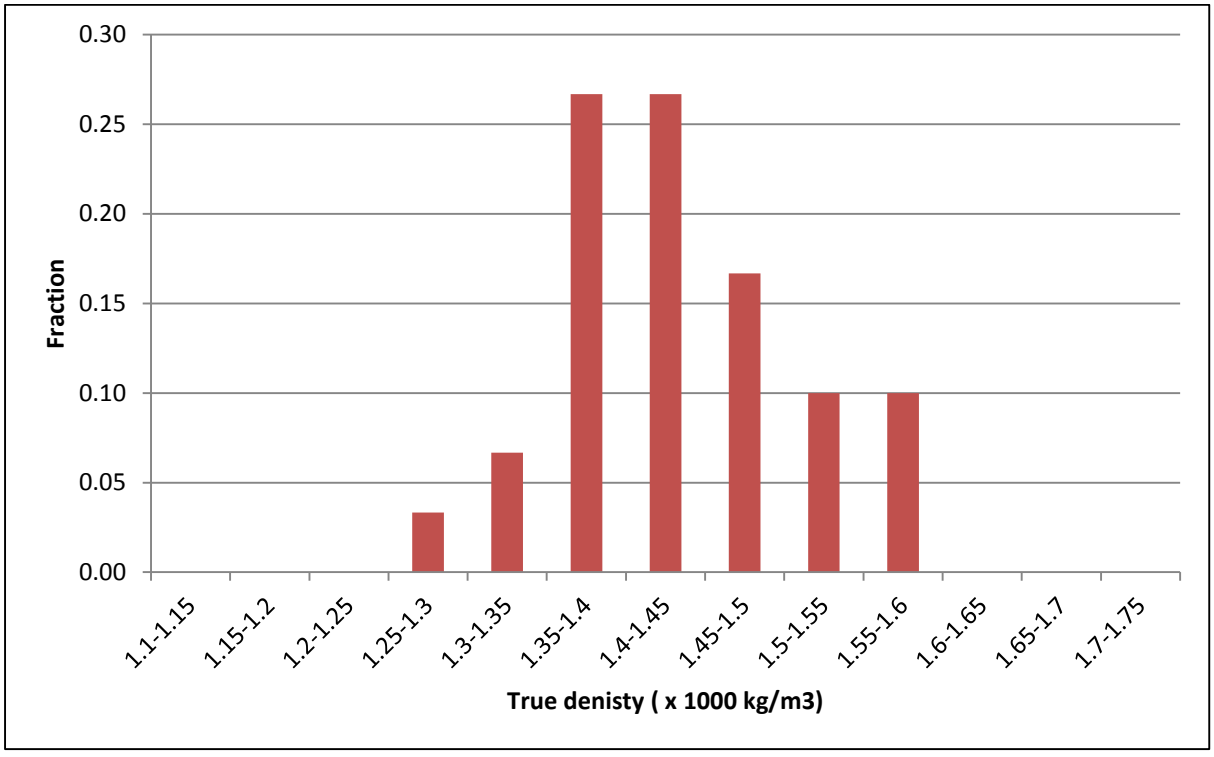

Figure C.3: Density distribution for 20mm HV1 particles.

In Figure C.4 the distribution curve for the 20mm HV2 particles are given.

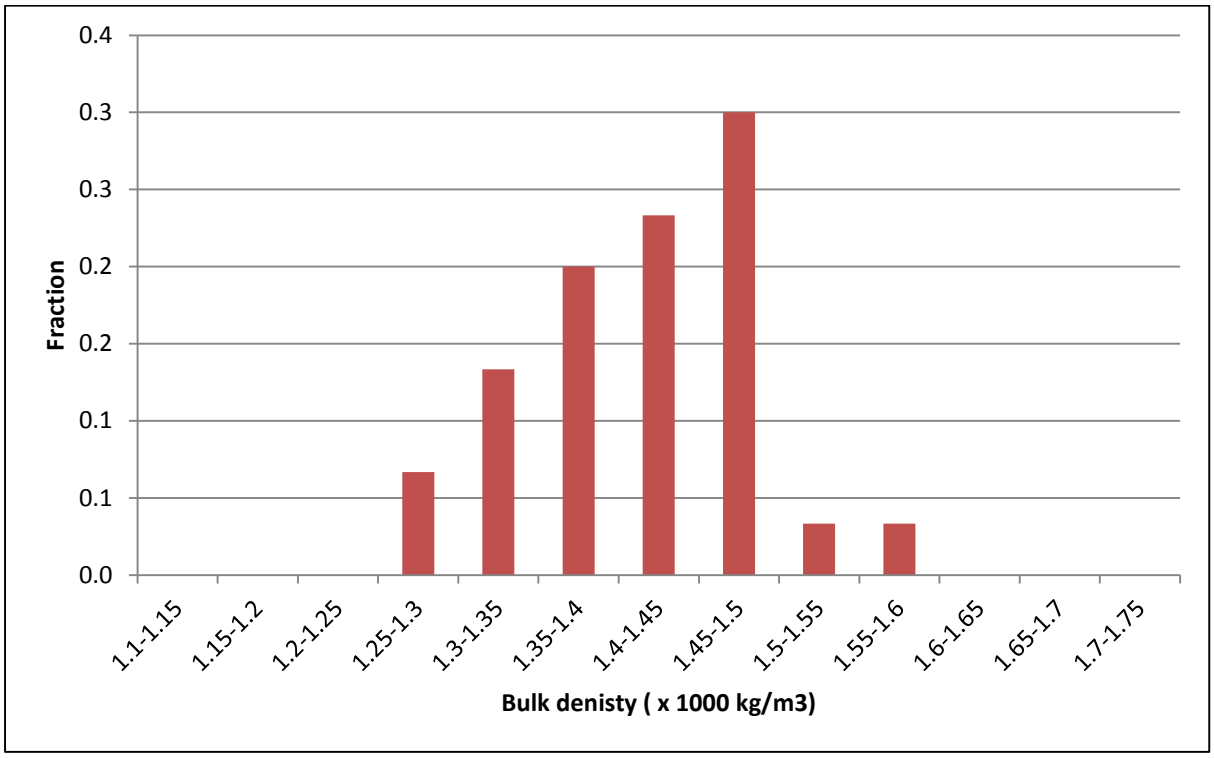

Figure C.4: Density distribution for 20mm HV2 particles.

In Figure C.5 the distribution curve for the 20mm HV Coking particles are given.

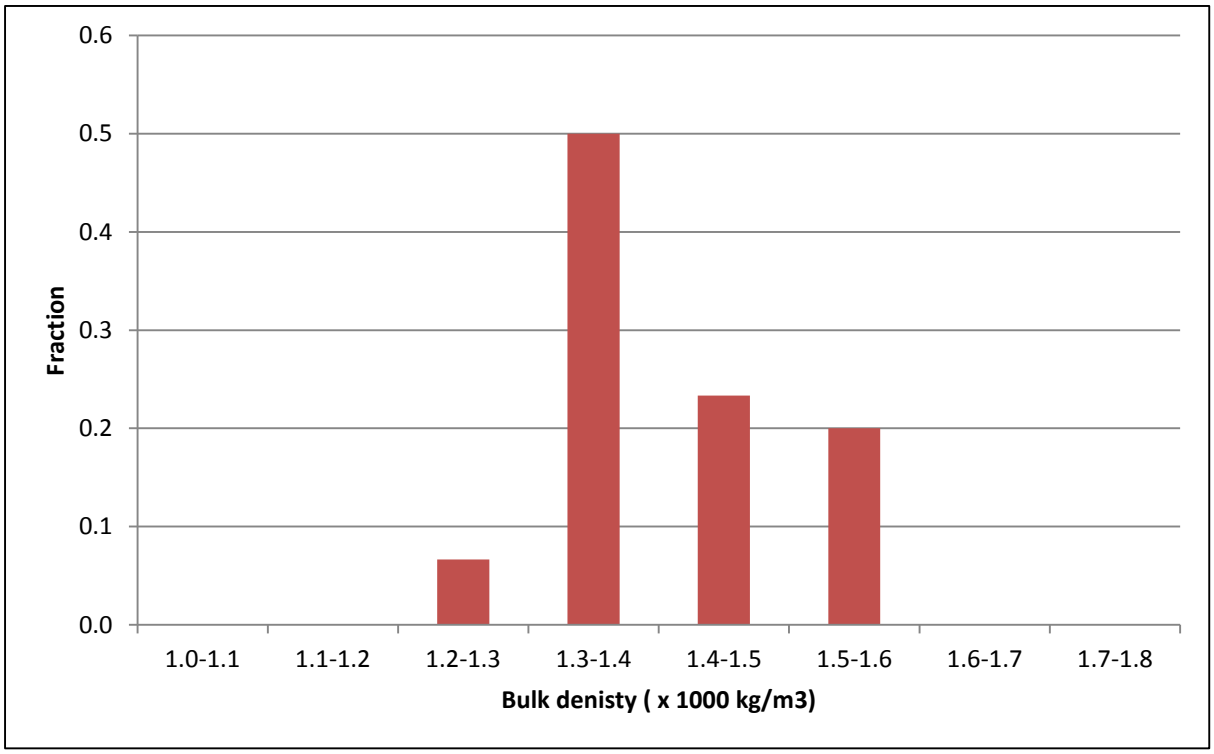

Figure C.5: Density distribution for 20mm HV Coking particles.

APPENDIX D: FRAGMENTATION RAW DATA

In this Appendix the raw data and errors for the fragmentation experiments (breakage index) are given (outliers already discarded). In Table D.1 breakage indices for each repeat as well as the average breakage index and error (confidence interval based on 95% confidence level) are given.

Table D.1: Raw breakage index data for fragmentation experiments.

Coal origin	Temperature (°C)	Size (mm)	Run 1	Run 2	Run 3	Run 4	Run 5	Run 6	Average	Error
LV1	**400**	**10**	1.00	1.00	1.00				**1.00**	**0.00**
LV1	**400**	**15**	1.00	1.00	1.00	1.00			**1.00**	**0.00**
LV1	**400**	**20**	1.00	1.00	1.00	1.00	1.00		**1.00**	**0.00**
LV1	**400**	**25**	1.00	1.00	1.00	1.00			**1.00**	**0.00**
LV1	**400**	**30**	1.00	1.00	1.00	1.00			**1.00**	**0.00**
LV2	**400**	**10**	1.00	1.00	1.00	1.00	1.00	1.00	**1.00**	**0.00**
LV2	**400**	**15**	1.00	1.00	1.00	1.00			**1.00**	**0.00**
LV2	**400**	**20**	1.00	1.00	1.00				**1.00**	**0.00**
LV2	**400**	**25**	1.00	1.00	1.00	0.97			**0.99**	**0.02**
LV2	**400**	**30**	1.00	1.00	1.00	0.97			**0.99**	**0.02**

HV1	**400**	**10**	1.00	1.00	1.00				**1.00**	**0.00**
HV1	**400**	**15**	1.00	1.00					**1.00**	**0.00**
HV1	**400**	**20**	1.00	1.00	1.00	1.00			**1.00**	**0.00**
HV1	**400**	**25**	1.00	1.00	1.00	1.00			**1.00**	**0.00**
HV1	**400**	**30**	0.99	0.92	0.93	0.98			**0.96**	**0.05**
HV2	**400**	**10**	1.00	1.00	1.00	1.00			**1.00**	**0.00**
HV2	**400**	**15**	1.00	1.00	1.00	1.00	1.00		**1.00**	**0.00**
HV2	**400**	**20**	0.85	1.00	0.69	1.41	0.36		**0.86**	**0.48**
HV2	**400**	**25**	0.85	0.83	1.00	0.66	1.00		**0.87**	**0.17**
HV2	**400**	**30**	0.79	0.81	0.78				**0.80**	**0.04**
HV Coking	**400**	**10**	1.42	1.42	1.42	1.42			**1.42**	**0.00**
HV Coking	**400**	**15**	1.00	1.00	1.99	1.41	0.91		**1.26**	**0.56**
HV Coking	**400**	**20**	1.00	1.34	1.29	0.74	1.02	1.14	**1.09**	**0.23**
HV Coking	**400**	**25**	0.50	1.90	0.86	1.41	0.50		**1.03**	**0.76**
HV Coking	**400**	**30**	0.92	0.60	0.71	1.05	0.88		**0.83**	**0.22**
LV1	**600**	**10**	1.00	1.00	1.00	1.00	1.00		**1.00**	**0.00**
LV1	**600**	**15**	1.00	1.00	1.00	1.00			**1.00**	**0.00**

LV1	**600**	**20**	1.00	1.00	1.00				**1.00**	**0.00**
LV1	**600**	**25**	0.90	0.96	1.00	0.94			**0.95**	**0.07**
LV1	**600**	**30**	0.63	0.90	0.96	0.87	0.78		**0.83**	**0.16**
LV2	**600**	**10**	1.00	1.00	1.00	1.00	1.00	1.00	**1.00**	**0.00**
LV2	**600**	**15**	1.00	1.00	1.00				**1.00**	**0.00**
LV2	**600**	**20**	0.81	0.66	1.00	0.46			**0.73**	**0.36**
LV2	**600**	**25**	0.68	1.00	1.00	0.80			**0.87**	**0.25**
LV2	**600**	**30**	1.00	0.46					**0.73**	**3.40**
HV1	**600**	**10**	1.00	1.00	1.00	1.00			**1.00**	**0.00**
HV1	**600**	**15**	1.00	1.00	0.68				**0.89**	**0.46**
HV1	**600**	**20**	1.00	1.00	1.00	1.00			**1.00**	**0.00**
HV1	**600**	**25**	0.97	1.00	1.00	0.91			**0.97**	**0.07**
HV1	**600**	**30**	0.58	0.72	0.70	0.46			**0.62**	**0.19**
HV2	**600**	**10**	1.00	1.00	0.81				**0.94**	**0.27**
HV2	**600**	**15**	1.00	1.00	1.00	1.00			**1.00**	**0.00**
HV2	**600**	**20**	1.00	0.85	0.72	1.00	0.72		**0.86**	**0.18**
HV2	**600**	**25**	1.00	1.00	0.88	1.00	0.74		**0.92**	**0.14**

HV2	**600**	**30**	1.00	0.77	0.86	0.60	0.89		**0.82**	**0.19**
HV Coking	**600**	**10**	0.61	2.00	2.00	0.94	0.98	0.27	**1.13**	**0.76**
HV Coking	**600**	**15**	0.86	0.99	0.77	0.85			**0.87**	**0.15**
HV Coking	**600**	**20**	1.41	0.48	1.41	0.93	1.00		**1.04**	**0.48**
HV Coking	**600**	**25**	1.02	1.13	1.13	1.04			**1.08**	**0.09**
HV Coking	**600**	**30**	0.92	1.18	0.42				**0.84**	**0.96**
LV1	**900**	**10**	1.00	0.87	1.00	0.78	0.97		**0.92**	**0.12**
LV1	**900**	**15**	0.81	0.50	0.84	0.59	0.93		**0.73**	**0.22**
LV1	**900**	**20**	0.49	0.47	0.49				**0.48**	**0.04**
LV1	**900**	**25**	0.47	0.39	0.40	0.29			**0.39**	**0.12**
LV1	**900**	**30**	0.37	0.26	0.31	0.29			**0.31**	**0.07**
LV2	**900**	**10**	1.00						**1.00**	**0.00**
LV2	**900**	**15**	1.00	0.57	0.86	0.78			**0.80**	**0.29**
LV2	**900**	**20**	0.39	0.46	0.52	0.39			**0.44**	**0.10**
LV2	**900**	**25**	0.24	0.20	0.23				**0.22**	**0.05**
LV2	**900**	**30**	0.18	0.36	0.48	0.49	0.20		**0.34**	**0.19**
HV1	**900**	**10**	1.00	1.00	1.00				**1.00**	**0.00**

HV1	**900**	**15**	1.00	1.00	1.00	1.00			**1.00**	**0.00**
HV1	**900**	**20**	0.71	0.83	0.67	0.96	0.57		**0.75**	**0.19**
HV1	**900**	**25**	0.93	0.83	0.69	0.63	0.86		**0.79**	**0.16**
HV1	**900**	**30**	0.66	0.40	0.51	0.61	0.82	0.27	**0.55**	**0.20**
HV2	**900**	**10**	1.00	1.00	1.00	1.00			**1.00**	**0.00**
HV2	**900**	**15**	1.00	1.00	1.00	0.90			**0.97**	**0.08**
HV2	**900**	**20**	0.52	1.00	1.00				**0.84**	**0.68**
HV2	**900**	**25**	0.48	0.55	0.46				**0.50**	**0.12**
HV2	**900**	**30**	0.57	0.58	0.58				**0.57**	**0.02**
HV Coking	**900**	**10**	1.42	2.00	1.42				**1.61**	**0.84**
HV Coking	**900**	**15**	1.41	1.19					**1.30**	**1.40**
HV Coking	**900**	**20**	1.00	1.32	0.89				**1.07**	**0.56**
HV Coking	**900**	**25**	0.75	0.74	0.51	0.58			**0.64**	**0.19**
HV Coking	**900**	**30**	1.12	0.47	0.52	1.41			**0.88**	**0.73**

APPENDIX E: STATISTICAL ANALYSIS ON NUMBER OF PARTICLES

In this Appendix (Table E.1) information on the amount of runs/repeats conducted (before discarding of outliers) for each coal-temperature-size combination is given.

Table E.1: Statistical analysis on number of particles.

Coal origin	Temperature (°C)	Size (mm)	Runs/Repeats
LV1	**400**	**10**	5
LV1	**400**	**15**	5
LV1	**400**	**20**	5
LV1	**400**	**25**	5
LV1	**400**	**30**	5
LV1	**600**	**10**	5
LV1	**600**	**15**	5
LV1	**600**	**20**	5
LV1	**600**	**25**	5
LV1	**600**	**30**	5
LV1	**900**	**10**	5
LV1	**900**	**15**	5
LV1	**900**	**20**	5
LV1	**900**	**25**	5
LV1	**900**	**30**	5
LV2	**400**	**10**	8
LV2	**400**	**15**	5
LV2	**400**	**20**	5
LV2	**400**	**25**	5
LV2	**400**	**30**	5

LV2	**600**	**10**	8
LV2	**600**	**15**	5
LV2	**600**	**20**	5
LV2	**600**	**25**	5
LV2	**600**	**30**	5
LV2	**900**	**10**	5
LV2	**900**	**15**	5
LV2	**900**	**20**	5
LV2	**900**	**25**	5
LV2	**900**	**30**	5
HV1	**400**	**10**	5
HV1	**400**	**15**	5
HV1	**400**	**20**	5
HV1	**400**	**25**	5
HV1	**400**	**30**	5
HV1	**600**	**10**	7
HV1	**600**	**15**	5
HV1	**600**	**20**	5
HV1	**600**	**25**	5
HV1	**600**	**30**	6
HV1	**900**	**10**	5
HV1	**900**	**15**	5
HV1	**900**	**20**	5
HV1	**900**	**25**	5
HV1	**900**	**30**	5
HV2	**400**	**10**	6

HV2	**400**	**15**	5
HV2	**400**	**20**	5
HV2	**400**	**25**	5
HV2	**400**	**30**	6
HV2	**600**	**10**	6
HV2	**600**	**15**	5
HV2	**600**	**20**	5
HV2	**600**	**25**	5
HV2	**600**	**30**	6
HV2	**900**	**10**	5
HV2	**900**	**15**	5
HV2	**900**	**20**	5
HV2	**900**	**25**	5
HV2	**900**	**30**	5
HV Coking	**400**	**10**	6
HV Coking	**400**	**15**	5
HV Coking	**400**	**20**	6
HV Coking	**400**	**25**	5
HV Coking	**400**	**30**	5
HV Coking	**600**	**10**	8
HV Coking	**600**	**15**	5
HV Coking	**600**	**20**	8
HV Coking	**600**	**25**	5
HV Coking	**600**	**30**	5
HV Coking	**900**	**10**	6
HV Coking	**900**	**15**	5
HV Coking	**900**	**20**	6

HV Coking	**900**	**25**	5
HV Coking	**900**	**30**	5